Doctoral Dissertation

PROMOTING DIRECT INTERSPECIES ELECTRON TRANSFER IN ANAEROBIC DIGESTION WITH MAGNETITE FOR ENHANCED BIOMETHANATION PERFORMANCE AND STABILITY

GAHYUN BAEK

Department of Urban and Environmental Engineering
(Environmental Science and Engineering)

Graduate School of UNIST

2019

PROMOTING DIRECT INTERSPECIES ELECTRON TRANSFER IN ANAEROBIC DIGESTION WITH MAGNETITE FOR ENHANCED BIOMETHANATION PERFORMANCE AND STABILITY

GAHYUN BAEK

Department of Urban and Environmental Engineering
(Environmental Science and Engineering)

Graduate School of UNIST

PROMOTING DIRECT INTERSPECIES ELECTRON TRANSFER IN ANAEROBIC DIGESTION WITH MAGNETITE FOR ENHANCED BIOMETHANATION PERFORMANCE AND STABILITY

A dissertation
submitted to the Graduate School of UNIST
in partial fulfillment of the
requirements for the degree of
Doctor of Philosophy

GAHYUN BAEK

July 15, 2019
Approved by

Advisor
Changsoo Lee

Promoting direct interspecies electron transfer in anaerobic digestion with magnetite for enhanced biomethanation performance and stability

Gahyun Baek

This certifies that the dissertation of Gahyun Baek is approved.

July 15, 2019

Changsoo Lee
Associate Professor in Department of Urban and Environmental Engineering
Ulsan National Institute of Science and Technology
Committee Chairperson

Young-Nam Kwon
Associate Professor in Department of Urban and Environmental Engineering
Ulsan National Institute of Science and Technology
Committee Member

Seokhwan Hwang
Professor in Division of Environmental Science and Engineering
Pohang University of Science and Technology
Committee Member

Changha Lee
Associate Professor in Department of Chemical and Biological Engineering
Seoul National University
Committee Member

Hyokwan Bae
Assistant Professor in Department of Civil and Environmental Engineering
Pusan National University
Committee Member

ABSTRACT

Anaerobic digestion (AD) is an attractive technology that stabilizes biodegradable organic compounds and converts them to CO_2 and CH_4 through a series of metabolic reactions of microorganisms. This process enables energy production and wastewater treatment, and biogas generated during AD can be used to produce electricity, thereby enabling wastewater treatment plants to achieve energy self-sufficiency. Biological processes primarily depend on the concerted activity of microorganisms involved in a series of microbial steps. Interspecies electron transfer (IET) between syntrophic partners plays an important role in oxidizing higher organic matters and reducing CO_2 to CH_4 in AD environments. Conventionally, this relationship is balanced by indirect IET (IIET) using electron carriers, such as hydrogen and formate. Direct IET (DIET) in AD environments has recently been suggested as an alternative to IIET. DIET is energetically more advantageous because it does not need hydrogen to be produced for use as an electron carrier. DIET can be realized between different species through biological electrical connections using redox-active proteins and electrically conductive pili.

However, recent studies suggest that cell-to-cell electron transfer can also be mediated through non-biological conductive materials, such as magnetite, granular activated carbon, biochar, and carbon cloth. The addition of conductive material is a simple and effective method of promoting DIET in AD, and its positive effect on process performance has been demonstrated in previous studies using various conductive materials. Such materials are suggested to serve as a conduit for electron flow between electroactive syntrophic partners. Early studies on this phenomenon were mostly performed using defined culture media with simple artificial substrates to confirm this effect. Also, most of the experiments have been conducted in a batch mode to figure out the fundamental mechanism of the conductive materials-mediated DIET. In the present study, this positive effect of conductive materials on biomethanation was further confirmed in real wastewater with a mixed-culture microbial source as an inoculum; this operating condition is similar to that in field-scale anaerobic digesters. Therefore, in the present study, we aimed to enhance the biomethanation performance from real wastewater by DIET stimulation accomplished by magnetite supplementation in a mixed-culture system.

For Study 1, the effect of (semi)conductive iron oxides in anaerobic batch reactors was investigated with cheese whey as substrate. The experimental data demonstrated that the addition of ferric oxyhydroxide (semi-conductive iron oxide) and magnetite (conductive iron oxide) significantly enhanced the AD performance in terms of energy recovery and organic removal over the control reactor. This finding implied that biostimulation with the (semi)conductive ferric oxides was beneficial for high-rate AD. In Study 2, the effect of magnetite addition was examined by long-term monitoring of the performance of continuous anaerobic digesters with and without magnetite. Results clearly demonstrated that magnetite supplementation benefited not only

methane productivity but also process stability likely by energetically providing favorable conditions for IET. DIET between exoelectrogenic bacteria and electron-capturing methanogens through conductive magnetite particles was presumably the dominant mechanism that led to enhanced biomethanation. In Study 3, an approach was designed to separate and recycle magnetite particles by magnetic force in a continuous process without adding extra magnetite for economic feasibility. The proposed magnetite recycling method effectively maintained enhanced DIET and methanogenic activities during a long-term operation (>250 days). Moreover, magnetite recycling helped retain a high biomass density (i.e., increased solid retention time) by returning active biomass aggregated with magnetite to the reactor. *Methanothrix* was likely the major methanogen group responsible for the DIET-based methanogenesis. In Study 4, the individual and combined effects of magnetite addition and external voltage application were explored. The overall results suggested that both individual applications stimulated DIET. However, magnetite had a more significant effect on enhancing AD performance than did external voltage; in particular, the digester with magnetite addition alone showed comparable organic removal efficiency and even higher methane yield at lower hydraulic retention time compared with the digester that combined both applications. Magnetite, as an electron transport conduit, appeared to have played an important role in developing electro-syntrophic associations between exoelectrogenic bacteria and electrotrophic methanogens in both the mixed liquor and electrode biofilms.

In conclusion, the Ph.D. study verified that magnetite-promoted DIET improved AD performance and stability. Furthermore, economic feasibility could be enhanced by the recycling method suggested in Study 3, and stability could be refined by a combination of magnetite addition with external voltage application. DIET is an interesting phenomenon that seems to provide a unique opportunity to improve AD processes at fundamental levels. The findings of this study provide useful information for an improved understanding of the effects of DIET-promoting strategies on AD performance, thereby helping advance the development of stable high-rate digesters.

CONTENTS

LIST OF FIGURES

LIST OF TABLES

1. INTRODUCTION

1-1. Anaerobic digestion

Organic compounds in waste and wastewater are generated from various municipal and industrial sources and can be treated by biological processes. Full-scale wastewater treatment plants use various biological processes, including activated sludge, extended aeration, tricking filter, and anaerobic digestion (AD), to stabilize biodegradable organic compounds via the metabolic activity of aerobic/anaerobic microorganisms [1]. In AD, organic matter is converted into CO_2 and CH_4 through a series of metabolic reactions of microorganisms. This process affords the advantages of both energy production and wastewater treatment. Typically, biogas obtained from AD has a methane content of 50%–60%; biogas with 55% CH_4 content has an upper calorific value of 6.0 KWh/m^3 at standard temperatures and pressure (STP) [2]. Furthermore, biogas is environmentally friendly and energy efficient owing to its low emission of hazardous pollutants [3]. Biogas can be used to produce electricity, thereby enabling wastewater treatment plants to achieve energy self-sufficiency. Therefore, studies have tried to improve the overall efficiency and reaction rates of biogas production through changes in operational conditions (e.g., pH, temperature, retention time, etc.), pretreatment methods, biogas upgrading, biostimulation, bioaugmentation, and co-digestion.

Biological processes primarily depend on the concerted activity of microorganisms involved in a series of microbial steps as seen in Fig. 1-1. Therefore, the key to enhancing AD efficiency is to harmonize and speed-up these activities [4]. Interspecies electron transfer (IET) between syntrophic partners plays an important role in oxidizing higher organic matters and reducing CO_2 to CH_4 in AD environments [5]. The balance of this syntrophic relationship provides thermodynamically favorable conditions for the degradation of carboxylic acids, and thus for realizing stable anaerobic digesters.

The conversion of complex organic matters into biogas proceeds through several series of microbial steps: hydrolysis, acidogenesis, acetogenesis, and methanogenesis. Four major functionally different microbial groups (i.e. hydrolytic bacteria, acidogenic bacteria, syntrophic acetogenic bacteria, and methanogenic archaea) are responsible for each step. First, complex organic matters are broken down into smaller molecules by hydrolytic bacteria. Acidogenic bacteria ferment these molecules to organic acids and alcohols, which are major intermediates in AD. Acetogenic bacteria further convert the fermentation products into acetate, carbon dioxide, and/or hydrogen which are the direct substrates for methanogenesis [6]. Methane-rich biogas produced from the last stage can replace the fossil fuels in production of power and heat.

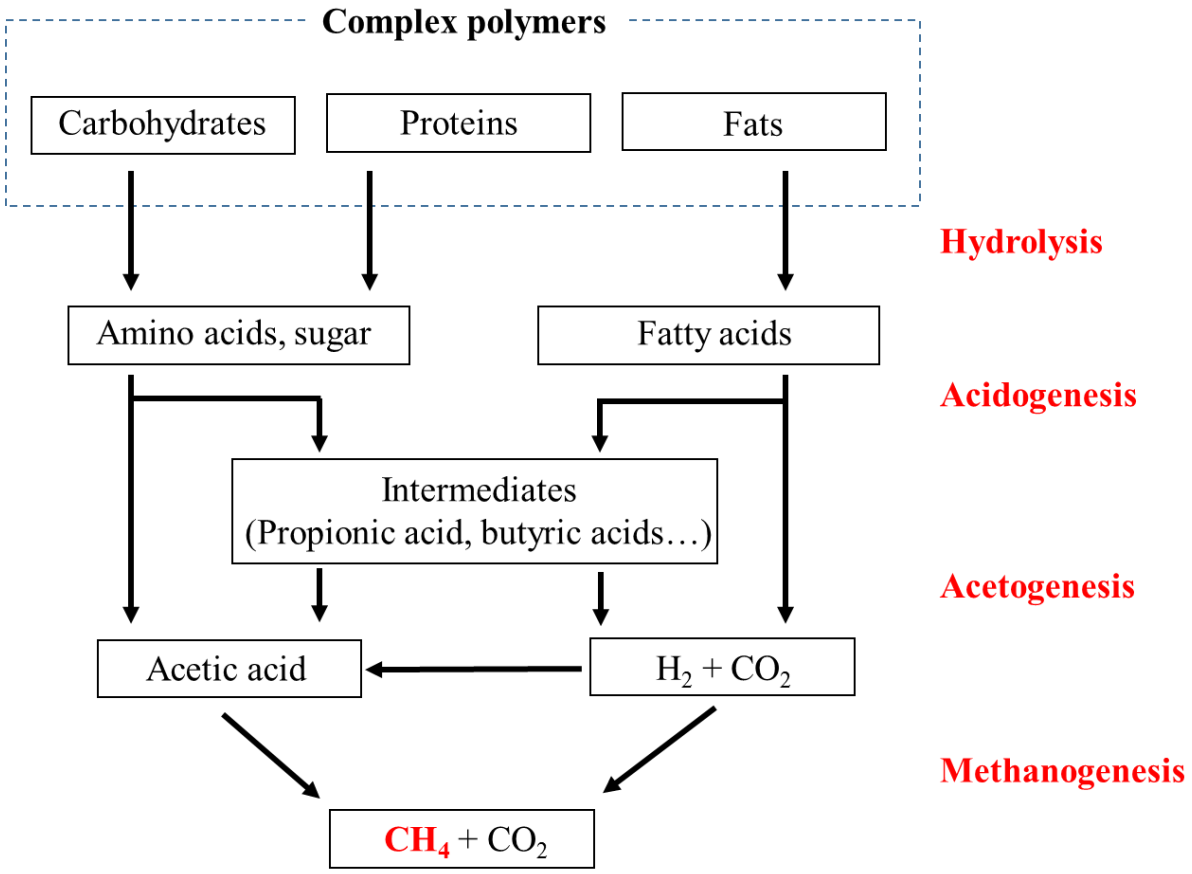

Fig. 1-1. The schematic diagram for anaerobic digestion flow

1-2. Indirect interspecies electron transfer (IIET)

In methanogenic environments, the syntrophic association between hydrogen-producing bacteria and hydrogen-consuming methanogens is the key to maintaining balanced and stable conditions. The slow syntrophic metabolism of propionate and butyrate in anaerobic digesters has often been reported as a crucial limiting factor for the overall reaction rate [7]. Indirect interspecies electron transfer (IIET) via hydrogen and formate as electron carriers is known as a major pathway for electron exchange between syntrophic microorganisms. The anaerobic degradation of major intermediates of AD, such as propionate and butyrate, is thermodynamically unfavorable (i.e., endergonic reaction under standard conditions) without a scavenging reaction (Table 1-1). Hydrogen or formate as a reducing equivalent should be consumed rapidly by methanogens for the growth and metabolism of syntrophs; in other words, the reaction is enabled by low hydrogen partial pressure or formate concentration. Therefore, many studies have tried to provide favorable conditions for syntrophic communities in anaerobic digesters. For example, intermicrobial distances can be shortened by producing compact aggregates or by providing proper mixing conditions [7-9]. Besides this,

mixing is an important factor that determines, for example, the distribution of input flow and the development of flocs and aggregates. This section discusses the mechanisms and microbial metabolisms of interspecies hydrogen transfer (IHT) and interspecies formate transfer (IFT) as well as their limitations.

Table 1-1. Major reactions of syntrophic metabolisms via interspecies hydrogen/formate transfer and their Gibbs free energy ($\Delta G^{\circ\prime}$) at pH 7.

Electron carrier	Major reactions		$\Delta G^{\circ\prime}$ (kJ/mol)
Hydrogen	Propionate degradation	$Propionate^- + 3H_2O \rightarrow Acetate^- + HCO_3^- + H^+ + 3H_2$	+76.5
	Methane production	$3/4HCO_3^- + 3/4H^+ + 3H_2 \rightarrow 3/4CH_4 + 9/4H_2O$	−101.7
	Overall reaction	$Propionate^- + 3/4H_2O \rightarrow Acetate^- + 1/4HCO_3^- + 1/4H^+ + 3/4CH_4$	−25.2
	Butyrate degradation	$Butyrate^- + 2H_2O \rightarrow 2Acetate^- + H^+ + 2H_2$	+48.3
	Methane production	$1/2HCO_3^- + 1/2H^+ + 2H_2 \rightarrow 1/2CH_4 + 3/2H_2O$	−67.8
	Overall reaction	$Butyrate^- + 1/2H_2O + 1/2HCO_3^- \rightarrow 2Acetate^- + 1/2H^+ + 1/2CH_4$	−19.5
Formate	Propionate degradation	$Propionate^- + 2H_2O + 2CO_2 \rightarrow Acetate^- + 3HCOO^- + H^+$	+65.3
	Methane production	$3HCOO^- + 3H^+ \rightarrow 3/4CH_4 + 9/4CO_2 + 3/2H_2O$	−144.5
	Overall reaction	$Propionate^- + 2H^+ + 1/2H_2O \rightarrow Acetate^- + 1/4CO_2 + 3/4CH_4$	−79.2
	Butyrate degradation	$Butyrate^- + 2H_2O + 2CO_2 \rightarrow 2Acetate^- + 2HCOO^- + 2H^+$	+38.5
	Methane production	$2HCOO^- + 2H^+ \rightarrow 1/2CH_4 + 3/2CO_2 + H_2O$	−96.3
	Overall reaction	$Butyrate^- + H_2O + 1/2CO_2 \rightarrow 2Acetate^- + 1/2CH_4$	−57.8

1-2-1. Interspecies hydrogen transfer

The conversion of complex organic compounds into methane via AD proceeds through several microbial steps: hydrolysis, acidogenesis, acetogenesis, and methanogenesis. These steps are respectively performed by four major functionally different microbial groups: hydrolytic bacteria, acidogenic bacteria, syntrophic acetogenic bacteria, and methanogenic archaea. First, complex organic compounds are broken down by hydrolytic bacteria into smaller molecules. Acidogenic bacteria ferment these hydrolytic products to organic acids and alcohols, including volatile fatty acids (VFAs) and ethanol, with hydrogen being evolved as a byproduct [10]. Acetogenic bacteria further oxidize more-reduced intermediates, such as lactate, ethanol, propionate, and butyrate, to acetate. Acetate is then converted to CO_2 and CH_4 by methanogens. Acetogenesis and methanogenesis should together constitute a healthy syntrophic relationship because acetogenesis is an endergonic reaction. It is important to ensure that hydrogen, an acetogenic product, is effectively removed by hydrogen consumers, especially methanogens, because high hydrogen partial pressure inhibits the regeneration of the cytoplasmic pool of oxidized coenzymes in acetogenic bacteria [11]. Syntrophic hydrogen consumption by methanogens helps keep the overall reaction exergonic (Table 1-1). Controlling the hydrogen concentration is crucial for realizing stable and effective AD.

Molecular hydrogen is a minor component in the environment; however, it plays an important role in AD metabolism as a convenient vehicle for electron transport between different organisms as seen in Fig. 1-2 [7, 12]. In sediments dominated by methanogenesis as a terminal electron-accepting step, hydrogen is an intermediate for approximately 40% of the electron flow [13]. Microorganisms that catalyze the hydrogen metabolism contain the key enzyme hydrogenase. Hydrogen can be consumed or produced by this metalloenzyme that catalyzes the reversible heterolytic cleavage of molecular hydrogen [14]. Fig. 1-3 shows the intracellular redox mediators for hydrogen production and consumption. Microorganisms that contain hydrogenases reduce protons through the oxidation of reduced ferredoxin, NADH, and $FADH_2$ [15]. The oxidation reactions of reduced ferredoxin and NADH are energetically favorable when methanogens keep the hydrogen partial pressure low enough, while the oxidation reaction of $FADH_2$ needs ATP to be feasible [16]. Most known methanogens are hydrogenotrophic methanogens that gain energy from the reduction of CO_2 to CH_4 by using hydrogen as an electron donor. Coenzyme F_{420} and oxidized ferredoxin are reduced by hydrogen-uptake hydrogenase as electron carriers, as shown in Fig. 1-3 [17]. Reduced ferredoxin ($Fd_{(red)}$) and reduced F_{420} (F_{420}-H_2) act as direct electron donors through successive steps from CO_2 to formyl, methylene, and methyl levels.

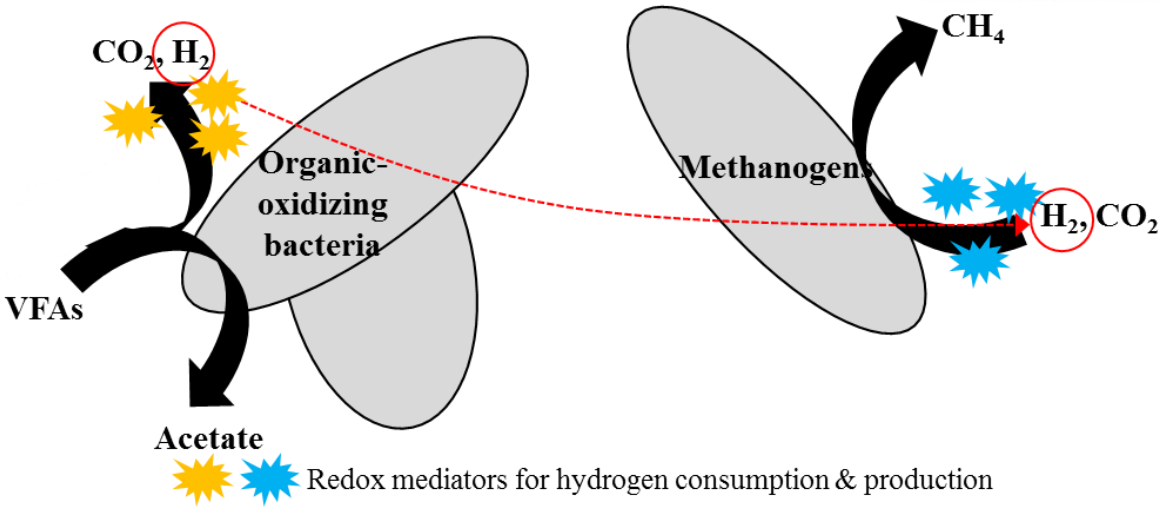

Fig. 1-2. The schematic drawing of interspecies hydrogen transfer

1-2-2. Interspecies formate transfer

Most hydrogenotrophic methanogens can use formate as well as hydrogen as major electron donors. Formate is oxidized to CO_2 by formate dehydrogenase (Fdh), following which CO_2 is reduced to methane [18]. Although most studies focus on IHT in syntrophic methanogenesis, IFT can sometimes function as a major route for electron transfer. For example, Boone et al. [19] reported that formate diffusion accounted for 98-fold more IET than hydrogen diffusion. Furthermore, Thiele et al. [11] observed that IFT was a major IET mechanism, whereas hydrogen was an insignificant intermediate in syntrophic ethanol-degrading flocs from an anaerobic digester treating whey. These studies demonstrated the significance of formate as a diffusive redox mediator in methanogenic cultures.

Hydrogen and formate function similarly in mediating electrons for IIET in AD processes; however, they have different physicochemical characteristics. Hydrogen has an advantage over formate in generating a concentration gradient because of its much lower solubility. This difference makes the concentration gradient between producing and scavenging microorganisms significantly higher (up to 1000-fold) with hydrogen than with formate [20]. On the other hand, hydrogen shows 30-fold higher diffusion rate in water compared to formate. Because of these different characteristics, IFT can be superior to IHT when the intermicrobial distances are large, and vice versa, in terms of generating a concentration gradient.

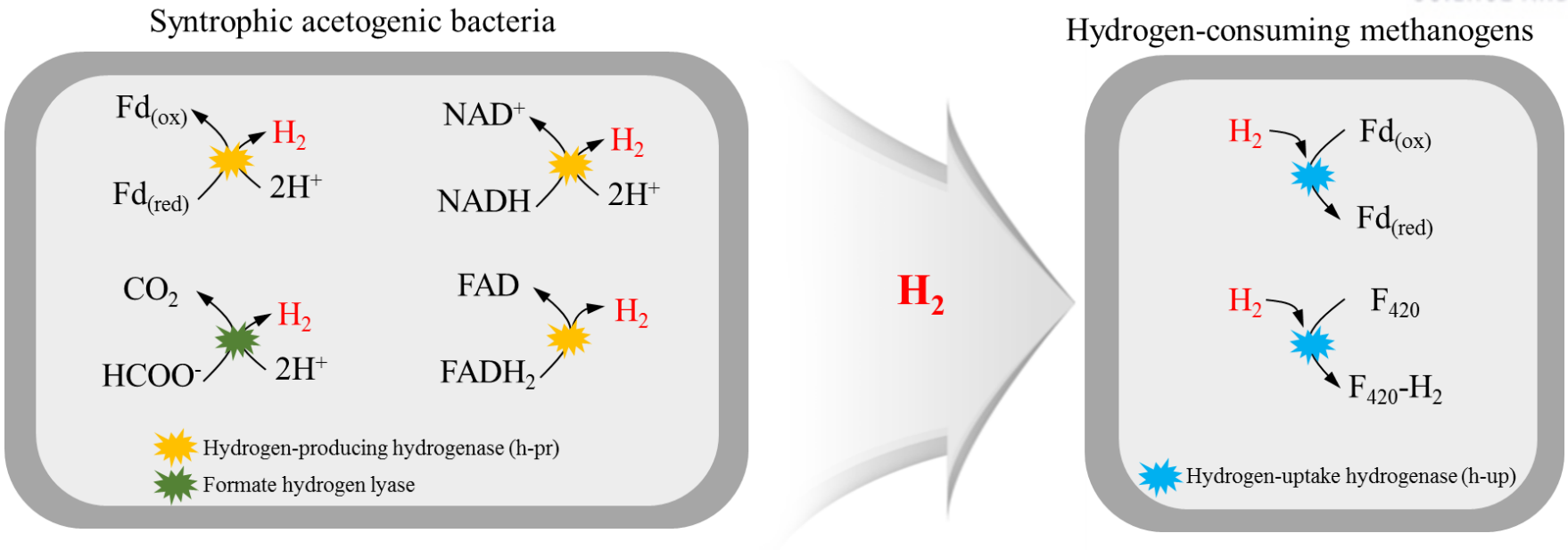

Fig. 1-3. Interspecies hydrogen transfer and intracellular redox mediators for hydrogen consumption and production

1-3. Direct interspecies electron transfer (DIET)

DIET has recently been identified as an important mechanism for IET between syntrophic microorganisms involved in the anaerobic degradation of VFAs in AD. In DIET communities, electrons released from exoelectrogenic microorganisms are directly transferred to electron-capturing microorganisms via membrane-associated cytochromes and conductive pili that form electrical connections between syntrophic partners. DIET could alternatively be mediated by abiotic conductive materials in methanogenic cultures. DIET has been suggested to be faster and energetically more efficient than IIET via hydrogen or formate as electron carriers; therefore, methanogenic performance can potentially be enhanced by promoting DIET in AD [21]. In this section, the fundamentals and mechanisms of DIET are briefly discussed based on observations in defined co-culture studies.

1-3-1. Comparison between DIET and IIET

The main limitation of the IIET mechanism is that any stagnation in this process causes the accumulation of VFAs, and high VFA concentrations (especially for propionate) are toxic to methanogens. The syntrophic association between acetogenesis and methanogenesis is often considered the rate-limiting step of the overall AD process [22]. Therefore, under high organic loading conditions, fast growth of acidogenic bacteria can lead to excessive accumulation of VFAs and hydrogen to levels that cannot be effectively handled by slow-growing methanogens and VFA degraders. This results in fast accumulation of excess fermentation products, in turn leading to unfavorable conditions for methanogens [23]. On the contrary, DIET has an advantage over IIET from a thermodynamic viewpoint because DIET does not need complex enzymatic steps to produce, consume, and diffuse the redox mediators (Fig. 1-2 and 1-4). For example, in the case of propionate oxidation by propionate-oxidizing bacteria (POB), the standard Gibbs free energy of IHT and DIET can be represented as equation (1-1) and (1-2), respectively [24].

$$C_2H_5COO^- + 3H_2O \rightarrow CH_3COO^- + HCO_3^- + H^+ + 3H_2 \quad (1\text{-}1)$$

$\Delta G^{o'}$ = 72.7 kJ/mol (37℃, pH 7)

$$C_2H_5COO^- + 0.75H_2O \rightarrow CH_3COO^- + 0.25HCO_3^- + 0.25H^+ + 0.75CH_4 \quad (1\text{-}2)$$

$\Delta G^{o'}$ = -26.4 kJ/mol (37℃, pH 7)

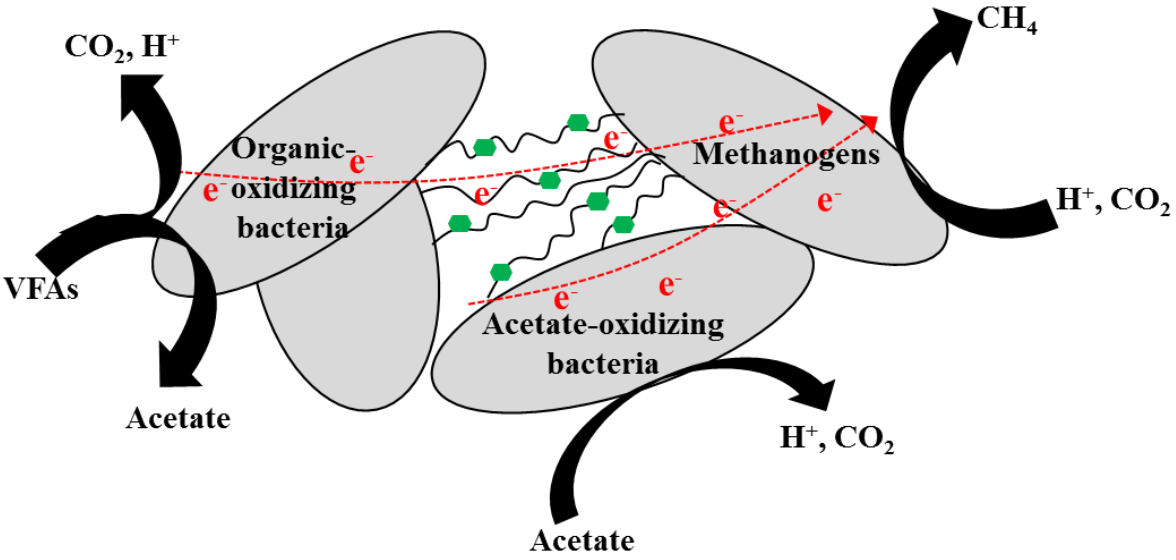

Fig. 1-4. The schematic drawing of direct interspecies electron transfer

As seen in the above equations, the oxidative half-reaction of propionate degradation is thermodynamically not favorable reaction, whereas methane is produced directly from H^+, e^-, and CO_2 via DIET. Furthermore, DIET is more energy-efficient than IHT, which loses energy owing to the formation and consumption of intermediates [21]. In IHT, the methanogenic reaction must be followed to keep lower H_2 concentration and negative Gibbs free energy to yield energy (Table 1-1). Jing et al. [24] calculated the Gibbs free energy value during the batch experiment under DIET-stimulated conditions and found that it was more negative for DIET than for IHT. They stated that higher propionate degradation rates could be achieved owing to the promotion of DIET. Furthermore, a recent study revealed that DIET showed even higher external electron transfer rates than hydrogen-based IET (44.9×10^3 and 5.24×10^3 e^-/cell pair/s for DIET and IHT, respectively) [25]. These authors reported that the main limiting factor for conventional IET is the mediator concentration gradient, whereas that for DIET is activation losses (overpotentials) when electrons are transferred between membrane-associated cytochromes and microbial nanowires.

1-3-2. DIET mechanisms

Extracellular electron transfer reportedly occurs through three different mechanisms: (1) soluble redox shuttles, (2) direct contact between the electron acceptor and the redox-active protein on the outer-membrane surface, or (3) conductive filamentous structures [26]. Biological DIET includes the second and third mechanisms in the form of cell-to-cell electron transfer via biological components like *c*-type cytochromes and conductive pili.

The *c*-type cytochrome is essential to the electron transfer mechanism of microbial species by undergoing oxidation and reduction. Most well-known exoelectrogenic microorganisms, such as *Geobacter* and *Shewanella*, are known to be capable of transporting electrons through a chain of cytochrome c toward extracellular electron acceptors [27]. They use cytochrome *c* to donate electrons to solid-state electron acceptors such as electrodes in bioelectrochemical systems (BES), insoluble chemical electron acceptors (iron oxides, sulfate, and nitrate), and soluble redox compounds (humic compounds or riboflavin). In *Shewanella oneidensis* MR-1, a well-known metal-reducing bacterium, *c*-type cytochromes (OmcA, MtrC, and CymA) play a role in transporting electrons from the quinone/quinol pool of the inner membrane, to the periplasm, to the outer membrane, and finally to extracellular electron acceptors like metal oxides [28]. *G. sulfurreducens* also contains *c*-type cytochromes (OmcS and OmcE); however, its conceptual model is quite different from that of *S. oneidensis* MR-1. Leang et al. [26] reported a close association between OmcS and conductive pili in *G. sulfurreducens* by suggesting a mechanism in which OmcS facilitates electron transfer from pili to ferric oxides. This model proposes that electron conduction is achieved through the conductive pili; however, OmcS should play a role in transferring electrons from pili to ferric oxides.

Another DIET mechanism, called microbial nanowires, also uses conductive pili. Conductive pili have been observed in many studies by atomic force microscopy (AFM), scanning electron microscopy (SEM), scanning tunneling microscopy (STM), and transmission electron microscopy (TEM) [29-32]. Conductive pili are protein filaments produced by microorganisms for long-range electron transfer under suitable conditions [33]. Through pili, longer-range electron transfer can occur without a direct contact mechanism to insoluble minerals, solid electrodes, other microorganisms, and even electrically conductive biofilm [34]. Two mechanisms have been proposed for how pili show electrical conductivity. The first mechanism is metal-like conduction in which charges are spread across the entire filament. This can occur through pi-pi orbital overlaps and charge delocalization, as has been observed frequently in many conductive organic materials [35]. Metallic-like conductivity in biological proteins was first reported with *G. sulfurreducens* pili; these show electronic conductivity of ~5 mS/cm, which is comparable to that of synthesized metallic nanotubes. The second mechanism is an electron hopping/tunneling mechanism in which electrons can move by hopping or tunneling through pili. In this mechanism, electrons jump from cytochrome to cytochrome; therefore, the involvement of cytochromes is a crucial factor. However, Malvankar et al. [33] found evidence of the irrelevance of cytochromes and electron transport in conductive *G. sulfurreducens* biofilms. AFM images showed that cytochromes were not located close enough on pili to enable the hopping or tunneling of electrons. Furthermore, the inactivation of cytochromes did not have any negative effect on biofilm conductivity. Thus, the authors reported that long-range electron transfer through nanowires in *G. sulfurreducens* is based on metallic-like filaments rather than on a hopping or tunneling mechanism between *c*-type cytochromes. On the other hand, Pirbadian et al. [36] reported that the conductive pili of *S. oneidensis* are an extension of the outer membrane and periplasm, which include multiheme cytochromes responsible for electron transport. They

proposed that *S. oneidensis* conducts electrons through a multistep cytochrome-to-cytochrome electron hopping/tunneling mechanism.

1-4. Objectives of the dissertation

Previous findings suggest that DIET can provide an interesting possibility to improve the energy efficiency and economic feasibility of anaerobic digesters. However, most prior studies investigated DIET in methanogenic communities using synthetic media with a single carbon source (e.g., ethanol or organic acids) under defined co-culture conditions to identify the fundamental mechanism. The influence of stimulated DIET may be more complicated in mixed-culture systems with complex microbial communities, which would have greater chances of containing more microbes potentially involved in electric syntrophy than defined co-culture communities. Therefore, in the present study, we aimed to enhance the biomethanation performance and improve the feasibility of the technique for treating complex wastewater by DIET stimulation accomplished by magnetite supplementation in a mixed-culture system. A brief flowchart of this study is illustrated in Fig. 1-5, and the objective of each study is listed as follows:

- Study 1: to investigate the effect of (semi)conductive iron oxides in anaerobic batch reactors;
- Study 2: to monitor the performance of continuous anaerobic digesters with and without magnetite for a long-term period;
- Study 3: to separate and recycle magnetite particles in a continuous process without adding extra magnetite for economic feasibility;
- Study 4: to investigate the individual and combined effects of magnetite addition and external voltage application.

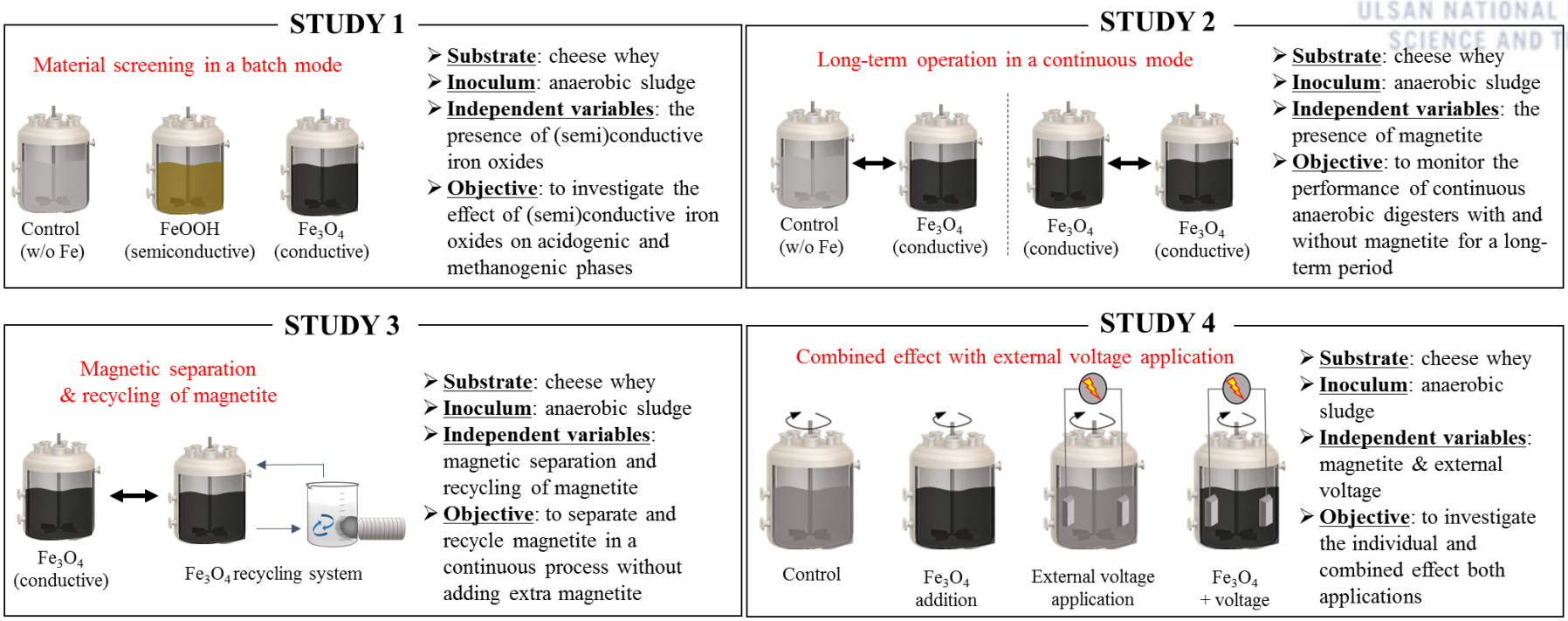

Fig. 1-5. The schematic flowchart of each study

2. LITERATURE REVIEW

2-1. Biological DIET observed in pure cultures

The DIET mechanism was first observed in defined co-cultures of *G. metallireducens* and *G. sulfurreducens* [32]. In the co-culture medium, ethanol and fumarate were the sole electron donor and acceptor, respectively, and they need to share electrons because *G. metallireducens* cannot use fumarate as an electron acceptor whereas *G. sulfurreducens* cannot oxidize ethanol. The authors observed that the co-culture oxidized ethanol through the formation of tight and electrically conductive aggregates. The deletion of the genes encoding the hydrogenase subunit did not affect the ethanol metabolism, and the abundance of genes for cytochrome OmcS and pili was closely correlated with the syntrophic co-culture. They concluded that DIET, and not IET via hydrogen or formate as electron carriers, was the predominant electron transfer mechanism under selective pressure for effective electron transfer. After this observation, similar experimental results demonstrating DIET under certain conditions were reported in defined co-cultures (Table 2-1).

Rotaru et al. [37] were the first to prove the ability of methanogens (*Methanosarcina barkeri*) to participate in DIET in a *G. metallireducens* co-culture. They presented evidence similar to that of the first experimental study conducted by [32], in which two species must give and take electrons for the metabolism of ethanol to methane. The experimental results strongly suggested that the direct use of electrons by *M. barkeri* occurred as shown in equation (2-1), rather than by conventional hydrogenotrophic methanogenesis.

$$8H^+ + 8e^- + CO_2 \rightarrow CH_4 + 2H_2O \quad (2\text{-}1)$$

Similar ability of DIET-mediated methanogenesis was observed in *Methanosaeta harundinaceae*. The *Methanosaeta* species is generally known to be able to utilize acetate only as substrate; however, it cannot convert hydrogen or formate to methane. Rotaru et al. [27] observed that the methanogenic aggregates collected from an anaerobic digester treating brewery wastewater were highly dominated by *Methanosaeta* species (over 90%) and capable of efficiently converting ethanol to methane. Given that *Methanosaeta* cannot use hydrogen or formate for electron donor, IIET cannot be the primary IET mechanism necessary for the syntrophic oxidation of ethanol for methanogenesis in the aggregates. Furthermore, these aggregates showed electrically conductive characteristics, and *Geobacter* species were predominant bacterial group (approximately 25% of the bacterial 16S rRNA sequences were recovered as *Geobacter* species). Based on these observations, the authors speculated that DIET was the primary mechanism for electron exchange within these aggregates. A significant volume of evidence was presented to support their speculation. Transcriptomic analysis revealed a highly abundant and complete complement of genes for the reduction of CO_2 to CH_4 in *M. harundinaceae*. Furthermore, highly expressed genes for ethanol metabolism and production of conductive

pili were detected in *G. metallireducens*. The authors checked that there was no methane production from ethanol oxidation in co-cultures of *G. metallireducens* with H_2- and formate-utilizing methanogens. This result excluded the possibility of IIET via H_2 or formate. Furthermore, radiotracer, stoichiometric modeling, and mutant strain experiments suggest that *Methanosaeta* species can participate in DIET. This interesting discovery suggests that *Methanosaeta* plays an important role in directly accepting electrons from other species as well as in acetate metabolism.

Table 2-1. Observational and experimental evidence for biological direct interspecies electron transfer (DIET) in defined co-cultures.

Electron-donating microorganism	Electron-accepting microorganism	Evidence	Reference
Geobacter metallireducens	*Geobacter sulfurreducens*	Ethanol oxidation under conditions in which IET is necessary Elimination of the possibility of IET via hydrogen or formate Formation of electrically conductive aggregates Knock-out mutation test (cytochrome OmcS and conductive pili)	[32]
Geobacter metallireducens	*Methanosarcina barkeri*	Ethanol oxidation under conditions in which IET is necessary Formation of close aggregates Knock-out mutation test (conductive pili)	[37]
Geobacter metallireducens	*Methanosaeta harundinacea*	Formation of close aggregates Lack of the ability of *G. metallireducens* to grow via IHT Transcriptomic analysis Isotopic labeling using $^{14}CO_2$ Knock-out mutation test (c-type cytochrome and conductive pili)	[27]

2-2. Conductive materials to promote DIET

As discussed in previous section, DIET usually involves biological electrical connections (i.e., cytochrome or pili) between microorganisms. However, DIET can also occur through conductive materials as nonbiological electric conduits, as shown in Fig. 2-1. Under a conductive-material-supplemented environment, microorganisms do not form tight aggregates of the kind that are necessary for direct physical contact or electrical connection through pili between cells; instead, they seem to be tightly attached to the surface of the conductive materials [38-40]. Furthermore, important biological tools for DIET, such as pili and cytochrome OmcS, are not required for electron exchange if conductive materials exist. Recently, DIET stimulation by the supplementation of conductive materials has been studied in engineered systems such as lab-scale anaerobic digesters as well as co-cultures. Most bioreactors are inoculated using an undefined mixed culture that has a much more complex microbial community structure than a defined co-culture. They may behave differently in response to different conductive materials, and this is an important point to address for practical applications.

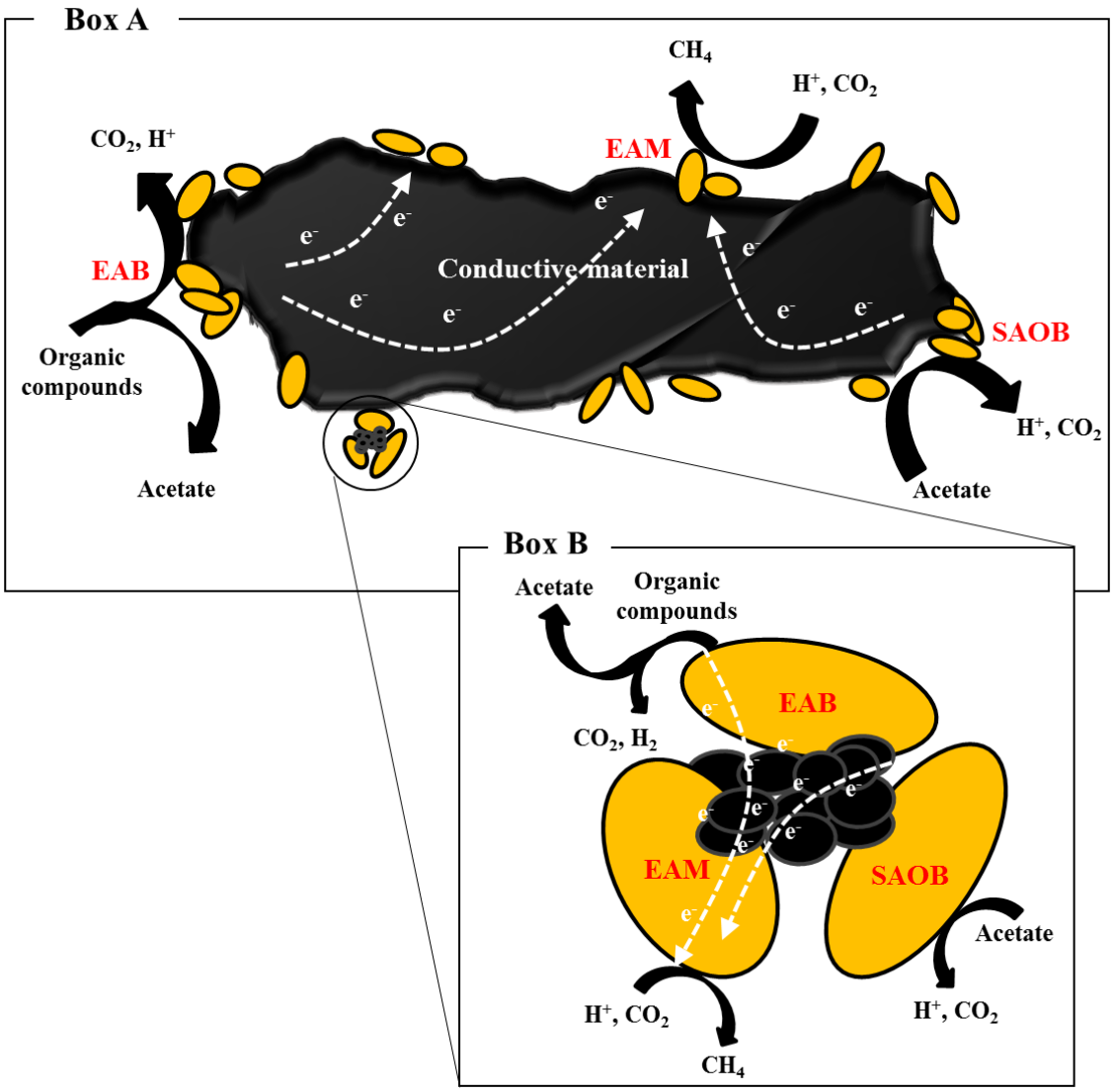

Fig. 2-1. Schematic of how conductive material serves to facilitate interspecies electron transfer. Boxes A and B represent the interactions between microorganisms and conductive materials when the conductive particles are larger or smaller than the associated microorganisms, respectively. EAB, electroactive bacteria; EAM, electroactive methanogens; and SAOB, syntrophic acetate-oxidizing bacteria.

2-3. (Semi)conductive iron oxides to promote DIET

Iron oxides on Earth are known to play an important role in biological and geological reactions. Given that there are different types of iron oxide particles with different conductivities, such as insulative (ferrihydrite), semiconductive (hematite and goethite), and conductive (magnetite), they are suitable for use in experiments to test whether the DIET mechanism is stimulated by conductive materials. Kato et al. [22] first explored the use of this characteristic (i.e., different conductivities of different types of iron oxides) to observe interactions in soil bacteria, and they found that nanosized iron oxide particles can facilitate the respiratory mechanism of soil microbial cultures. Kato et al. [41] further confirmed that the conductivity of iron oxides can determine the methanogenesis rate from enriched microbial communities from rice paddy soils. In this study, three different iron oxides with different conductivities (magnetite, hematite, and ferrihydrite) were investigated. It was found that (semi)conductive iron oxides could facilitate methanogenesis from acetate and ethanol, with improvements in both lag time and production rate. Any other effect of ferrous ions, including acting as a nutrient or electron shuttle, was excluded upon the detection of an extremely small amount of ferrous ions under hematite- and magnetite-supplemented conditions. This explained the reason for enhanced methanogenesis with the establishment of an electrical syntrophic relationship between *Geobacter* and *Methanosarcina* via (semi)conductive iron oxides. This hypothesis was supported by real-time PCR results in the presence and absence of methanogenesis inhibitors. The abundance of *Geobacter* was not dependent on the presence of an inhibitor in the ferrihydrite-supplemented conditions, but was strongly affected in hematite- and magnetite-supplemented conditions. The results suggest that the *Geobacter* used (semi)conductive iron oxides as electron conduits towards *Methanosarcina*, making them candidates for syntrophic partnership (Fig. 2-2).

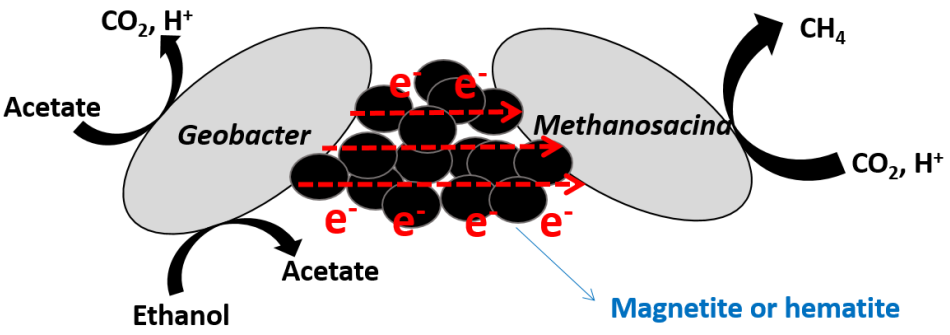

Fig. 2-2. Schematic of suggested mechanisms under hematite- and magnetite-supplemented conditions.

Since Kato's [22] study, magnetite has attracted much attention as a promoter for DIET. It is the main component of iron ores on Earth, and it has conductive and ferrimagnetic characteristics. Among all naturally

occurring minerals on Earth, it is the most magnetic and is harmless to the environment and to living things. Therefore, it has attracted interest in various application fields including drug delivery, contrast agents for magnetic resonance imaging, immunoassays, and molecular biotechnology [42, 43]. Furthermore, magnetite can be synthesized easily by the addition of stoichiometric amounts of Fe^{2+} and Fe^{3+} in ammonia, and basic solution and size control is possible; this suggests its various potential applications [44]. The most important characteristic of magnetite as a promoter for DIET is its conductivity. The electrical conductivity and resistivity of magnetite are 2.5×10^2 $\Omega \cdot cm^{-2}$ and 0.000005 $M\Omega \cdot cm$, respectively (electrical resistivity values of hematite and goethite are 2 and 16 $M\Omega \cdot cm$, respectively) [45].

Kato et al. [46] investigated the possibility of DIET in co-cultures of *G. sulfurreducens* and *Thiobacillus denitrificans* when stimulating DIET by supplementation with magnetite and not by a naturally formed biological electrical connection. As in other experiments with defined co-cultures, *G. sulfurreducens* can oxidize acetate but cannot reduce nitrate; the opposite is true for *T. denitrificans*. The authors could not observe any reaction (i.e., oxidation of acetate or reduction of nitrate) in the co-culture of the two species, suggesting that electron exchange via direct biological electrical connections like pili or cytochromes is not possible between them. IIET mediated by H_2 or formate also cannot occur in this environment because *T. denitrificans* is not capable of using these electron carriers as electron donors. However, supplementation with semiconductive and conductive iron oxides induced the reaction, where magnetite stimulated much faster electron transfer. The electron transfer curve, X-ray diffraction (XRD) spectra pattern, and SEM images supported the possibility of DIET between two species via electric currents through conductive magnetite.

Thereafter, magnetite addition to stimulate DIET has been studied in various substrates in mixed cultures. Cruz Viggi et al. [47] first reported the effect of magnetite addition to facilitate the degradation of propionate, a central intermediate in AD with rice paddy soil as an inoculum. Indeed, the addition of micrometer-sized (100–150 nm) magnetite triggered a methane production rate that was 33% higher than that of a control reactor; they proposed that this stimulatory effect was derived from the DIET mechanism with magnetite particles acting as an electron conduit between microorganisms. Similarly, Li et al. [48] reported the improvement of butyrate degradation by magnetite supplementation in paddy soil enrichments. They used nanosized (30 nm) magnetite particles to accelerate the methane production rate in the whole subculture enrichment. The addition of anthraquinone-2-sulfonate (AQS), which acted as an electron shuttle outside the cells, did not facilitate methane production, and the stimulatory effect of magnetite disappeared completely when it was insulated by a silica coating. Both observations suggested that the electrical conductivity of magnetite particles is the key to enhanced methanogenesis. Yamada et al. [49] tested the effect of magnetite addition under thermophilic conditions, unlike other studies that were conducted in a mesophilic environment. Observations of the putative electric syntrophy between VFA-oxidizing bacteria and *Methanosarcina* species suggested that faster degradations of acetate and propionate occurred successfully even under thermophilic conditions. Mixed VFAs containing an equimolar mixture of acetate, propionate, butyrate, valerate, and caprotate were used as an

artificial substrate for the methanogenic test with magnetite supplementation [50]. The degradation rate of C2-C6 VFAs was improved significantly by magnetite addition, and this effect was particularly pronounced for longer-chain VFAs. Zhuang et al. [51] used benzoate, an intermediate in the methanogenesis of aromatic compounds, as a substrate; its degradation rates were increased remarkably in the presence of hematite (25%) and magnetite (53%) compared to a control.

3. [STUDY 1] INVESTIGATION OF THE EFFECTS OF (SEMI) CONDUCTIVE IRON OXIDE ADDITION IN BATCH MODE

3-1. Introduction

A recent study on a rice paddy soil microbial community reported that the addition of semiconductive hematite and conductive magnetite clearly increased methanogenesis rates from acetate and ethanol, with a stimulated growth of *Geobacter* [41]. The authors observed a marked increase in methane production from acetate and ethanol when magnetite or hematite was supplied at 20 mM Fe. Methane production was higher by approximately 31–60% for acetate and 38–58% for ethanol with magnetite and by approximately 33–68% for acetate and 44–48% for ethanol with hematite compared with the control, which had no added iron compounds. The leaching of iron ions and their contribution as a nutrient or electron shuttle for enhanced methanogenesis were considered insignificant because the concentration of Fe(II) was very low (<2 mM) in these cultures. The addition of insulative ferrihydrite had a suppressive effect likely due to the competition between the methanogens and iron-reducing bacteria (IRB) on the same substrates. Although knowledge about the underlying mechanism remains insufficient, these observations suggested that methanogenic performance can be influenced by the type of iron oxides added to anaerobic digesters; furthermore, the electrical conductivity is the major characteristic that determines the direction and extent of the effect.

This study aimed to investigate the effect of crystalline (semi)conductive ferric oxides on the evolution of microbial community structure in AD, particularly during startup, and the process performance when the substrate used has a complex composition. Three anaerobic batch reactors, namely, one control and two supplemented with different ferric oxides, were operated to treat cheese-processing wastewater for comparison. The primary focus was on how the different biostimulation amendments affected the reaction course throughout acidogenesis and methanogenesis. The results of this study will provide information about proper material screening in stimulating DIET in future studies. Variations in physicochemical parameters and microbial community structure between the reactors during the operation period were comparatively analyzed to obtain comprehensive insights into the microbial and process responses.

3-2. Materials and methods

3-2-1. Bioreactor operation

Three completely-mixed tank reactors with a working volume of 2 L, designated as R1 to R3, were run to anaerobically treat whey, a byproduct from cheese production, in batch mode for a period of 30 days. Whey has widely been treated by AD due to its high organic strength and biodegradability [52, 53]. Basic

characteristics of the substrate and inoculum are presented in Table 3-1. Most organic matter in the substrate existed in soluble form more easily available for microorganisms. Each reactor was filled with dilute whey (5 g/L as chemical oxygen demand (COD)) and inoculated with anaerobic sludge from a municipal sewage treatment plant (seeding ratio, 1% (v/v)). R2 and R3 were supplemented with ferric oxyhydroxide (FeOOH) and magnetite (Fe_3O_4), to give a final Fe concentration of 20 mM, respectively. The reactor operating temperature was maintained at 35 ± 2°C using an automatic controller combined with a heating tape, and the pH was kept above 7.0 by dosing 3 N NaOH solution with a pH controller. Each reactor was routinely sampled and monitored for a set of physicochemical parameters.

Table 3-1. Basic physicochemical characteristics of anaerobic seed sludge and whey substrate

Parameter	Unit	Anaerobic sludge	Whey
Total COD	mg/L	16,968 (93)[a]	4,941 (221)
Soluble COD	mg/L	1,035 (42)	4,226 (108)
Total solids	mg/L	19,900 (141)	5,750 (71)
Total volatile solids	mg/L	11,500 (71)	5,250 (71)
Total suspended solids	mg/L	17,600 (566)	1,000 (283)
Volatile suspended solids	mg/L	11,200 (566)	600 (283)

[a] Standard deviations are in parentheses.

3-2-2. DNA extraction

Community DNA was purified from the reactor samples using an automated nucleic acid extractor (ExiProgen, Bioneer, Daejeon, Korea) according to the manufacturer's instructions. A 1-mL aliquot of a sample was centrifuged in a 1.5-mL microtube at 13,000 *g* for 3 min, and the pelleted biomass was then washed with distilled water by repeated centrifuging (13,000 *g*, 1 min), decanting (900 μL), and resuspending (up to 1 mL in distilled water) to get rid of cell debris and other impurities. A 200-μL portion of the resuspension was loaded on the extractor with the ExiProgen Bacteria Genomic DNA Kit (Bioneer). The purified DNA was eluted in a DNase-free elution buffer solution (200 μL) and stored at –20°C until use.

3-2-3. Molecular fingerprinting and sequencing analysis

Denaturing gradient gel electrophoresis (DGGE), a widely used molecular fingerprinting method to analyze microbial community structure, was employed to monitor the variations in archaeal and bacterial community structures in the reactors. Archaeal and bacterial 16S rRNA gene fragments for DGGE analysis were prepared by polymerase chain reaction (PCR) using ARC787F/1059R and BAC338F/805R primer sets

[54], respectively. A 40-base GC clamp was added to the 5'-end of each forward primer (i.e., ARC787F and BAC338F) for stable melting behavior and better separation of the amplicons on a gel [55]. A touch-down thermal cycling protocol was applied for PCR: initial denaturation at 94°C for 10 min; 20 cycles of denaturation at 94°C for 30 s, annealing at 65 to 55°C for 30 s (decrease in temperature by 0.5°C/cycle), and extension at 72°C for 30 s; additional 25 cycles of 94°C for 30 s, 55°C for 30 s, and 72°C for 30 s; and further extension at 72°C for 7 min. The PCR fragments (20 μL) were loaded on 8% (w/v) polyacrylamide gels with denaturant gradients of 35–65% and 20–60% for the archaeal and bacterial DGGE runs (100% denaturant contains 7 M urea and 40% (v/v) formamide), respectively. Electrophoresis was run in a D-code system (Bio-Rad, Hercules, CA) for 16 h at 80 V. The DGGE gels were stained with SYBR Safe dye (Molecular Probe, Eugene, OR) and scanned under blue light to visualize the band patterns. Bands of interest were cut out of the gels and eluted in 40 μL of sterile water. A 2-μL aliquot of each elution was reamplified with the same primer sets as used for the DGGE analysis but without the GC clamp. The resulting PCR products were gel-purified, cloned, and sequenced. The recovered sequence information was compared against the GenBank and RDP databases. The RDP classifier was used for taxonomic classification at a bootstrap confidence threshold of 80%. All nucleotide sequences retrieved in this study have been deposited in the GenBank database: KP241962-KP241975.

3-2-4. Cluster analysis and ordination of DGGE fingerprints

A binary matrix was constructed from the archaeal and bacterial DGGE fingerprints each by recording the presence or absence of individual DGGE bands as 1 or 0, respectively, in all lanes. Cluster analysis on the resulting matrices was performed using UPGMA (unweighted pair group method with arithmetic means) algorithm to measure the relatedness between the analyzed community structures. Cluster dendrogram construction was conducted using PAST 3.03 software [56]. Non-metric multidimensional scaling (NMS), one of the most effective ordination methods for ecological community data [57], was employed to visualize the shifts in archaeal and bacterial community structures over time in each reactor. NMS compresses a complex data set (e.g., band profile of a DGGE lane) into a point in a low dimensional space so the distance between two points in a NMS plot reflects the dissimilarity between the corresponding data sets. NMS calculation was performed using PC-ORD software 5.0 (MjM software, Gleneden Beach, OR, USA). UPGMA clustering and NMS were both performed using the Sorensen distance measure generally recommended for community data [57].

3-2-5. Real-time polymerase chain reaction

The *Methanosaeta* and *Trichococcus* 16S rRNA gene concentrations in the reactors were determined by real-time PCR using Mst primers and probe set [54] and Trich primer set [58], respectively. Real-time PCR

amplification was performed in a Quantstudio 12K Flex system (Life Technologies, Singapore). A reaction mixture for *Methanosaeta* detection (20 μL) was prepared using the THUNDERBIRD Probe qPCR mix (Toyobo, Osaka, Japan): 10 μL of the premix, 2 μL of the TaqMan probe (final concentration, 200 nM), 1 μL of each primer (final concentration, 500 nM), 4 μL of PCR-grade water, and 2 μL of template DNA. On the other hand, for *Trichococcus* detection based on SYBR Green I chemistry, a reaction mixture was prepared using the THUNDERBIRD SYBR qPCR mix (Toyobo): 10 μL of the premix, 1 μL of each primer (final concentration, 500 nM), 7 μL of PCR-grade water, and 1 μL of template DNA. Both target sequences were amplified in a two-step thermal procedure: predenaturation for 10 min at 95°C followed by 40 cycles of 15 s at 95°C and 1 min at 60°C. All *Trichococcus* runs were checked for amplification specificity by melting curve analysis (60 to 95°C with a ramping rate of 0.05°C/s) after the amplification cycles.

The quantitative standard curve for *Methanosaeta* was generated as previously described using an equimolar mixture of the standard plasmids as the standard template [59]. A 10-fold serial dilution series (10^2–10^8 copies/μL) of the standard template was prepared and analyzed by real-time PCR with Mst-set. The crossing point (CP) values determined from the standard dilutions were plotted against the logarithm of their corresponding initial copy concentrations of template. The target sequence concentration in an unknown sample was quantified against the linear regression line of the resulting plot. The *Trichococcus* standard curve was prepared in the same manner using a standard plasmid made in this study as the standard template. The standard plasmid was constructed by cloning the target sequence PCR-amplified from the day 12 sample of R3 using Trich-set into pGEM-T Easy vector (Promega, Madison, WI, USA). A wide linear range ($r^2 > 0.999$) over eight log units was observed for each standard curve. Each DNA sample was analyzed in duplicate, and real-time PCR data were acquired and processed using Quantstudio 12K Flex Software ver. 1.2 (Life Technologies).

3-2-6. Analytical methods

COD was measured spectrophotometrically using HS-COD-MR kit (HUMAS, Daejeon, Korea). Solids were measured following the protocols in Standard Methods [60]. VFAs (C_2-C_7) were analyzed using a gas chromatograph (7820A, Agilent, Palo Alto, CA) equipped with a flame ionization detector and an Innowax column (Agilent). The same gas chromatograph equipped with a thermal conductivity detector and a ShinCarbon ST column (Restek, Bellefonte, PA) was used to analyze biogas composition. Soluble COD and VFA analyses were performed with samples prepared by filtering through a membrane filter (pore size, 0.45-μm). All analyses were performed at least in duplicate. Biogas volume was measured by water displacement and converted to standard temperature and pressure (STP; 0°C and 1 atm).

3-3. Results and discussion

3-3-1. Reactor performances

The three reactors showed visibly different reaction profiles during the 30 days of batch operation. The residual soluble COD (sCOD) concentration decreased rapidly along with an immediate production of hydrogen during the first 2 days of incubation and remained fairly constant around 3.7 g/L until day 12 in all reactors (Fig. 3-1). Afterwards, however, the sCOD removal rates in the reactors diverged substantially, and its removal efficiency on day 30 was 82.5%, 59.3%, and 31.9% in R3, R2, and R1, respectively. Correspondingly, the cumulative methane production during the operation period was highest in R3 (2,529 mL), followed by R2 (1,730 mL) and R1 (577 mL). Such differences in organic removal rates are also reflected in the VFA profiles (Fig. 3-2). The total VFA (tVFA) level accumulated up to about 4 g COD/L during the initial few days in all reactors. Similarly to the sCOD removal patterns, the lowest residual tVFA level (i.e., largest tVFA consumption) after 30 days of operation was observed in R3 (0.8 g COD/L), followed by R2 (1.8 g COD/L) and R3 (3.7 g COD/L). These indicate clearly that the organic removal and methanogenesis rates were significantly higher in R2 and R3 supplemented with ferric oxides than in the control reactor R1. Acetate, propionate, and butyrate were the dominant acidogenic products in all reactors. Complete degradation of both acetate and butyrate was achieved within 30 days in R3. On the other hand, a significant level of acetate remained undegraded in R1 (2.2 g COD/L) and R2 (1.2 g COD/L) on day 30 while butyrate was almost completely removed. Especially in R1, the residual acetate concentration increased gradually with the degradation of butyrate till the end of the reactor operation. One mole of butyrate is broken down syntrophically to two moles of acetate and further converted to CH_4 and CO_2 via methanogenesis [61]. The delayed acetate consumption, particularly in R1, may indicate that aceticlastic methanogenic activity was not high enough to efficiently handle the released acetate in the system. The faster and more effective stabilization of acetate in R2 and R3, on the other hand, may reflect a positive effect of ferric oxides (FeOOH and Fe_3O_4 in R2 and R3, respectively) on aceticlastic methanogenesis. In line with these observations, the cumulative methane production for 30 days was significantly higher in R2 and R3 than in R1 (Fig. 3-1B). Meanwhile, no apparent degradation of propionate was shown in all reactors. This suggests that a 30-day operation period was not sufficient for effective syntrophic propionate oxidation, a highly endergonic ($\Delta G_0' = +76.1$ kJ/mol) process, in the reactors [61]. Because of the thermodynamic hindrance, propionate oxidation occurs after other easily utilizable VFAs are fully consumed in AD processes [62]. The residual propionate concentration on day 30 was considerably higher in R1 (821 mg COD/L) than in R2 (412 mg COD/L) and R3 (549 mg COD/L).

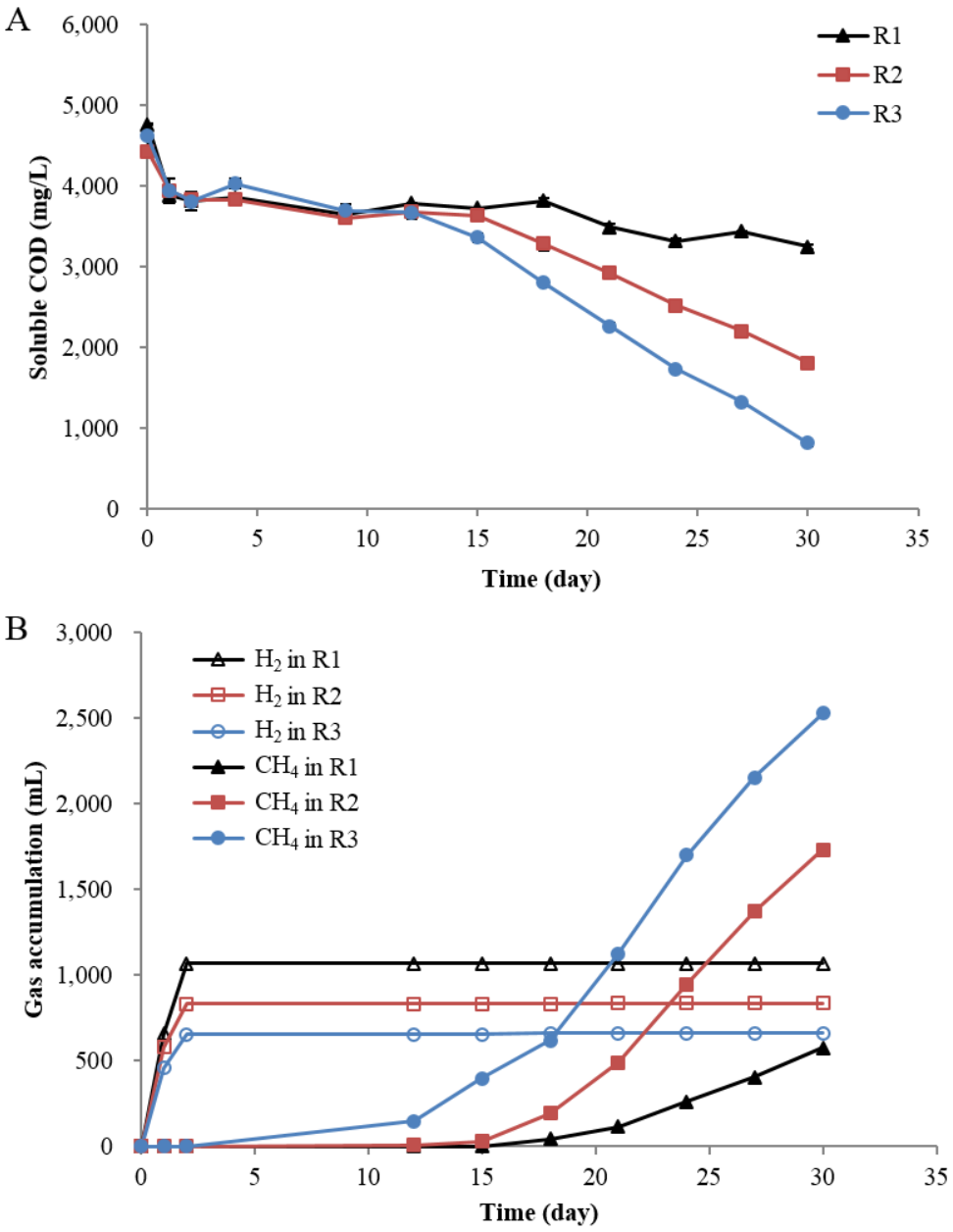

Fig. 3-1. Soluble COD removal (A) and biogas production (B) profiles during the batch operation.

An interesting thing to note is that the cumulative production of hydrogen was highest in R1 (1,068 mL), followed by R2 (835 mL) and R3 (661 mL), which is contrary to the methane production profiles (Fig. 3-1B). This, together with the VFA composition data on day 9 (Fig. 3-3), implies that the reactors varied in acidogenic fermentation pathway likely due to the effect of the ferric oxides added. There are more than one pathways for mixed-culture fermentation of organic matter, particularly when the substrate includes diverse organic compounds like whey used in this study [63]. Figs. 3-2 and 3-3 show the evident differences in acid production profiles between the ferric oxide-supplemented and the control reactors. Although acetate accounted for the

largest portion in all reactors, its proportion to tVFA concentration on day 9 (i.e., the point of maximum tVFA accumulation) differed significantly among the reactors: 37.7% in R1, 50.3% in R2, and 55.1% in R3. Correspondingly, the reactors showed high variations in the propionate/acetate (0.53 in R1, 0.19 in R2, and 0.23 in R3) and the butyrate/acetate (0.91 in R1, 0.64 in R2, and 0.45 in R3) ratios. It is generally known that butyric-type fermentation benefits biohydrogen production and thus the butyrate/acetate ratio correlates positively with hydrogen yield [64, 65]. This accords well with the hydrogen production profiles observed in the reactors tested. Changes in the butyrate/acetate ratio reportedly represent alterations in the metabolic characteristics of reactor microbial communities [66]. The metabolic shifts towards acetic-type fermentation observed in R2 and R3 were supposedly induced by the ferric oxides added. The less production of hydrogen in the ferric oxide-supplemented reactors may also be in part attributed to the iron reduction consuming hydrogen as an electron donor [67, 68].

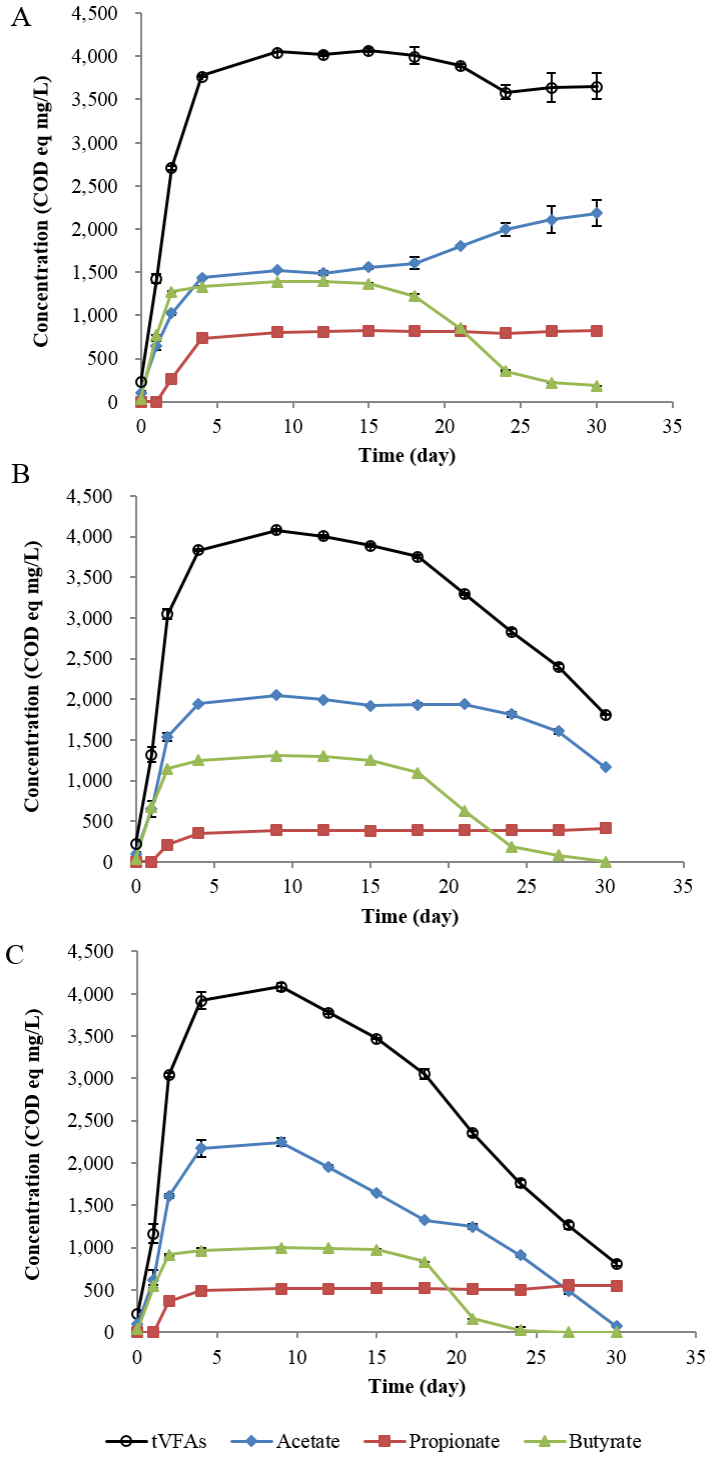

Fig. 3-2. Production and consumption profiles of VFAs in the tested reactors: R1 (A), R2 (B), and R3 (C)

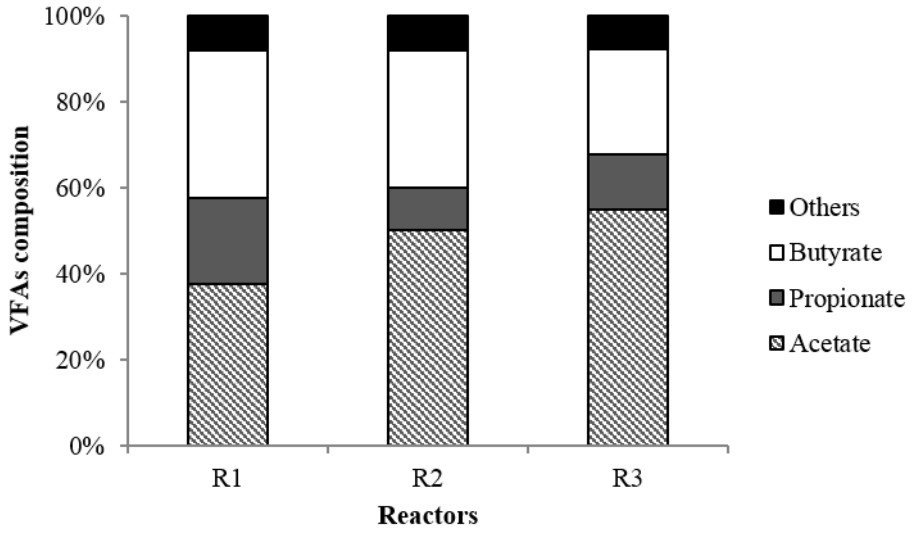

Fig. 3-3. The composition of accumulated VFAs in each reactor on day 9.

Hydrogen production ceased on day 2, before which the biogas was composed mostly of hydrogen (≥90% (v/v)), in all reactors, and methane evolved after different lengths of delays in the reactors (Fig. 3-1B). The 30-day cumulative methane production was high in order of R3, R2, and R1. This could be attributed to the higher production of acetate, along with the lower formation of longer-chain VFAs, during the acidogenesis in the ferric oxide-supplemented reactors (Figs. 3-2 and 3-3). It is well known that acetate is a more favorable substrate than other longer-chain VFAs for methanogenesis, and thus a higher acetate/other VFAs ratio generally leads to a higher methanogenesis rate [61]. The methanogenesis profile was further described by fitting the cumulative methane production data to a modified Gompertz equation (Eq. 3-1) for each reactor as previously described [69].

$$M(t) = P \cdot \exp\left[-\exp\left\{\frac{R_m \cdot e}{P}(\lambda - t) + 1\right\}\right] \qquad (3\text{-}1)$$

where $M(t)$ is the cumulative methane production (mL) at time t, P is the methane production potential (mL), R_m is the maximum methane production rate (mL/d), λ is the lag phase length (day), and t is the incubation time (day). The estimated P and R_m values were much greater in R2 (>2-fold) and R3 (>3-fold) than in R1, while the lag time was estimated to be longer in R1 than in the other reactors (Table 3-2). These, according well with the reaction profiles observed, suggest again that the ferric oxide addition had a positive effect on the reactor performance in both terms of methanogenesis rate and yield. The total energy production as hydrogen plus methane during the experimental period, calculated based on the net heating value, was 32.2,

71.0, and 97.7 kJ (at STP) in R1, R2, and R3, respectively. This is due to the greater methane production in the ferric oxide-supplemented reactors and the higher heating value of methane (35.8 kJ/L) than of hydrogen (10.8 kJ/L). COD recovery as biogas was also examined in each reactor by balancing the sum of COD equivalents of hydrogen and methane produced against the substrate COD removed. Interestingly, COD recovery was nearly 100% in both R2 and R3 while a significantly lower value of 79% was obtained in R1. This implies that the production of hydrogen and methane served as the absolutely dominant electron sink in R2 and R3 while a substantial fraction was used for other metabolic functions in R1. This is another indication of changes in reactor metabolic functions likely induced by the addition of ferric oxides.

Table 3-2. Modified Gompertz parameters estimated for the reactors tested

Parameter	Unit	R1	R2	R3
Maximum methane potential (P)	mL	1,139.3	2,490.4	3,944.6
Methane production rate (R_m)	mL/d	150.2	409.5	455.8
Lag phase (λ)	day	19.5	17.8	14.1

3-3-2. DGGE analysis and phylogenetic affiliation

DGGE and further phylogenetic analysis were performed to characterize the archaeal and bacterial community structures in the reactors tested. The seed sludge and the reactor samples on days 1, 12, and 30 were examined to monitor the shifts in community structures during the 30-day operation period (Fig. 3-4). Two archaeal (WA1 to 2) and twelve bacterial (WB1 to 12) bands were excised from the DGGE gels and sequenced for phylogenetic affiliation (Table 3-3). Both the archaeal sequences were closely related (≥97% sequence similarity) to a well-known methanogen species while two out of twelve bacterial were not. WA1 and 2 were both closely related to *Methanosaeta concilii* and detected in all lanes as the prevailing methanogen bands, indicating that the aceticlastic pathway was probably the main route for methanogenesis in all reactors. These bands appeared with significantly higher band intensity, although not robustly quantitative, in the 30-day samples of R2 and R3. This corresponds to the general knowledge that *Methanosaeta* species often dominate methanogen communities in stabilized AD systems with low levels of residual VFAs [61]. Ten out of twelve bacterial sequences were assigned to known bacterial species across three phyla, *Firmicutes* (WB1, 2, 4, 8, 10, and 12), *Proteobacteria* (WB6 and 9), and *Bacteroidetes* (WB3). The remaining two were classifiable only at the order (WB5) and the genus (WB11) level, respectively, but both affiliated with the phylum *Firmicutes*. Six *Firmicutes* sequences (WB1, 2, 4, 8, 10, and 11) were assigned to the obligatory anaerobic genus *Clostridium* of which members are frequently found in abundance in anaerobic fermentation processes. *Clostridium* species are metabolically very versatile and capable of utilizing a wide range of organic

substances to produce different organic acids and hydrogen [70]. The *Clostridium*-related bands showed up from the early period, where acidogenesis with hydrogen production actively occurred, in all reactors. Most of the *Clostridium* sequences were affiliated with saccharolytic species, and the *Clostridium* populations in the reactors were likely responsible for the rapid fermentation of carbohydrate (mainly lactose) during the initial operation period. WB3 showed a high sequence similarity of 99.1% to *Macellibacteroides fermentans* and *Parabacteroides chartae* both of which can ferment carbohydrates, including lactose, into diverse organic acids [71, 72]. Differentiating between *M. fermentans* and *P. chartae* strains based on the 16S rRNA gene sequence information is often difficult due to their high sequence similarity. For example, their type strains share a 16S rRNA gene sequence similarity of 99.7% [73]. WB3 was meanwhile assigned to the genus *Parabacteroides* by the RDP classifier at a confidence threshold of 80%. WB6, 7, and 9 were all affiliated with the genus *Acinetobacter* originally known to be aerobic. The presence of *Acinetobacter* has, however, been extensively reported in anaerobic or oxygen-limited environments [74-77], and the *Acinetobacter*-related populations in the reactors supposedly played a functional role in the AD reactions. WB12 was affiliated with a fermentative genus *Trichococcus* which utilizes various sugars and polysaccharides [78]. The metal-reducing capability of *T. pasteurii* under anoxic/anaerobic conditions has recently been suggested. Abundant growth of *T. pasteurii* was reported with the microbial U(VI) and Fe(III) reduction in trench slurry [79] and the Cr(VI) reduction in the cathode biofilm of a microbial fuel cell [80]. Accordingly, considering the prominent occurrence of WB12 in R2 and R3, the corresponding *Trichococcus*-related population was suggested to be electroactive and directly involved in the functioning of the ferric oxides. WB5, the only band not affiliated to a known genus, was classified to the order *Clostridiales*, indicating that the corresponding population to this band probably took part in the fermentation of substrate organics.

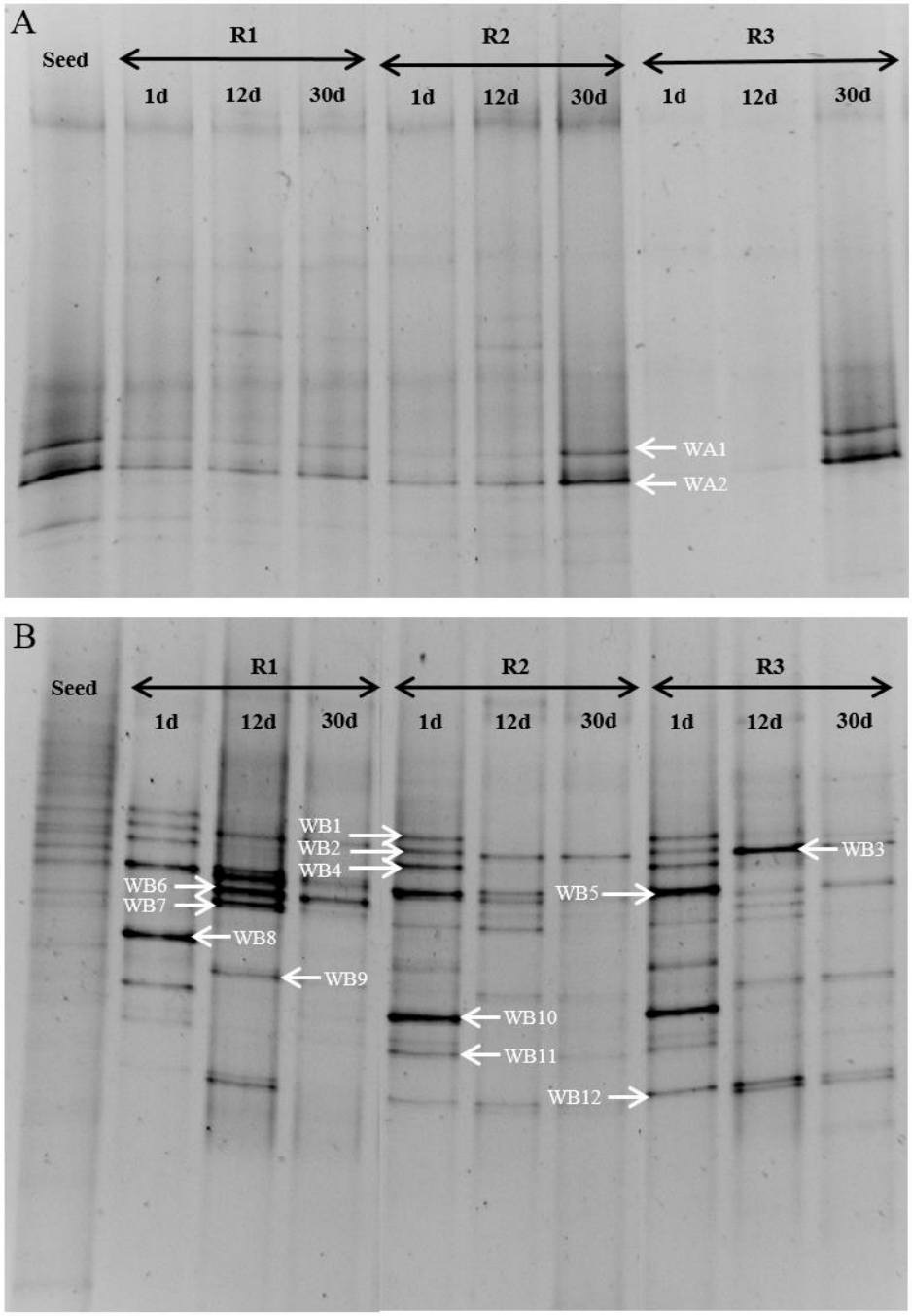

Fig. 3-4. Archaeal and bacterial 16S rRNA gene DGGE profiles analyzed from reactor samples (labeled with the time of sampling in days) and anaerobic seed sludge (labeled as seed).

Table 3-3. Phylogenetic affiliation of archaeal and bacterial 16S rRNA gene sequences retrieved from DGGE bands

Band	Closest relative	Accession number	Similarity (%)	Classification[a]
Archaea				
WA1	*Methanosaeta concilii*	NR102903	100	Genus *Methanosaeta*
WA2	*Methanosaeta concilii*	NR102903	99.6	Genus *Methanosaeta*
Bacteria				
WB1	*Clostridium butyricum*	KF611983	99.1	Genus *Clostridium*
	Clostridium saccharobutylicum	GU060306	98.6	
WB2	*Clostridium sartagoforme*	KF611989	99.1	Genus *Clostridium*
	Clostridium tertium	JX267105	98.9	
WB3	*Parabacteroides chartae*	NR109439	99.1	Genus *Parabacteroides*
	Macellibacteroides fermentans	HQ020488	99.1	
WB4	*Clostridium beijerinckii*	KF746386	99.8	Genus *Clostridium*
	Clostridium saccharobutylicum	CP006721	99.8	
	Clostridium butyricum	AB647330	99.8	
WB5	Bacterium enrichment culture clone HY35	JX473590	98.4	Order *Clostridiales*
	Uncultured bacterium clone FB1_6A	JX296075	97.0	
WB6	*Acinetobacter junii*	JF915345	99.4	Genus *Acinetobacter*
	Acinetobacter seohaensis	DQ518593	98.7	
WB7	*Acinetobacter junii*	JF915345	99.8	Genus *Acinetobacter*

	Acinetobacter seohaensis	DQ518593	99.1	
WB8	*Clostridium quinii*	NR026149	99.3	Genus *Clostridium*
	Clostridium cellulovorans	KF528156	98.9	
WB9	*Acinetobacter seohaensis*	NR115299	99.8	Genus *Acinetobacter*
	Acinetobacter sp. SAL_13	FJ482069	99.6	
WB10	*Clostridium chauvoei*	KF372578	100	Genus *Clostridium*
	Clostridium sp. T28_4	JQ739656	100	
	Clostridium tertium	JX267105	100	
WB11	Uncultured bacterium clone GAH72_115	JQ640370	100	Genus *Clostridium*
	Uncultured microorganism clone YLB20	KC841524	100	
WB12	*Trichococcus pasteurii*	KF387711	100	Genus *Trichococcus*
	Trichococcus flocculiformis	NR042060	100	
	Trichococcus collinsii	EF111215	100	

[a] The lowest rank assigned by RDP Classifier at a 80% confidence threshold.

3-3-3. Microbial community structure

Although the intensity of *Methanosaeta*-related bands (WA1 and 2) varied with time and among the reactors, no marked differences or changes in the archaeal band patterns (Sorensen distance (D_S) < 0.15) were observed (Fig. 3-4). In contrast, the bacterial DGGE patterns showed clear variations over time and among the reactors (D_S < 0.55). These mean that the magnitude of changes in community structure was significantly greater for bacteria (i.e., acidogens) than for archaea (i.e., methanogens) and that the changes in bacterial community structure affected little the evolution of methanogen community structure in the reactors. This could be ascribed to the much less diverse and dynamic characteristics of methanogens than of acidogens in AD environments largely due to the limited substrate spectrum of methanogens [81, 82]. The cluster dendrogram shown in Fig. 3-5A illustrates the relationships between the bacterial community structures analyzed. The bacterial community structures of three reactors grew apart with the progress of batch digestion, with the R1 community being remotely located from those of R2 and R3 on day 30. This, together with the acid production profiles (Figs. 3-2 and 3-3), further supports that the metabolic pathways of the reactor microbial communities were changed by the influence of the ferric oxides added in R2 (FeOOH) and R3 (Fe_3O_4). Changes in microbial community structure lead to changes in metabolic functioning in a bioreactor as the functional attributes of a biological process depend on the activity of the microbes working in the system [83]. The direction and magnitude of the temporal variations in bacterial community structure in each reactor were visualized by NMS analysis (Fig. 3-5B). The first two ordination axes accounted for 71.0% (r^2 = 0.710) and 18.1% (r^2 = 0.181) of the total variance in the analyzed community structure data, respectively, and thus 89.1% (cumulative r^2 = 0.891) of the variability in the data can be explained by the two-dimensional plot. The final stress (<5) and instability (<10^{-4}) of the solution were sufficiently low to provide a reliable NMS solution [57]. As in the cluster analysis, the community profiles of three reactors were closely clustered initially but gradually became more distantly related as the reaction proceeded. The seed bacterial community structure was located in the down-right corner of the NMS plot and shifted with time in all reactors towards the upper-left region of the plot. The bacterial communities in the control and the ferric oxide-supplemented reactors evolved in visibly different directions after day 12, and the community profile of the control reactor was distantly located from those of R2 and R3 at the conclusion of the batch test. Correspondingly, WB12 retrieved from a putative metal-reducing bacterium likely engaged in the utilization of the ferric oxides added was detected in R2 and R3 only. The NMS results linked with the reactor performance data suggest that the ferric oxides induced the bacterial communities in R2 and R3 to develop and function differently from that in R1.

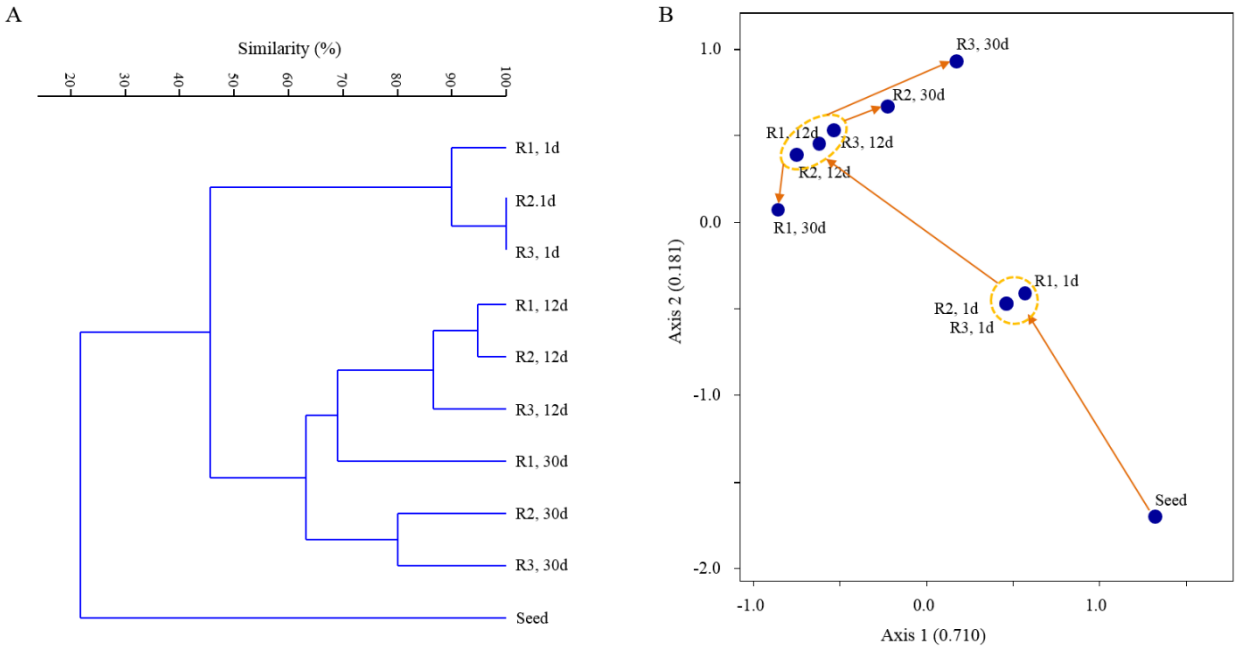

Fig. 3-5. Cluster dendrogram (A) and NMS plot (B) illustrating the relationships between the bacterial community structures analyzed over the experimental period. Each data point was labeled with the reactor name and time of sampling in days. Arrows indicate the time-course community structure shifts in each reactor.

3-3-4. Microbial quantification

Real-time PCR analysis revealed that both *Methanosaeta* and *Trichococcus* were present in all reactors with a 16S rRNA concentration of $>10^6$ copies/mL during the operation period (Fig. 3-6). All reactors showed a continuous increase in the *Methanosaeta* level over time. This increase was much more pronounced in the ferric oxide-supplemented reactors, particularly in R3 with magnetite. On day 30, the *Methanosaeta* 16S rRNA gene concentrations in R2 and R3 were 5.1- and 16.4-fold higher than that in R1, which seems to reflect the more stabilized AD environment in R3 [61]. The *Trichococcus* 16S rRNA gene concentration was also visibly higher in the ferric oxide-supplemented reactors compared to that in R1. Its abundance after 30 days of batch incubation was 2.9- and 10.4-fold higher in R2 and R3, respectively, than in R1 while decreasing with the stabilization of organic matter over incubation time (Figs. 3-1 and 3-2). These suggest that the supplementation with (semi)conductive ferric oxides likely formed a favorable environment for *Methanosaeta* and *Trichococcus* to flourish in the AD systems.

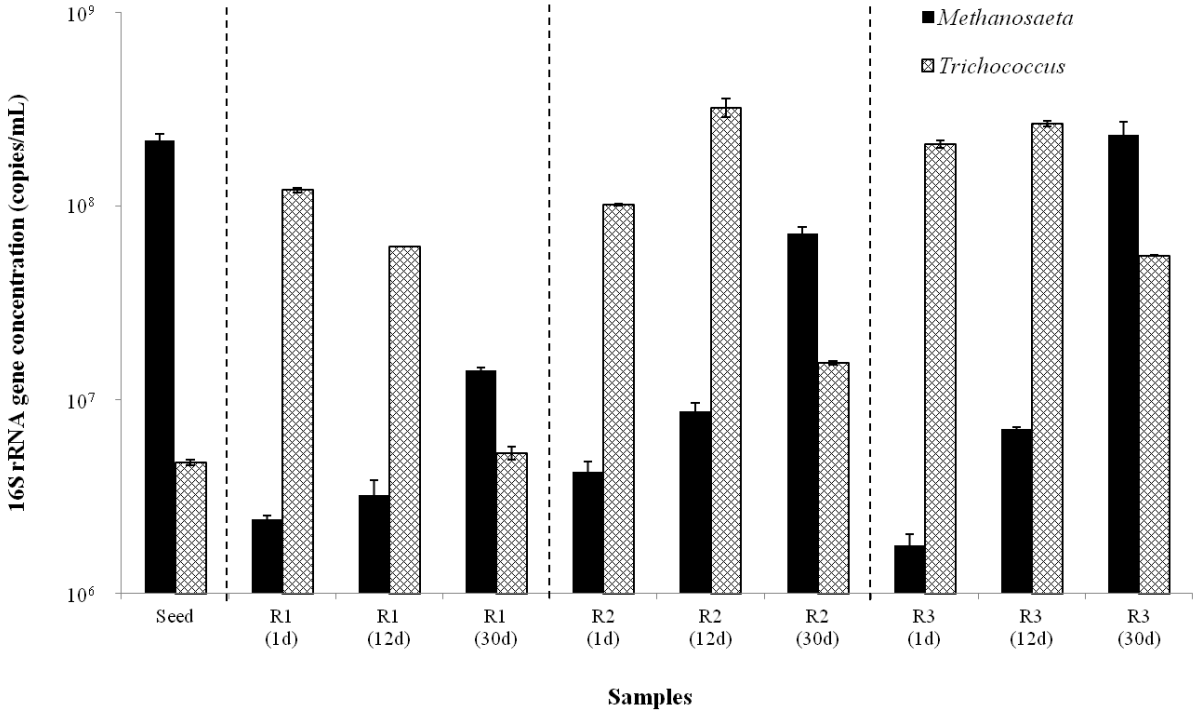

Fig. 3-6. The 16S rRNA gene concentrations of *Methanosaeta* and *Trichococcus* determined by real-time PCR. The time of sampling in days is indicated in parentheses.

3-4. Discussion

Our overall experimental data demonstrated that the addition of ferric oxyhydroxide (R2) and magnetite (R3) significantly enhanced the AD performance, in terms of energy recovery as well as organic removal, over the control reactor (R1). This implies that the biostimulation with the (semi)conductive ferric oxides was beneficial for high-rate AD. An interesting point is that the performance enhancement was more pronounced in R3 than in R2, suggesting that the conductivity of the ferric oxides added potentially influenced the performance variations among the reactors. Kato et al. [41] have recently reported that methanogenesis rate was improved by adding (semi)conductive ferric oxides (i.e., hematite and magnetite) in enrichment cultures of a rice paddy soil microcosm using synthetic media with acetate or ethanol as sole substrate. On the other hand, no positive effect was recorded with insulative ferrihydrite for both carbon sources. Limited solubilization of Fe(III) to Fe(II) was observed in the cultures supplemented with ferric oxides, and therefore the authors attributed the accelerated methanogenesis mainly to the electric syntrophy rather than the nutritional effects or electron shuttling of soluble iron. They also revealed that H_2-mediated syntrophy did not work in the ferric oxide-supplemented cultures and suggested that the syntrophy between electroactive bacteria (i.e., *Geobacter*) and methanogens (i.e., *Methanosarcina*) mediated by direct electron flow through the ferric

oxide particles supposedly led to enhanced methanogenesis. Similarly, more recent studies reported an accelerated methanogenesis from propionate by magnetite addition under mesophilic [47] and thermophilic [49] conditions. Such observations correspond well with the results from our reactors fed with whey, a real wastewater containing various organic matters, except that neither *Geobacter*- nor *Methanosarcina*-related sequence was found in our DGGE analysis. *Methanosaeta* strains, the dominant methanogens in our reactors, have been thought to be able to grow exclusively on acetate and not to directly utilize electrons as electron donor for methane generation, whereas *Methanosarcina* and several hydrogenotrophic methanogens have been suggested to have the ability to directly accept electrons from conductive materials [84-86]. However, a recent study on the genome sequence of *Methanosaeta* revealed the existence of a complete set of genes required for the reduction of carbon dioxide to methane [87]. Additionally, more recent metagenomic and metatranscriptomic investigations on the anaerobic granules in an upflow anaerobic sludge blanket reactor treating synthetic brewery wastewater showed the dominance of *M. concilii* with high expression of the genes for CO_2 reduction to CH_4 [27, 88]. These imply the potential of *Methanosaeta* to directly accept electrons and participate in the electric syntrophy given that they cannot utilize H_2 or formate as an electron donor to reduce CO_2 [41]. In our experiment, accordingly, an electric syntrophy between *M. concilii*-related methanogens (WA1 and 2) and electroactive bacteria, particularly a *Trichococcus*-related population corresponding to WB12, was suggested to be formed in the ferric oxide-supplemented reactors (Fig. 3-4 and Table 3-3). Supportively, real-time PCR analysis showed that both *Methanosaeta* and *Trichococcus* occurred in markedly higher abundance in R2 and R3 than in R1 (Fig. 3-6). This implies that the growth of putative electric-syntrophy partners was stimulated by the (semi)conductive ferric oxides added. Interestingly, the *Trichococcus* 16S rRNA gene concentration was 3.6- and 10.4-fold greater in R3 than in R2 and R1, respectively, on day 30 despite the residual level of utilizable organics was lowest in R3 (Figs. 3-1 and 3-2). The high abundance of *Trichococcus* in R3 may have been formed by the enhanced electric syntrophy owing to the conductive nature of magnetite. The different rates of methanogenesis in R2 and R3 may be attributed to the difference in conductivity between semiconductive ferric oxyhydroxide and conductive magnetite. Such differences in chemical and microbial properties were well reflected by the gradual divergence between the bacterial community structures of R2 and R3 with the progress of batch culture (Fig. 3-5).

IRBs are capable of oxidizing poorly biodegradable organic compounds such as aromatic hydrocarbons [89]. Enhanced degradation of refractory organics through ferric reduction may therefore also lead to an increase in methanogenesis rate. A recent work on the AD of waste activated sludge reported an increase in methane production by ferric oxyhydroxide addition concurrent with a significant increase (2.3-fold) in the soluble Fe(II) concentration [75]. This indicates that at least some of the ferric oxide particles added were reduced and consumed as final electron acceptor (i.e., iron reduction) rather than used as conduits for electron transfer (i.e. electric syntrophy). Not like sewage sludge, however, whey used as the substrate for our batch reactors is readily biodegradable and has little refractory organics. In such a case, active iron reduction can

negatively affect methanogenesis because IRBs and methanogens compete for acetate [90], and a system dominated by slow-growing *Methanosaeta* like our experimental reactors is known to be more sensitive to the competition. However, acetate consumption was much faster and more effective in R2 and R3 than in R1, implying that the ferric oxides rather benefited aceticlastic methanogens (Figs. 3-1 and 3-2). Therefore, the accelerated methanogenesis in the ferric oxide-supplemented reactors was more likely attributed to the electric syntrophy mediated by (semi)conductive ferric oxides between methanogens and electroactive bacteria. Supportively, a recent study revealed that magnetite facilitates extracellular electron transfer in a similar manner to *c*-type cytochromes and further demonstrated the compensation of the deficiency of the functions of a *c*-type cytochrome (OmcS) by magnetite [91].

Another point to consider is the fact that several *Clostridium* species are capable of using Fe(III) as a minor electron acceptor (<5% of the reducing equivalent) for fermentative growth [92]. Although these bacteria do not conserve energy from ferric reduction, thermodynamic estimations proved that fermentation coupled with ferric reduction is energetically more favorable than without it [93]. This implies that the growth of fermentative iron reducers can potentially be stimulated by providing ferric iron. It is therefore interesting to observe that WB10, a DGGE band assigned to *Clostridium*, showed up with substantially greater intensity in R2 and R3 than in R1 during the active acidogenesis period (Figs. 3-2 and 3-4B). In addition, a previous study actually reported the increase in cellular activity of *Clostridium chauvoei*, which WB10 was most closely related to, by the addition of ferric salts [94]. These suggest that the *Clostridium*-related population corresponding to WB10 was likely a fermentative iron reducer and stimulated to active growth in R2 and R3. Given that both *C. chauvoei* and *Clostridium tertium* (Table 3-3) are able to ferment lactose and produce acetate followed by butyrate generally as the major fermentation products [78], this stimulated growth may have contributed to the alteration in the composition of VFAs produced (i.e., higher proportion of acetate) in the reactors (Figs. 3-2 and 3-3). Such a shift in metabolic characteristics towards more acetic-type fermentation seems to be beneficial to methanogenesis (Fig. 3-1). Biostimulation of fermentative iron reducers and its influence on methanogenesis have been little explored, and this interesting potential deserves further study.

3-5. Summary

Our overall experimental data demonstrated that the addition of ferric oxyhydroxide (R2) and magnetite (R3) significantly enhanced the AD performance in terms of energy recovery as well as organic removal over the control reactor (R1). This implies that biostimulation with the (semi)conductive ferric oxides was beneficial for high-rate AD. An interesting point is that the performance enhancement was more pronounced in R3 than in R2, suggesting that the conductivity of the iron oxides potentially influenced the performance variations among the reactors. The potential electric syntrophy formed between *Methanosaeta concilii*-like methanogens

and electroactive iron-reducing bacteria, particularly *Trichococcus*, was likely responsible for the enhanced performance.

4. (STUDY 2) LONG-TERM STUDY ON THE EFFECT OF MAGNETITE SUPPLEMENTATION IN CONTINUOUS MODE: ENHANCEMENT OF PROCESS PERFORMANCE AND STABILITY

4-1. Introduction

Previous findings suggest that DIET can provide an interesting possibility to improve the energy balance and economic feasibility of an anaerobic digester. The influence of stimulated DIET may be more complicated in mixed-culture systems with complex microbial communities, which would have greater chances of containing more microbes potentially involved in electric syntrophy than defined co-culture communities. Most previous studies have investigated DIET in methanogenic communities using synthetic media containing ethanol or organic acids under co-culture conditions. A study of study 1 demonstrated the positive effect of conductive iron oxides, particularly magnetite, on the biomethanation of real waste-product of cheese production, in a batch mode [95]. However, little has been learned regarding the long-term influence of magnetite supplementation in a continuous AD process treating real waste stream.

To address this gap, the study in study 2 seeks to monitor and compare the performance of continuous anaerobic digesters with and without the addition of magnetite over a period of one year. The primary focus of this study is whether magnetite supplementation facilitates methanogenesis and helps avoid process imbalance in continuous culture and whether its effect is maintained for a long period. The outcomes of this study can help improve our understanding of the complex syntrophic relations involved in AD and open new possibilities for high-rate biomethanation.

4-2. Materials and methods

4-2-1. Bioreactor operation

Two anaerobic continuously stirred tank reactors (CSTRs) with a working volume of 2 L (total volume, 2.4 L), namely RC and RM, were operated with cheese whey as substrate for 376 days. Each reactor was initially filled with equal volumes of whey (diluted to 5 g/L as soluble COD) and anaerobic sludge from a biogas plant treating sewage sludge (seeding ratio, 50% [v/v]). The physicochemical characteristics of the seed sludge and the whey substrate are shown in Table 4-1. The soluble-to-total COD ratio of the whey substrate was as high as 94.7% whereas the volatile-to-total-solids ratio was 89.2%. This result indicates that the whey substrate is highly organic and that the majority of the organic matter involved is soluble. Whey was selected as the substrate because it contains the majority of the essential nutrients for microbial growth and has been widely treated anaerobically with no additives. The reactors were run in batch mode during the first 5 days for start-

up and then switched to continuous mode with daily feeding. RM was supplemented with magnetite (particle size, 100–700 nm; Fig. 4-1) through the substrate to achieve a final Fe concentration of 20 mM; RC was not amended and served as a control. The experimental period was divided into six and four phases for RC (PC1 to 6) and RM (PM1 to 4), respectively, according to the operating conditions. The time period and operating conditions for each phase are presented in Table 4-2. Both reactors were maintained at approximately pH 7.0 and 35 ± 2˚C throughout the experiment with automatic pH and temperature control units. The reactors were continuously agitated by bottom stirring for complete mixing of the mixed liquor.

Table 4-1. Physicochemical characteristics of inoculum and substrate

Parameter	Unit	Anaerobic sludge	Cheese whey
Total COD	mg/L	13,356 (84)[a]	5,114 (9)
Soluble COD	mg/L	620 (47)	4,845 (37)
Total solids	mg/L	17,000 (236)	5,550 (71)
Total volatile solids	mg/L	10,167 (236)	4,950 (71)
Total suspended solids	mg/L	14,500 (236)	250 (71)
Volatile suspended solids	mg/L	9,333 (0)	100 (0)
C	%	–[b]	35.3 (0.3)
H	%	–	7.3 (0.1)
O	%	–	45.8 (0.5)
N	%	–	1.5 (0)
S	%	–	0.2 (0)

[a] Standard deviations are in parentheses.

[b] Not measured.

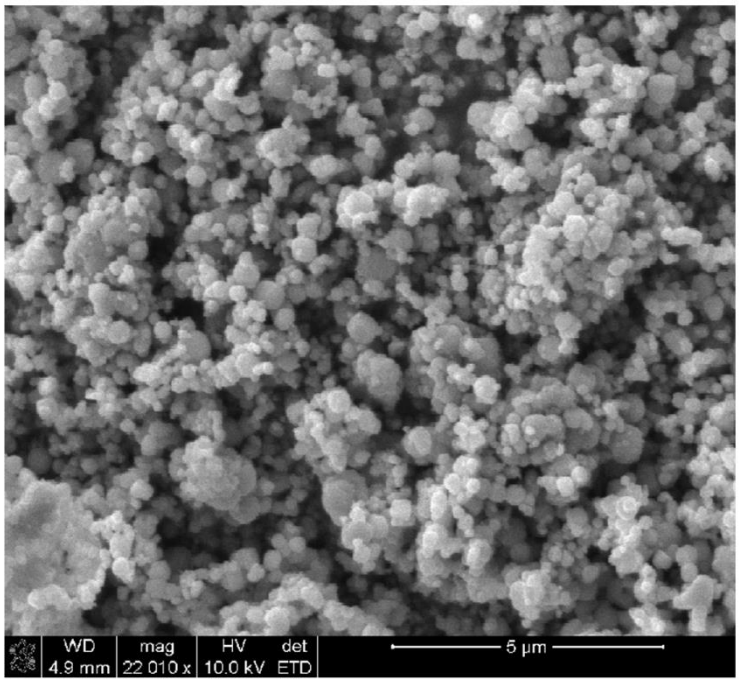

Fig. 4-1. Scanning electron microscopy image of magnetite particles

4-2-2. Real-time PCR

The experimental procedures for DNA extraction and DGGE analysis are same with the methods shown in study 1. The nucleotide sequences obtained in this study have been deposited in the GenBank database under accession numbers KX255698-KX255716. For real-time PCR, two order-specific primers/probe sets, MBT-set for *Methanobacteriales* and MMB-set for *Methanomicrobiales*, and two family-specific primers/probe sets, Msc-set for *Methanosarcinaceae* and Mst-set for *Methanosaetaceae*, were used to amplify their target methanogen sequences [54]. A reaction mixture (20 μL) was prepared using the THUNDERBIRD Probe qPCR mix (Toyobo, Japan): 10 μL of the premix, 2 μL of the TaqMan probe (final concentration, 200 nM), 1 μL of each primer (final concentration, 500 nM), 4 μL of PCR-grade water, and 2 μL of template DNA. The same two-step thermal cycling procedure as for DGGE was employed for real-time PCR amplification. A standard curve was generated for each primers/probe set using an equimolar mixture of the standard templates as previously described [59]. The copy concentration of each target sequence in an unknown sample was determined from the corresponding standard curve. All samples were analyzed in duplicate.

4-2-3. Statistical analysis of community structure data

The archaeal and bacterial DGGE gel images were each converted to an intensity matrix based on the relative contribution of individual bands to the total band intensity (i.e., the sum of the intensities of all bands) in each

lane. Band detection and intensity measurement were performed using TotalLab 1D image-processing software (TotalLab, UK). Cluster analysis with the unweighted pair group method with arithmetic means (UPGMA) algorithm and nonmetric multidimensional scaling (NMS) were conducted on the obtained matrices to describe the variations in the microbial community structure of each reactor during the experiment. Clustering and NMS ordination were performed based on the Sorensen distance measure, the most recommended measure for ecological community data [96], using PAST 3.03 and PC-ORD 5 (MjM software, USA), respectively. In an NMS plot, the axes were scaled in proportion to the longest axis (%Max scaling) as recommended by the software to accurately illustrate the similarity relations among the analyzed community profiles.

4-2-4. Scanning electron microscopy

Mixed liquor was taken from each reactor on days 181 and 272 and analyzed by SEM and energy-dispersive X-ray spectroscopy (EDX) to characterize the surface morphology of the digestates. Mixed liquor (20 mL) was centrifuged at 1,900 *g* for 10 min, followed by washing three times with 0.1 M phosphate buffer (pH 7.4). Then, the pellets were fixed in 0.1 M phosphate buffer (pH 7.4) containing 2.5% glutaraldehyde for 4 h at 4˚C. The fixed pellets were washed another three times with 0.1 M phosphate buffer (pH 7.4), followed by serial ethanol dehydration (50%, 70%, 90% and 100%) for 15 min at each step and air drying. The prepared specimens were mounted on SEM stubs using carbon tape, sputter-coated with platinum, and analyzed using a field-emission SEM system (NanoSEM 230, FEI, USA) equipped with an EDX spectrometer.

4-2-5. Analytical methods

Cation concentrations, including ammonium, were determined using an ion chromatograph (Dionex ICS-1100, Thermo Scientific, USA) equipped with a Dionex Ionpac CS12A column (Thermo Scientific, USA). A 20-mM methanesulfonic acid solution was used as the eluent. Samples for measuring sCOD, VFAs, and ions were filtered through a 0.45-μm membrane filter prior to analysis. The contents of C, H, O, N, and S were determined on a dry weight basis using an organic elemental analyzer (Flash 2000, Thermo Scientific, The Netherlands). XRD analysis was performed using a D/MAX2500 diffractometer (RIGAKU, Japan) installed with an ultra 18 kW Cu-rotating anode source. All analyses were performed at least in duplicate. Biogas volume was measured by water displacement and corrected to standard temperature and pressure (STP; 0˚C and 1 bar).

Table 4-2. Reactor operating conditions and performance data during experimental phases

	RC						RM			
Phase	PC1	PC2	PC3	PC4	PC5	PC6	PM1	PM2	PM3	PM4
Period (day)	6–71	72–111	112–145	146–181	182–218	219–376	6–71	72–111	112–119	120–376
HRT (day)	25	20	B[a]	20	B	20	25	20	B	20
Magnetite addition	No	No	No	No	Yes	Yes	Yes	Yes	Yes	Yes
MPR (mL/d)[b]	102.4	58.8	–[c]	43.7	–	133.4	89.4	72.2	–	127.4
CH_4 content (%)	76.8	84.7	–	77.5	–	66.5	78.0	81.0	–	64.5
SCOD removal (%)	99.0	71.9	–	67.3	–	99.3	98.8	80.8	–	99.3
Y_M (L/g CODr)[d]	0.267	0.169	–	0.128	–	0.277	0.233	0.185	–	0.265

[a] B, batch operation with interrupted feeding.

[b] MPR, methane production rate.

[c] Not applicable.

[d] Y_M, methane yield.

4-3. Results and discussion

4-3-1. Effects of magnetite supplementation

Fig. 4-2 shows the changes in the residual concentrations of sCOD and VFAs in RC and RM. In both reactors, sCOD was rapidly reduced by over 70% during the 5 days of batch start-up and then further stabilized to below 100 mg/L (>98% sCOD removal) during the continuous operation at an HRT of 25 days (i.e., PC1 and PM1). Because the reactors showed comparable performances in terms of substrate removal and methane production, the HRT was reduced to 20 days to increase the hydraulic stress (i.e., PC2 and PM2; Table 4-2). An immediate accumulation of sCOD, mostly propionic acid, in addition to a drastic decrease in methane production was observed with the reduction in HRT in both reactors. Accumulation of VFAs, particularly propionic acid, is a signal of imbalance between acidogenesis and methanogenesis, which may result in system failure. Both reactors showed an extremely high propionic to acetic acid ratio of approximately 9 on day 107, which indicates that the process is severely imbalanced (propionic to acetic acid ratio > 1.4; [97]. This process deterioration was attributed to the limitation of the nitrogen source; the residual NH_4^+-N concentration on day 80 was below 1 mg/L. The reactors were fed with the substrate amended with 100 mg NH_4Cl/L (26 mg NH_4^+-N/L) from day 84. However, the residual VFA level continued to increase in both reactors although the accumulation rate was apparently lower in RM. The amended concentration of NH_4Cl was doubled (52 mg NH_4^+-N/L) from day 104. The accumulation of sCOD continued in RC (1,569 mg/L on day 107) but ceased in RM (915 mg/L on day 107). Both reactors were subjected to interrupted feeding for restoration from day 112. The sCOD concentration in RM dropped to below 100 mg/L in a week (i.e., PM3), and continuous feeding was resumed on day 119 and continued to the conclusion of the experiment (i.e., PM4). Although the sCOD was maintained at a somewhat higher level during early PM4 (250–350 mg/L) compared with the steady-state level in PM1, the sCOD decreased gradually to below 100 mg/L after increasing the amended concentration of NH_4Cl to 400 mg/L (105 mg NH_4^+-N/L) from day 161. However, it took 34 days for RC to be stabilized (<100 mg sCOD/L) with interrupted feeding (i.e., PC3). The sCOD in RC accumulated rapidly after resuming continuous feeding on day 146 to reach >2,000 mg/L on day 181 (i.e., PC4) despite the increase in NH_4Cl amendment to 400 mg/L from day 161. The residual NH_4^+-N concentration was maintained at 50–100 mg/L after day 161 whereas the concentration was below 25 mg/L before then in both reactors (data not shown). It has been noted that the NH_4^+-N concentration in the reactor must exceed 40–70 mg/L to prevent a reduction in methanogenic activity [98]. Therefore, the different responses of RC and RM to the changes in operating conditions (i.e., PC2 to 4 and PM2 to 4), particularly after day 161, were attributable to the influence of magnetite supplemented to RM only.

Notably, acetic and propionic acids accumulated simultaneously during the build-up of VFAs in PC4 and accounted for 45.2% and 48.4% of the residual sCOD, respectively, on day 181, which contrasts with the

observation that the sCOD accumulation in PC2 was caused primarily by propionic acid (89.4% on day 107). This observation indicates that not only syntrophic propionate oxidation but also aceticlastic methanogenesis activities were limited during PC4. Meanwhile, RM experienced no process imbalance after being restored by interrupted feeding during PM3 and performed fairly stably until the end of the experiment. These results suggest that magnetite had a beneficial effect in stabilizing VFAs and thus producing biogas (Table 4-2). Supportively, some previous studies have demonstrated that (syntrophic) degradation of VFAs was facilitated by DIET via magnetite particles in different methanogenic cultures [41, 47, 48]. RC was subjected to another round of interrupted feeding from day 182 (i.e., PC5), but this time with the same dose of magnetite supplementation as for RM (20 mM Fe), to confirm the effect of magnetite on biomethanation. The accumulated VFAs were completely degraded after 37 days of batch cultivation, and the sCOD degradation rate during PC5 (57.4 mg/L·d) was significantly higher than the rate during PC3 (48.1 mg/L·d). After resuming continuous feeding from day 219 (i.e., PC6), the residual sCOD increased to 726 mg/L in 25 days and then gradually decreased over the next 2.5 months to below 100 mg/L. Notably, acetic acid was the major component accumulated (up to 92.1% of the residual sCOD) whereas the propionic acid level remained fairly low ($\leq$120 mg/L) during this period. This result may be because of the enhancement of syntrophic propionate oxidation by magnetite-mediated DIET [47]. Another possibility is that the reactor metabolic characteristics shifted in the presence of magnetite toward more acetic-type fermentation rather than the propionic-type [95]. Both cases are beneficial to stable methanogenesis given that anaerobic degradation of propionic acid is thermodynamically quite unfavorable ($\Delta G^{\circ\prime} = +76.1$ kJ/mol) and occurs only when a well-balanced syntrophy between hydrogen-producing propionate oxidizers and hydrogen consumers exists.

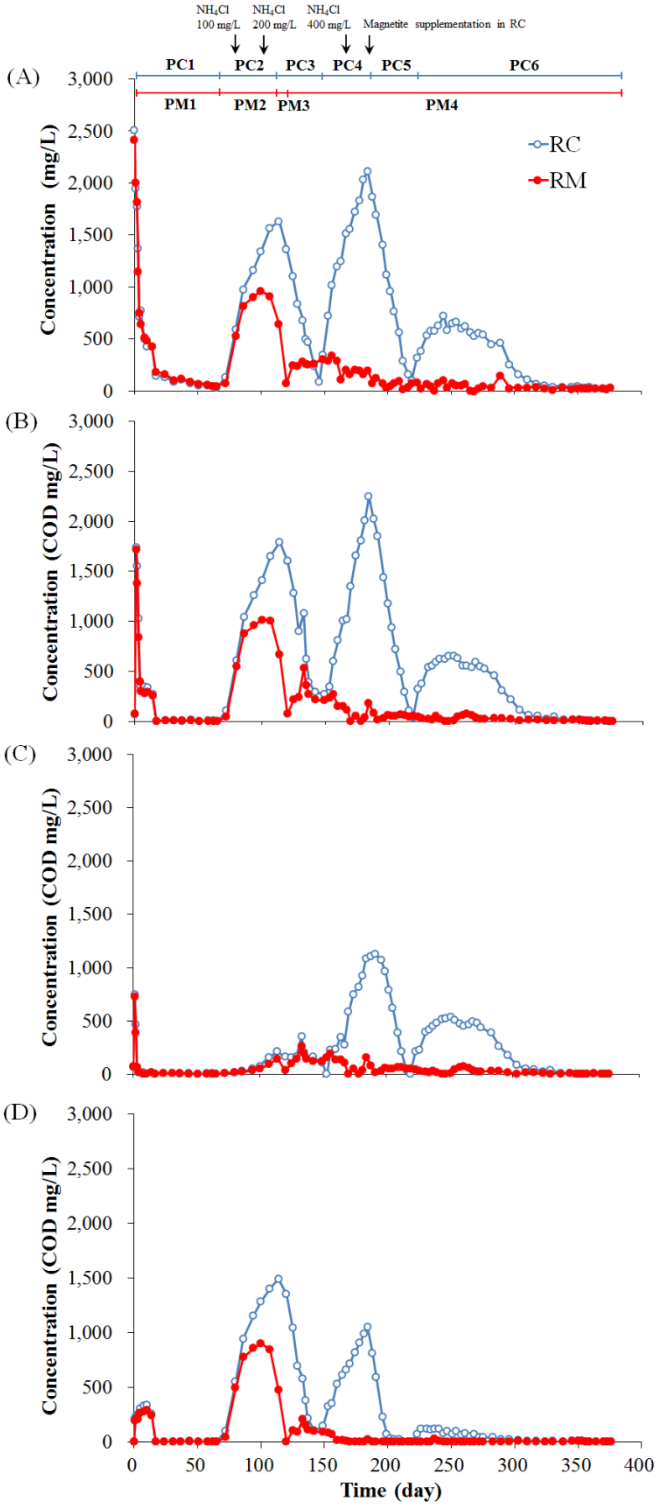

Fig. 4-2. Changes in the residual concentrations of soluble COD (A), total VFAs (B), acetic acid (C), and propionic acid (D) in the reactors community structure shifts in each reactor.

The reactors were operated for another three turnovers of the HRT after RC was stabilized (sCOD < 100 mg/L) to confirm the effect of magnetite and examine whether the effect lasts over a long period. During the final two-month period of the experiment, both reactors reached steady state and achieved complete removal of sCOD (<50 mg residual sCOD/L) with comparable methane production rates (Fig. 4-2 and Table 4-2). The steady-state methane yield (i.e., methane production per removed substrate COD; L CH_4/g CODr) was 0.277 and 0.265 L/g CODr for RC and RM, respectively. These values are consistent with previously reported yields from cheese whey, although lower than the theoretical methane yield of 0.350 L/g CODr. This result is understandable given that substrate is utilized for cell growth (i.e., anabolic flux) as well as methane production (i.e., catabolic flux). The reactor experimental results clearly demonstrate that the 20-mM Fe magnetite supplementation had a significant beneficial effect not only on the robustness of the reactor performance but also in curing a process imbalance.

4-3-2. Fate of magnetite

The SEM-EDX analysis results of the reactor digestate samples are shown in Fig. 4-3. The day-181 sample of RC (before adding magnetite) shows cells with clean, smooth surfaces (Fig. 4-3A); however, the sample taken on day 272 (under magnetite supplementation) shows a completely different morphology with aggregates of fine particles with irregular shapes attached to cell surfaces (Fig. 4-3B). The samples from RM, which was supplemented with magnetite from the initiation, also show similar morphology to the morphology of the day-272 sample of RC (Figs. 4-3C and 4-3D). The EDX spectra show that the day-181 digestate of RC mostly comprises C, N, and O (i.e., organic components) whereas the other samples contained a substantial amount of Fe on the cell surfaces. XRD analysis was performed on the digestates collected from the reactors at the end of the experiment to investigate the fate of the added magnetite (Fig. 4-4). The XRD peak patterns obtained from both samples matched the patterns of pure magnetite, indicating that chemical change did not occur in magnetite particles during the experiment. These patterns suggest that the magnetite added to the reactors adhered to microbial cell surfaces and formed aggregate structures bridging cell connections with its conductive nature [47, 48]. It is possible that Fe(III) released from magnetite may shuttle electrons for extracellular electron transfer via the redox cycling of Fe(II)/Fe(III) under anoxic conditions (i.e., dissimilatory Fe[III] reduction). However, the Fe(II) concentration remained below 1 mg/L during both PC6 and PM4 (data not shown), and it was unlikely that microbial reduction of Fe(III) and/or the nutritional effect of Fe(II) contributed to the enhancement of methanogenesis. It may therefore be concluded that DIET via conductive magnetite particles was the key mechanism that facilitated methanogenesis and improved the process stability. This electric syntrophy has been observed, and several recent studies on methanogenic cultures using synthetic media containing organic acids or ethanol have suggested that electric syntrophy is beneficial to methanogenesis [47, 48, 99].

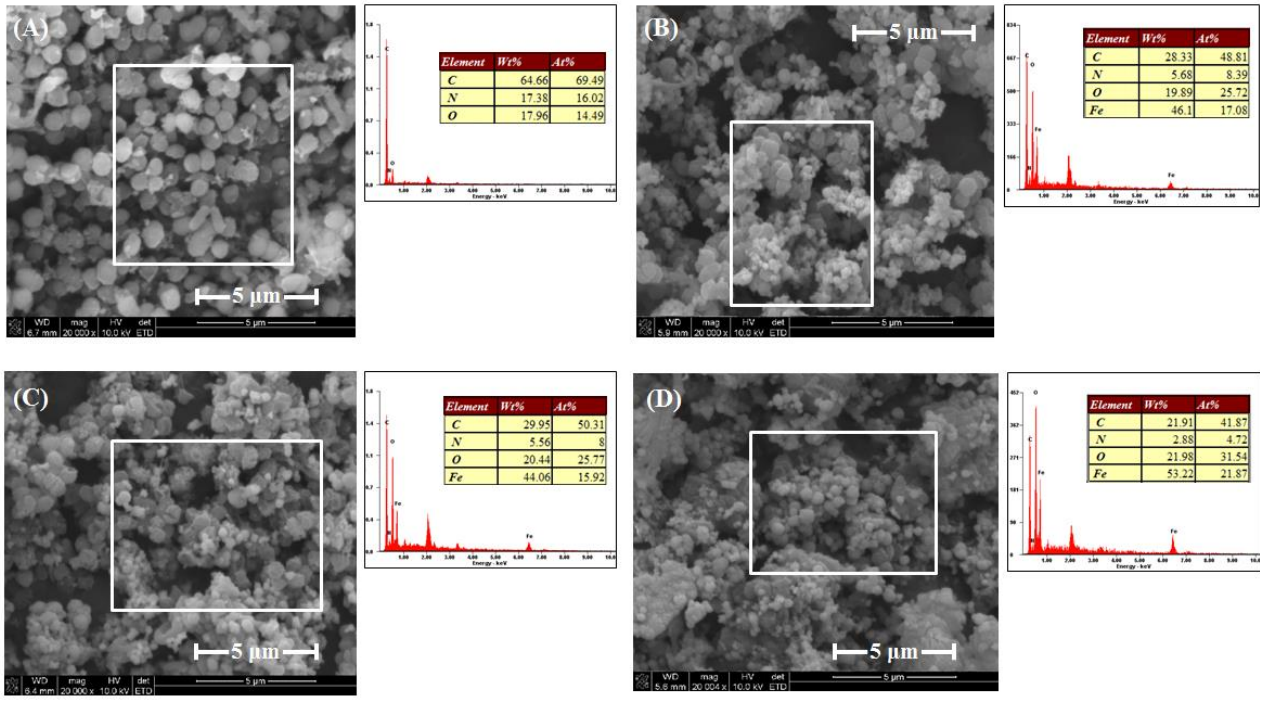

Fig. 4-3. SEM-EDX images of the digestate samples from RC on day 181 (A) and 271 (B) and from RM on day 181 (C) and day 272 (D).

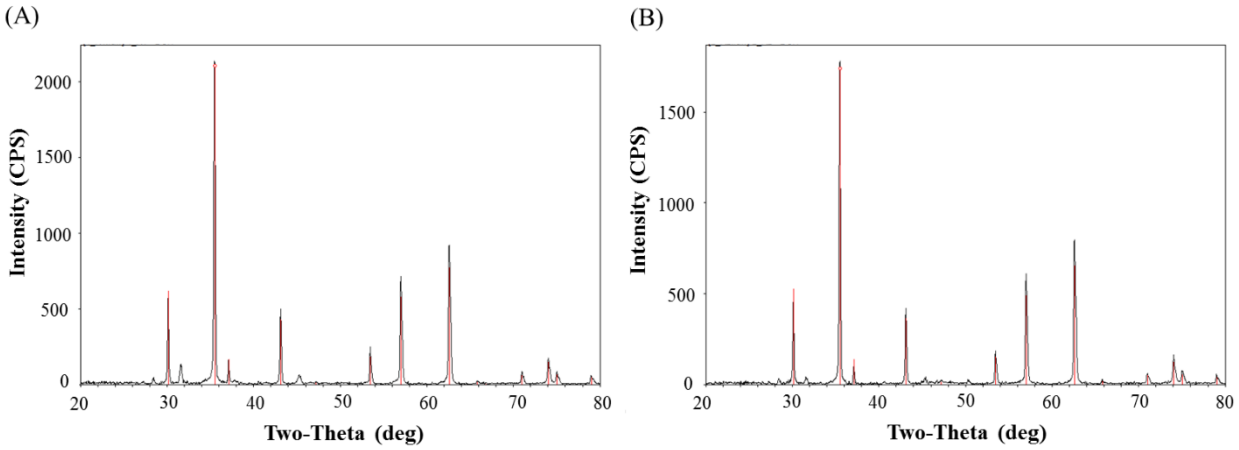

Fig. 4-4. XRD spectra of the reactor digestate samples from RC (A) and RM (B). The spectrum of pure magnetite (red line) is shown for reference.

4-3-3. Phylogenetic affiliation of the DGGE band sequences

DGGE was conducted to investigate the variations in microbial community structures in RC and RM over the experimental phases. Six DNA samples were prepared from each reactor (days 62, 149, 181, 216, 296, and 376) and analyzed parallel to samples from the seed sludge (Fig. 4-5). Seven archaeal 16S rRNA gene sequences (WWA1 to 7) were retrieved from the gel and assigned across three methanogenic orders, *Methanobacteriales*, *Methanomicrobiales*, and *Methanosarcinales* (Table 4-3). Six of the seven sequences were closely related (≥97% sequence similarity) to known aceticlastic (WWA4 and 6) and hydrogenotrophic (WWA2, 3, 5, and 7) methanogen species. WWA1 was not closely related to any known archaeal species but was identified from AD cultures to uncultured clones (accession nos. JX110159 and JF527479). It was assigned by the RDP Classifier to a recently discovered hydrogenotrophic genus, *Methanomassiliicoccus*, which dwells in various anaerobic environments, including wetland soils and animal feces [100]. Given that WWA1 appeared only on day 216 in RC, the hydrogen supply from the rapid degradation of VFAs combined with the electric syntrophy facilitated by magnetite supplementation may have stimulated the growth of the methanogen corresponding to WWA1 during PC5. WWA2, 3 and 5 were affiliated with the *Methanospirillum*, *Methanolinea*, and/or *Methanoculleus* species, which belong to the order *Methanomicrobiales* and frequently occur in methanogenic. WWA2 and 3 appeared with markedly higher band intensity in RM than in RC, and WWA3 in particular emerged to a visible band after the addition of magnetite in RC. This may imply that the hydrogenotrophic methanogens corresponding to these bands were involved in the syntrophy via magnetite-aided DIET. WWA4, detected as the dominant band in all lanes, showed 100% similarity to *Methanosaeta concilii*, an aceticlastic species known to thrive under stable conditions with low concentrations of residual VFAs. Correspondingly, its intensity was apparently lower on day 181 during PC4 in which RC experienced a serious imbalance in addition to an accumulation of acetic and propionic acids. Another *Methanosaeta*-related band WWA6 also occurred in all lanes but with much weaker intensity than WWA4. WWA7 was closely related to the *Methanobacterium* species of the order *Methanobacteriales*, whose relatives are often observed in abundance in AD processes treating different waste streams.

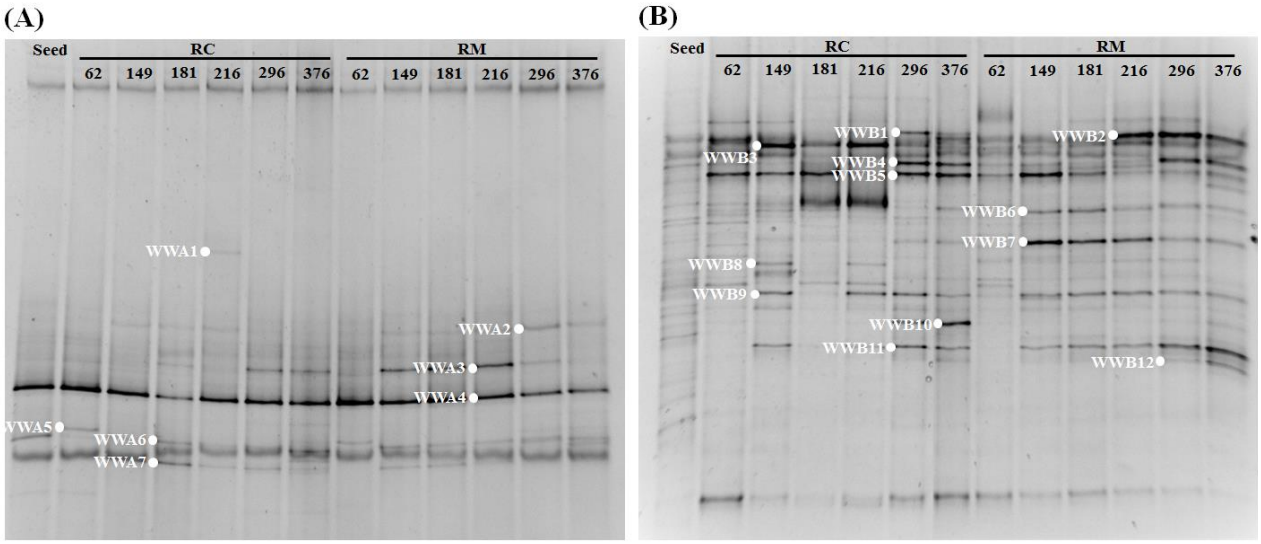

Fig. 4-5. Archaeal (A) and bacterial (B) 16S rRNA gene DGGE fingerprints analyzed from the reactor samples (labeled with the time of sampling in days for each reactor) and seed sludge (labeled as seed)

The bacterial DGGE analysis produced apparently more complicated and dynamic band patterns than does the archaeal analysis. This difference may be related to the limited substrate range of methanogens compared with acidogens. A total of twelve bacterial bands (WWB1 to 12) were sequenced, and only six (WWB2, 5, 6, 7, 8, and 9) were classified at the genus level (Table 4-4). WWB2 and 5, assigned to the genus *Parabacteroides*, were closely related to both *Parabacteroides chartae* and *Macellibacteroides fermentans* with strong similarity. This relation can be attributed to the high rRNA gene sequence homology between the *M. fermentans* and *P. chartae* strains, which renders their differentiation by 16S rRNA gene sequencing difficult [73]. These species are known to ferment various sugars to produce organic acids such as acetic, butyric, and lactic acids [71, 72]. Notably, these bands were also closely related to a Fe(Ⅲ)-reducing fermentative bacterium (accession no. FJ862827) capable of reducing Fe(III) using glucose, yeast extract, and sodium lactate as electron donors [101]. This phenomenon suggests that the *Parabacteroides*-related populations corresponding to WWB2 and 5 may be able to exoelectrogenically oxidize acidogenic products such as VFAs. WWB2 occurred with dominant intensity in RM after the reactor performance was stabilized during PM4 (days 216, 296, and 376) although showing an extremely weak signal or no signal in the other lanes. Conversely, WWB5 was detected in all lanes but with rather greater intensity in the RC samples. The bacterium corresponding to WWB2 may therefore have been involved in electric syntrophy in the experimental reactors whereas the bacterium deduced from WWB5 presumably played a role in the fermentation of whey sugars [101]. WWB6 and WWB7 were assigned to the fermentative genera *Petrimonas* and *Saccharofermentans*, respectively. These genera are mesophilic and capable of fermenting various sugars to produce organic acids, including acetic acids, and H_2/CO_2 [102, 103]. The populations corresponding to these bands were likely involved in the acidogenic fermentation of whey. A notable point is that WWB7 also shared a considerable similarity of 96.7% with an uncultured clone

from the anode biofilm of a microbial fuel cell (accession no. JX491538). This similarity implies that the WWB7-related bacterium may be electroactive. This possibility may explain the dominance shift between the two major bands WWB2 and 7 at approximately day 216 in RM as a result of the transition of the dominant exoelectrogenic population over time. WWB8 was assigned to the genus *Rhodopseudomonas*, which is characterized by its great metabolic versatility. This purple nonsulfur bacterium can grow both aerobically and anaerobically by switching between four different metabolic modes: photoautotrophic, photoheterotrophic, chemoautotrophic, and chemoheterotrophic [104]. WWB8 appeared on days 149 and 216 when residual VFAs that accumulated during PC2 and PC4 were stabilized. This appearance suggests that its corresponding population was presumably responsible for degrading VFAs, particularly propionic acid, or the degradation products. WWB9 was affiliated with the genus *Syntrophobacter*, which oxidizes propionate to acetate in cooperation with hydrogen-consuming partners, for example, hydrogenotrophic methanogens [20]. The consistent appearance of WWB9 after the HRT was shortened to 20 days in both reactors, except for the day-181 sample of RC taken under imbalanced conditions, suggests that the corresponding bacterium to this band was most likely responsible for syntrophic propionate oxidation and thus containment of the process imbalance.

Among the remaining band sequences, four (WWB1, 3, 4, and 12) were classified only at the phylum level whereas the other two (WWB10 and 11) were unclassified even at the phylum level (Table 4-4). WWB1, 3, and 4 were assigned to phylum *Bacteriodetes*, whose members are commonly found in AD environments and closely related to uncultured clones from anaerobic digesters treating different wastes. Notably, WWB4 emerged while WWB3 decayed with the stabilization of RC after magnetite supplementation was applied (Fig. 4-2). This dominance shift between the putatively fermentative bacteria may be related to the environmental changes caused by the addition of magnetite. WWB4 was closely related to several uncultured clones from different bioelectrochemical systems inoculated with anaerobic sludge, indicating that its corresponding population may be electroactive. This phenomenon suggests that this bacterium was possibly involved in electric syntrophy in the experimental reactors and that its growth was favored under magnetite supplementation. WWB12 was assigned to the phylum *Chloroflexi* that often occurs in abundance in AD processes [105]. Additionally, there is growing evidence that *Chloroflexi* bacteria have exoelectrogenic activity [106, 107]. Given that WWB12 appeared in the later period of PC6 and PM4 (days 296 and 376; Fig. 4-2), the corresponding *Chloroflexi*-related bacterium may have participated in DIET within the reactor communities. WWB10 and 11 were closely related to uncultured clones from anaerobic treatment processes although the functions of their corresponding populations are unclear.

Table 4-3. Phylogenetic affiliation of archaeal 16S rRNA gene sequences retrieved from DGGE bands

Band	Closest relative	Accession number	Similarity (%)	Classification[a]
WWA1	Uncultured archaeon clone LB12C11	JX110159	100	*Methanomassiliicoccus*
	Uncultured archaeon clone GDIC2IK01EWX39	JF527479	99.2	
	Candidatus Methanoplasma termitum strain MpT1	CP010070	96.9	
WWA2	*Methanospirillum hungatei*	NR_074177	99.6	*Methanospirillum*
	Methanospirillum stamsii	NR_117705	99.6	
	Methanospirillum psychrodurum	NR_133782	99.2	
WWA3	*Methanolinea mesophila*	NR_112799	97.2	*Methanomicrobiales*
	Uncultured archaeon clone Annu5	HM630578	97.2	
WWA4	*Methanosaeta concilii*	KM408635	100	*Methanosaeta*
WWA5	*Methanolinea tarda*	NR_028163	98.0	*Methanomicrobiales*
	Methanolinea mesophila	NR_112799	97.7	
	Methanoculleus receptaculi	NR_043961	97.3	
WWA6	*Methanosaeta harundinacea*	KM408632	99.2	*Methanosaeta*
	Methanosaeta pelagica	NR_113571	97.7	
WWA7	*Methanobacterium beijingense*	NR_028202	99.6	*Methanobacterium*
	Methanobacterium sp. SMA-27	KJ432636	97.7	

[a] The lowest rank assigned by RDP Classifier at an 80% confidence threshold.

Table 4-4. Phylogenetic affiliation of bacterial16S rRNA gene sequences retrieved from DGGE bands

Band	Closest relative	Accession number	Similarity (%)	Classification[a]
WWB1	Uncultured bacterium clone CloningB8D06	AB998023	100	*Bacteriodetes*
	Uncultured bacterium clone GBL1-02	KM046958	100	
	Uncultured bacterium clone GB2	KJ679865	100	
	Uncultured bacterium clone MR3	DQ661705	100	
WWB2	*Parabacteroides chartae*	NR_109439	100	*Parabacteroides*
	Macellibacteroides fermentans	NR_117913	99.6	
	Bacteroides sp. W7	FJ862827	99.3	
WWB3	Uncultured bacterium clone UB2	KF803571	99.8	*Bacteriodetes*
	Uncultured bacterium clone LA86	FJ799150	99.8	
	Uncultured bacterium clone paintanode52	KC597203	99.5	
WWB4	Uncultured bacterium clone MISEQ01_89_000000000-A647M_1_1107_2246_12378	KP348423	100	*Bacteriodetes*
	Uncultured bacterium clone MFC-GIST450	EU704659	99.8	
	Uncultured bacterium clone MFC-GIST14	EU704544	99.5	
WWB5	*Parabacteroides chartae*	NR_109439	99.8	*Parabacteroides*
	Macellibacteroides fermentans	NR_117913	99.8	
	Bacteroides sp. W7	FJ862827	99.3	
WWB6	*Petrimonas sulfuriphila*	NR_042987	100	*Petrimonas*
	Petrimonas sulfuriphila	KT183420	99.5	
WWB7	Uncultured bacterium clone W-16S-34	HM445961	100	*Saccharofermentans*
	Uncultured bacterium clone ANAER_V1_5G	KC110305	99.8	

	Uncultured bacterium clone R3B10L	GQ423908	99.8	
	Uncultured bacterium clone Wcon1_O11	JX491538	96.7	
WWB8	*Rhodopseudomonas faecalis*	KT180200	100	*Rhodopseudomonas*
	Rhodopseudomonas palustris	KT824854	100	
	Rhodopseudomonas sp. JFANr	HQ693554	99.8	
	Rhodopseudomonas oryzae	AB241410	99.8	
WWB9	*Syntrophobacter pfennigii*	NR_026232	97.6	*Syntrophobacter*
	Uncultured bacterium clone KB-1	AY780561	99.6	
WWB10	Uncultured bacterium clone KIST-JJY029	EF654698	99.1	*Bacteria*
	Uncultured bacterium clone QEDS1CF05	CU921570	98.8	
	Uncultured bacterium clone B074	HG007954	97.9	
WWB11	Uncultured bacterium clone BLB06	AB248628	99.8	*Bacteria*
	Uncultured bacterium clone MADSa78	AB669261	99.5	
WWB12	Uncultured bacterium clone ORSFAM_	EF393281	99.3	*Chloroflexi*
	Uncultured bacterium clone SB1B_8F_c12	KC713023	98.4	

[a] The lowest rank assigned by RDP Classifier at an 80% confidence threshold.

4-3-4. Changes in archaeal and bacterial community structures

The cluster dendrograms and NMS plots that were constructed based on the archaeal and bacterial DGGE profiles are shown in Fig. 4-5. The cumulative r^2 for ordination axes was 0.892 and 0.789 in the archaeal and bacterial NMS plots, respectively, indicating that 89.2 and 78.9% of the total variance in the archaeal and bacterial community data, respectively, are explained by the NMS ordination results. The final stress and instability were acceptable for both plots to provide a reliable picture of the relatedness between the analyzed community profiles [96]. The archaeal community profiles from RM were clustered separately from the RC profiles, except that the day-62 profiles from two reactors were quite closely related (Sorensen distance (*Ds*) < 0.04). The same clustering pattern with a clear divergence between the RC and RM profiles was observed by the archaeal NMS ordination (Fig. 4-6A). These results show that the archaeal community structures in RC and RM developed in significantly different manners during the experiment. Notably, the day-181 RC profile was located remotely from all other profiles. This placement appears to reflect the visible change in the abundance of methanogen populations (i.e., DGGE band intensity), particularly *Methanosaeta*-related (WWA4 and 6) and *Methanobacterium*-related (WWA7) populations, after the serious imbalance during PC4. Notably, in the NMS plot, the largest jump between two consecutive points (i.e., the most significant change) was observed between days 181 and 216 in RC and between days 62 and 149 in RM. These jumps suggest that the addition of magnetite presumably triggered the most significant change in archaeal community structure in RC whereas the process was upset following the decrease in HRT to 20 days in RM (Fig. 4-2 and Table 4-2). This result represents a significant effect of magnetite on the evolution of AD archaeal communities.

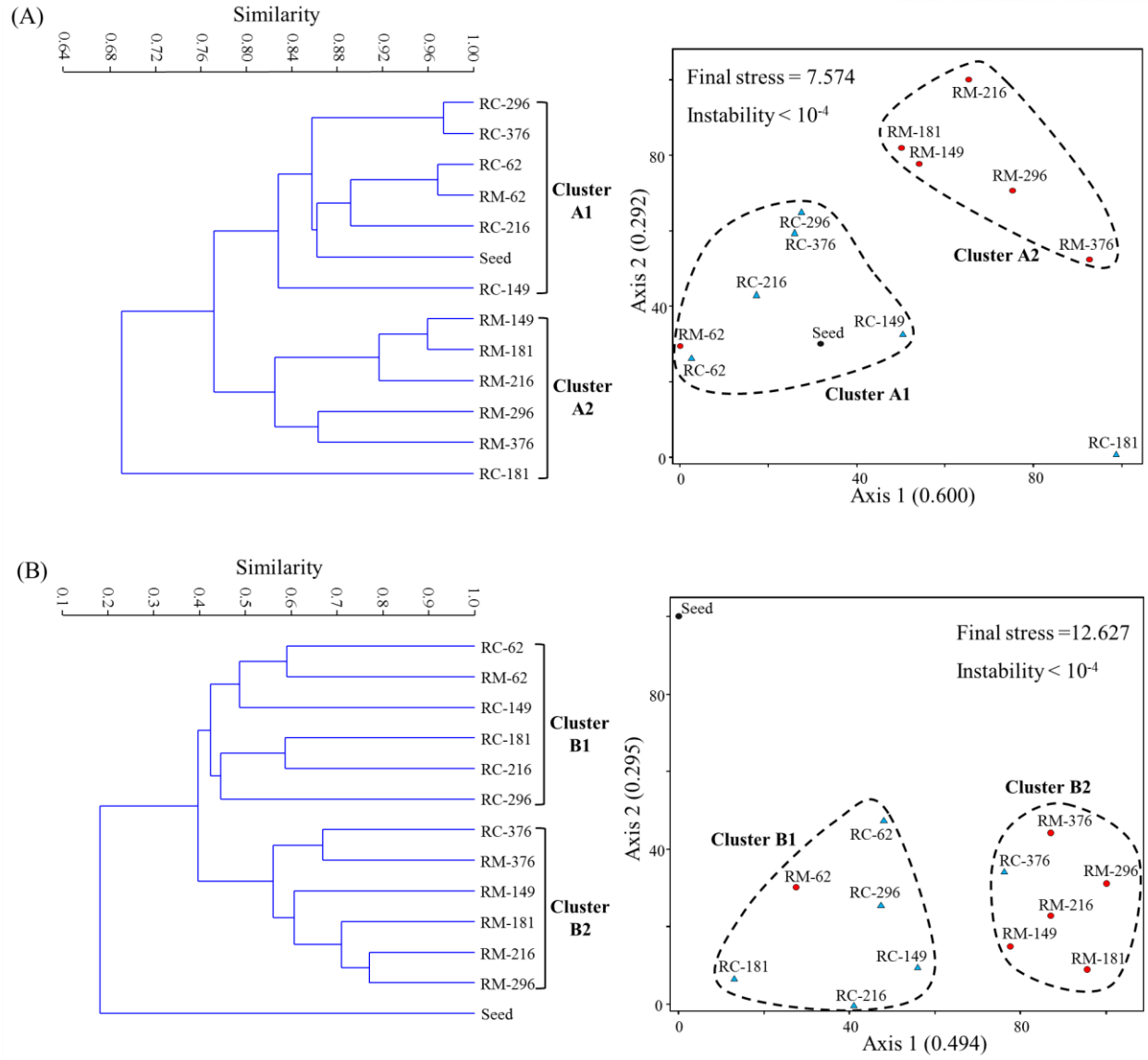

Fig. 4-6. Cluster dendrograms and NMS plots generated based on the archaeal (A) and bacterial (B) DGGE profiles. Each community profile is labeled with the reactor name followed by the time of sampling in days, with the seed sludge profile being labeled as "Seed".

The bacterial cluster analysis produced a clustering pattern similar to the archaeal cluster dendrogram, in which the bacterial community profiles from RM and RC were generally clustered separately (Fig. 4-6B). Notably, the day-376 RC profile was most closely related to the day-376 RM profile and grouped in a cluster with other RM profiles. The same converging pattern was shown in the NMS plot. Given the reactor performance profiles and operating conditions (Fig. 4-2 and Table 4-2), this pattern may be related to the influence of magnetite (supplemented from time 0 in RM but from day 181 in RC) and to the extremely stable treatment efficiency in both reactors (i.e., substrate-limited environment). The NMS plot shows that both RC and RM bacterial community structures changed significantly between days 62 and 149. This change may be

related to a process imbalance after the decrease in HRT (Fig. 4-2). The bacterial community structure in RC changed dynamically until day 376 whereas the structure in RM remained relatively stable with little significant change afterwards. This result corresponds to the fact that RC was subjected to more severe variations in the reactor environment related to, for example, repeated VFA build-up, interrupted feeding, and magnetite addition than RM. Particularly with magnetite supplementation in RC from day 181, the bacterial community structures in two experimental reactors gradually became more closely related over time, suggesting that magnetite may have a significant influence on the development of bacterial communities in AD processes. It was demonstrated overall that both archaeal and bacterial community structures developed in evidently different directions between RC and RM and that the community structure transitions were well correlated with the changes in the reactor environment.

4-3-5. Quantitative analysis of methanogen community composition

The changes in methanogen community composition in the experimental reactors were analyzed based on the 16S rRNA gene abundance of the target methanogen groups. The total methanogen population (MET; the sum of the measured 16S rRNA gene concentrations of all target methanogen groups) remained fairly constant, at approximately 10^8 copies/mL, except for the day-181 sample of RC (2.7×10^7 copies/mL). The apparently lower MET was primarily a result of the drastic decrease in *Methanosaetaceae*, which typically thrives at low acetic acid concentrations (Fig. 4-7). The lower MET appears to reflect the effect of the process imbalance along with VFA accumulation at approximately day 181 in RC (Fig. 4-2).

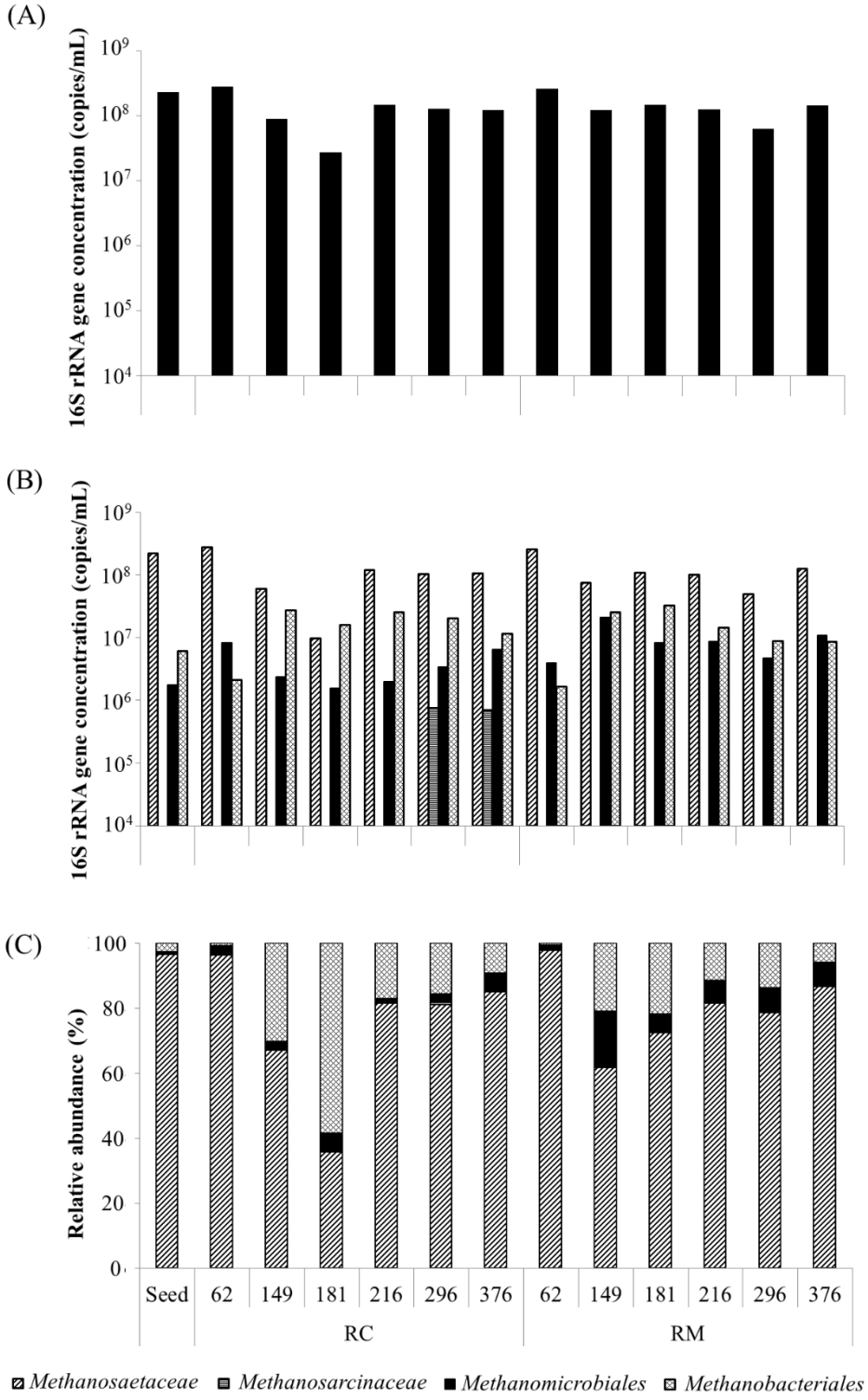

Fig. 4-7. Changes in the total methanogen population (A) and the absolute (B) and relative (C) abundance of each methanogen group analyzed based on the 16S rRNA gene quantification results.

The methanogen communities in the seed sludge and the 62-day samples of both reactors were absolutely dominated by *Methanosaetaceae* (>96% of MET). This result agrees with the general understanding that the members of this family form the dominant methanogen group in stable AD systems [108]. The community composition changed significantly in both reactors to have a remarkably increased proportion of hydrogenotrophic methanogens over the subsequent experimental period. The marked increase in hydrogenotrophs, particularly *Methanobacteriales* (>12-fold), between days 62 and 149 was perhaps supported by hydrogen produced from the degradation of accumulated propionic acid and also, particularly in RM, by DIET. This potential syntrophic relation likely involved *Syntrophobacter*-related (WWB9) and *Methanobacterium*-related (WWA7) microbes as the major syntrophic partners (Fig. 4-5 and Tables 4-3 and 4-4). Of note is that the abundance of hydrogenotrophic methanogens, particularly *Methanomicrobiales*, was generally higher in the RM samples. This reading may suggest that magnetite stimulated their growth by facilitating electric connections with syntrophic VFA degraders via DIET. Supportively, the involvement of *Methanobacteriales* (e.g., *Methanobacterium*; WWA7) and *Methanomicrobiales* (e.g., *Methanospirillum* and *Methanolinea*; WWA2, 3, and 5) strains in DIET has been demonstrated in recent studies [48, 86, 109]. In particular, Lee et al. [116] and Li et al. [48] reported that these hydrogenotrophic methanogens, combined with putative exoelectrogenic bacteria, were preferentially enriched in the presence of conductive material (i.e., granular activated carbon and magnetite nanoparticles) from sewage sludge digestate and paddy soil, respectively. The relative abundance of the two hydrogenotrophic orders increased from <1% on day 62 to 9.3% in RC (1.7×10^7 copies/mL; 1.7-fold increase in absolute concentration) and to 5.9% in RM (1.9×10^7 copies/mL; 3.5-fold increase in absolute concentration) on day 376.

Methanosaetaceae remained the most dominant methanogen group (61.7%– 97.8% of MET) throughout the experiment in both reactors, except for day 181 in RC. This result is consistent with the archaeal DGGE results in which the dominant *Methanosaeta*-related band WWA4 appeared with markedly diminished intensity on day 181 (Fig. 4-5A). This result is interesting given that this family is generally known to be strictly aceticlastic and unable to reduce carbon dioxide to methane. However, Smith et al. [87] revealed that *Methanosaeta* has a complete set of genes encoding the enzymes required for methanogenesis from carbon dioxide. A more recent study reported that *Methanosaeta* can directly accept electrons by electrical connections and DIET can prevail over hydrogen/formate-mediated IET during AD [27]. Correspondingly, some previous studies observed the dominance of *Methanosaeta*-related populations in methanogenic cultures under electrically conductive conditions [40, 95]. These suggest that *Methanosaeta* was likely responsible for methane production by DIET-mediated CO_2-reducing as well as aceticlastic pathways in the experimental reactors.

Another point to note is that *Methanosarcinaceae* accounted for a negligible proportion of the methanogen community (<0.6% of MET) in all reactor samples (Fig. 4-7C). Given that this metabolically versatile family reportedly outcompetes *Methanosaetaceae* and dominates the aceticlastic methanogenesis at high acetic acid

concentrations, the limited abundance of *Methanosarcinaceae* even on days 216 and 296 in RC appears unusual. It may be speculated that a portion of the acetic acid, particularly when acetic acid accumulates to high levels, was oxidized by syntrophic acetate-oxidizing bacteria instead of being converted to methane by aceticlastic methanogens. Syntrophic acetate oxidation associated with hydrogenotrophic methanogenesis is often observed to be an important methanogenic route, and sometimes such oxidation can even contribute more than a direct aceticlastic pathway [110]. Acetate oxidation may also exoelectrogenically provide electrons to methanogens via DIET whereby an electric syntrophy can be supported. The overall results support the assumption that the reactor communities formed a stable three-way syntrophic interaction between fermenters, methanogens, and exoelectrogens under magnetite supplementation.

4-4. Summary

This study examined the influence of magnetite supplementation in continuous AD processes treating cheese whey during a long-term operation of 376 days. It was well demonstrated that magnetite supplementation had a beneficial effect not only on the methane productivity but also on the process stability, likely by providing energetically more favorable conditions for IET. DIET between exoelectrogenic bacteria and electron-capturing methanogens through conductive magnetite particles was presumably the dominant mechanism that led to enhanced biomethanation. *Methanosaeta* predominated the methanogen communities in both reactors and appeared to be responsible for methanogenesis via DIET-aided carbon dioxide-reducing as well as aceticlastic pathways.

5. (STUDY 3) LONG-TERM STUDY ON THE EFFECT OF MAGNETITE SUPPLEMENTATION IN CONTINUOUS MODE: SEPARATION AND RECYCLING OF MAGNETITE

5-1. Introduction

The authors have demonstrated the beneficial effect of magnetite supplementation on the biomethanation of cheese whey, a high-strength dairy wastewater, in a batch mode (Study 1) and a continuous mode (Study 2). The magnetite-supplemented reactor used in these studies maintained enhanced process performance and stability over a continuous operation period of one year. A drawback of applying this strategy in practice is the need for continuous supply of magnetite to facilitate DIET, which may offset the benefits from enhanced methanation. Therefore, the manner of minimizing the consumption of magnetite while maintaining a desired level of performance enhancement is critical to the economic feasibility of this approach.

To address this question, this study was designed to test magnetic separation and recycling of magnetite as a method to support magnetite-promoted DIET in a continuous AD process without adding extra magnetite. Recycling magnetite from the effluent seems to be a feasible approach given previous observations that magnetite particles supplemented to AD processes did not change chemically, even after long-term operation [48, 111]. This study focused on whether magnetite recycling without addition of extra magnetite can support continuous AD for a long period (more than 10 months) while maintaining performance comparable to an AD process continuously supplemented with magnetite. To the best of our knowledge, this is the first study that attempts magnetic separation and recycling of magnetite to promote DIET for enhanced biomethanation in continuous mode. The outcomes of this study provide insight into the possibility of magnetite-promoted DIET as a novel and practical approach for stable, high-rate biomethanation of organic waste.

5-2. Materials and methods

5-2-1. Bioreactor operation

Two identical CSTRs, each with a working volume of 2 L, were operated anaerobically to treat whey. Each reactor was initially filled with equal amounts of diluted whey (5 g/L, sCOD) and anaerobic sludge from a full-scale digester treating sewage sludge (seeding ratio, 50% [v/v]). Temperature and pH were maintained at approximately 35 ℃ and 7.0, respectively, for both reactors throughout the experiment. Further details of the reactor operating conditions and the physicochemical characteristics of the inoculum and substrate can be found in previous paper about study 2 [111], where biomethanation performance was compared between a reactor with magnetite supplementation (RM) and a reactor without it (RC) (final Fe concentration, 20 mM) for over a year. As an extension, in this study, two reactors were operated in continuous mode for a further 10

months. The RC was run with continuous supplementation of magnetite while extra magnetite was not added to RM, which recycled magnetite (Table 5-1).

A schematic diagram of the operation of RM with magnetite recycling is shown in Fig. 5-1. Magnetite was separated from the effluent of RM using neodymium magnets of 4820 gauss and recycled by mixing it with the influent, while the remaining effluent was discharged (Fig. 5-2). The reactors were periodically analyzed for treatment efficiency and biogas production. Steady-state data for comparison of the performance of RC and RM with changes in operating conditions were analyzed at three different time point after the reactors had stabilized.

Table 5-1. Reactor operating conditions.

	RC			RM		
Period (days)	0–61	62–194	195–317	0–61	62–194	195–317
Magnetite addition	Yes	Yes	No	Yes	No	No
Magnetite recycling	No	No	No	No	Yes	Yes
HRT (day)	20	20	20	20	20	20
OLR (g COD/L·d)	0.255	0.255	0.255	0.255	0.255	0.255

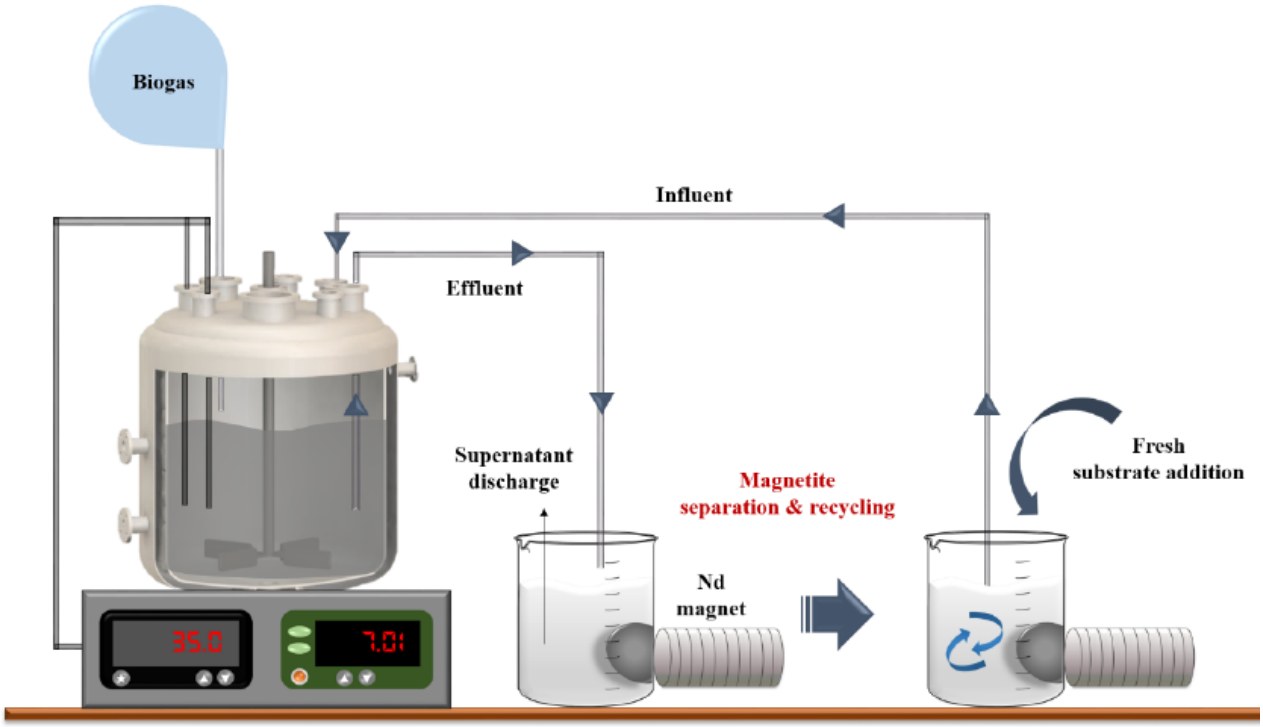

Fig. 5-1. Schematic diagram of the operation of RM with magnetic separation and recycling.

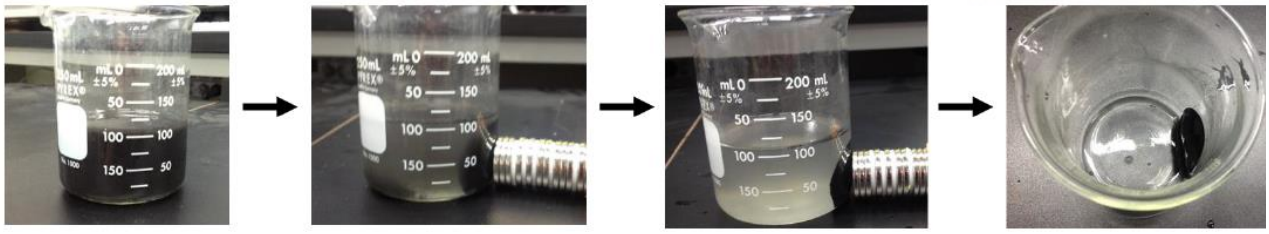

Fig. 5-2. Magnetic separation of magnetite from the effluent of RM.

5-2-2. Next-generation sequencing

Libraries for next-generation sequencing (NGS) were prepared from the total DNA and cDNA samples by PCR amplification with 515F and 806R as the universal primers for prokaryotic 16S rRNA gene sequences [112]. An Illumina adapter sequence was added to the 5' end of each primer. The PCR was performed with the following thermal cycling profile: an initial denaturation at 94 ℃ for 10 min, 30 cycles of amplification (30 s at 94 ℃, 30 s at 55 ℃, and 30 s at 72 ℃), and a final extension at 72 ℃ for 7 min. The PCR products were submitted to Macrogen, Inc. (Korea) for NGS on the Illumina MiSeq platform. Readings with low quality scores (<20), ambiguous bases, or potential chimeric sequences were removed. The trimmed sequences were aligned and clustered using CD-HIT-OTU (http://weizhongli-lab.org/cd-hit-otu/) with an operational taxonomic unit (OTU) definition of <3% divergence. Taxonomic classification was performed using the RDP Classifier (https://rdp.cme.msu.edu/classifier/). The sequence data generated in this study have been deposited in the NCBI Sequence Read Archive (SRA) under the bioproject accession number PRJNA382304.

For each of the obtained 16S rRNA gene and 16S rRNA libraries, a bacterial matrix and an archaeal matrix were constructed based on the OTU relative abundances. Cluster analysis was conducted for each matrix using the unweighted pair group method with arithmetic means (UPGMA) algorithm based on the Sorensen distance measure using PAST 3.03.

5-3. Results and discussion

5-3-1. Reactor performances

The experimental reactors, RM with magnetite supplementation (final Fe concentration, 20 mM) and RC without magnetite supplementation, had been operated for more than one year in a preceding study, to examine the effect of magnetite supplementation on continuous biomethanation of whey [111]. That study demonstrated that magnetite had a significant beneficial effect on process performance and stability. Both reactors in that study were operated with magnetite supplementation after the comparative study of methanation performance with and without magnetite supplementation. RC stabilized gradually with magnetite supplementation to show

similar organic removal and methane productivity to those of RM after five turnovers of working volume (days 219–317). During further operation for three turnovers (days 318–376), which were conducted to examine the long-term stability of the reactions, the reactors showed comparable, stable methane production while maintaining residual sCOD concentrations below 100 mg/L. The present study, as an extension of the preceding study, attempted magnetic separation and recycling of magnetite from the effluent to investigate the potential for maintaining enhanced performance without a continuous supply of magnetite. In this study, to avoid confusion, the point where RC stabilized (<100 mg residual COD/L) after applying magnetite supplementation (day 317 in the preceding study) was set as day 0 for the following experiments with RC and RM.

Both reactors maintained very stable performance, showing complete removal of sCOD and VFAs during the operation with magnetite supplementation for the first three turnovers of the working volume since day 0 (Figs. 5-3 and 5-4). During this period, RC and RM showed similar performance in terms of methane production rate (MPR) and sCOD removal (Table 5-2). The methane yield (Y_M, methane produced per substrate COD removed) was 0.277 and 0.265 L/g CODr in RC and RM, respectively, which is comparable to previously reported values for cheese whey [111, 113]. Although the measured values are lower than the theoretical yield of 0.350 L/g CODr, this result is reasonable given that substrate is utilized not only for methane production but also for cell growth.

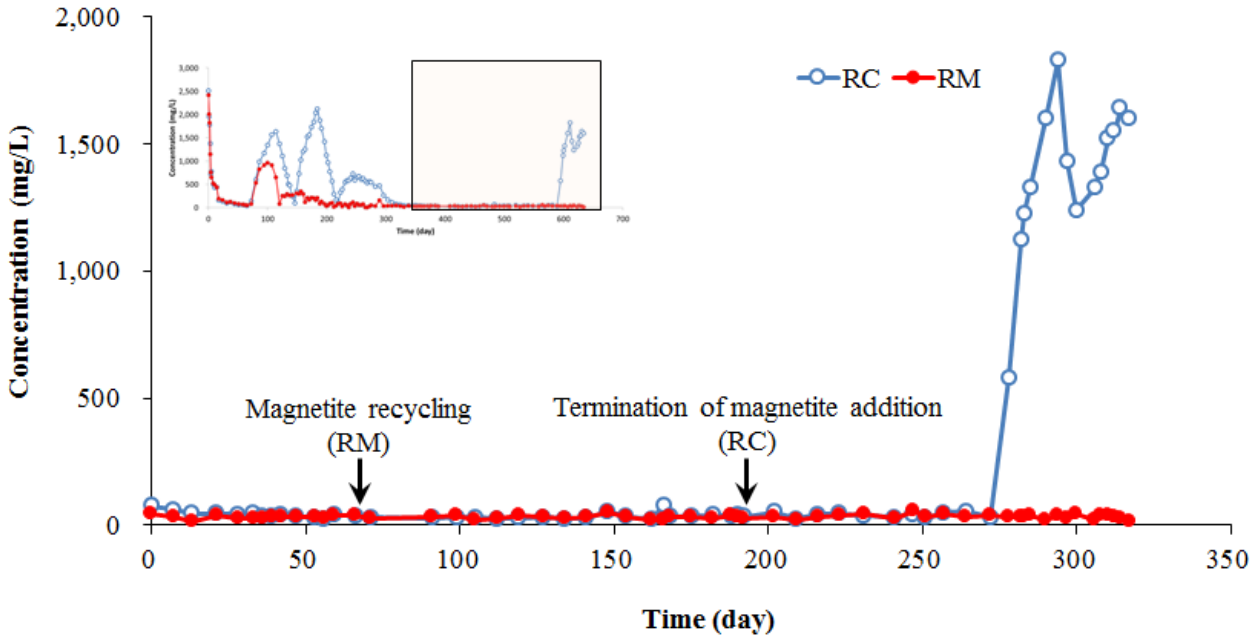

Fig. 5-3. Changes in the residual concentration of soluble chemical oxygen demand in the reactors. The shaded area in the inset indicates the observation period in this study.

Magnetite supplementation to RM was stopped on day 62, and thereafter, the reactor was run with recycled magnetite magnetically separated from the effluent. With no addition of extra magnetite, RM maintained

comparable performance to RC, which was continuously supplemented with magnetite for more than six turnovers of the working volume (Fig. 5-3 and Table 5-2). The sCOD removal remained over 99% (residual VFAs/L, <50 mg), with MPR also being maintained at a high level (around 150 mL/d), in both reactors during this period. This suggests that the enhanced DIET activity was robustly supported by the magnetite recycling method. It is worth noting that an apparent increase in methane production was observed in RM after the operation with magnetite recycling. This is likely to be attributed to the retention of increased biomass concentration in the reactor due to the recycling of cells aggregated with magnetite particles.

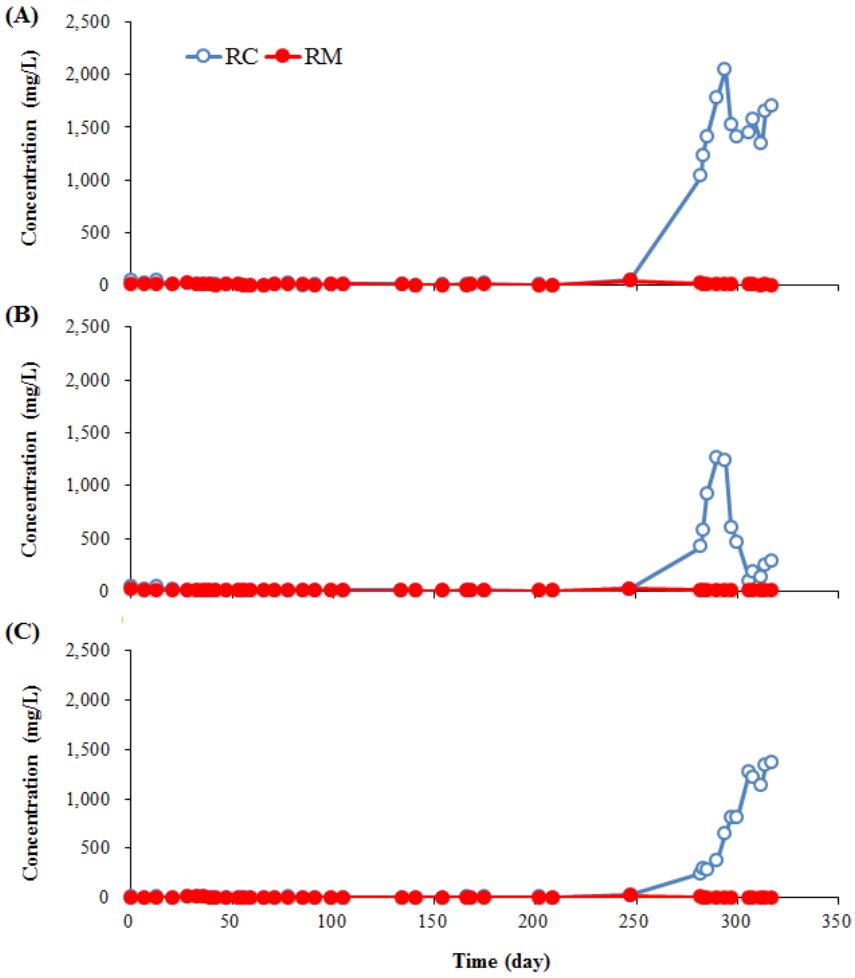

Fig. 5-4. Changes in the residual concentrations of total volatile fatty acids (A), acetic acid (B), and propionic acid (C) in the reactors.

For further confirmation, RC was operated without magnetite supplementation from day 195, while running RM with magnetite recycling to the end of the experiment on day 317. A sudden increase in the residual sCOD concentration was observed in RC after four turnovers of the working volume (Fig. 5-3). With a rapid buildup of VFAs, the methanation performance deteriorated severely in terms of both MPR and Y_M (Fig. 5-4 and Table 5-2). This sudden process upset was probably related to the washout of magnetite from

RC, and its performance was not restored during the next two operation turnovers. On the other hand, RM maintained stable, enhanced performance until the end of the experiment without the addition of extra magnetite. These observations reconfirm again the stimulatory effect of magnetite on AD performance. It is noteworthy that in RC, the acetic and propionic acids, as well as the major VFAs produced, showed markedly different time profiles (Fig. 5-4). Acetic acid initially accumulated faster but soon decreased to a stable level (<100 mg COD/L), while propionic acid steadily accumulated to the end of the observation period. As a result, the propionic to acetic acid (P/A) ratio exceeded 1.4 and reached 11.8 after day 300. It is well accepted that residual VFA concentrations can serve as an indicator of process imbalance and a P/A ratio above 1.4 is considered a sign of impending process failure [114]. This accords with the significant performance deterioration observed in RC during this period. An important point to recognize here is that the conversion of VFAs, particularly propionic acid, was very stable and efficient without fluctuations throughout the experiment in RM. Propionic acid is potentially toxic to methanogenic activity and energetically difficult to be oxidized to acetic acid for methanogenesis ($\Delta G^{\circ\prime}$ = 76.1 kJ/mol). Therefore, its efficient degradation by syntrophic propionate oxidation is crucial for stable and complete AD [115]. A key step in this syntrophic pathway is transfer of electrons between syntrophic partners, and recent studies have shown that this step can be facilitated by promoting DIET with the addition of magnetite [47, 111]. These observations suggest that the magnetic recycling method robustly supports magnetite-promoted DIET in RM, effectively enhances methanation performance, and prevents process imbalance. Whey is a problematic industrial by-product produced in substantial amounts from cheese manufacturing industry, and its proper treatment is a challenging task due to its highly organic and easily perishable characteristics. AD has been extensively used to treat this strong wastewater and recover energy, and recently different approaches to the same goal have been applied using, for example, bioelectrochemical systems [116]. The reactor experimental results suggest that DIET-promoted AD can provide an advanced way of valorizing whey and possibly other high-strength organic wastewaters.

Table 5-2. Reactor performance data.

	RC			RM		
Period (days)	0–61	62–194	195–317	0–61	62–194	195–317
MPR (mL/d)[a]	133.4	146.5	37.1	127.4	150.8	138.9
Methane content (%)	66.5	69.1	77.2	64.5	71.0	67.4
sCOD removal (%)[b]	99.3	99.2	67.1	99.3	99.4	99.5
Y_M (L/g CODr)[c]	0.277	0.299	0.110	0.265	0.306	0.288

5-3-2. Characteristics and morphology of the digestate

Fig. 5-5 shows SEM-EDX images of the digestate samples taken before the termination of magnetite supplementation to RC (day 192) and at the end of the experiment (day 317). All the samples show complex aggregate structures with fine irregular-shaped particles on their surfaces. This is supported by EDX spectra, which indicate the presence of a substantial amount of Fe on the cell surfaces. XRD analysis was conducted on the day-317 digestate of RM to investigate the fate of magnetite during the long-term continuous operation with magnetic recycling for over 250 days (Fig. 5-6). The Fe^{2+} concentration remained below 1 mg/L throughout the experiment in both reactors, and it was unlikely that dissimilatory reduction of Fe^{3+} and/or the nutritional effect of Fe^{2+} contributed to the enhanced methanation performance. These results suggest that magnetite-promoted DIET was likely the main mechanism leading to the enhancement of reactor performance and stability that the applied magnetite recycling method supports the beneficial effect without the need for adding extra magnetite.

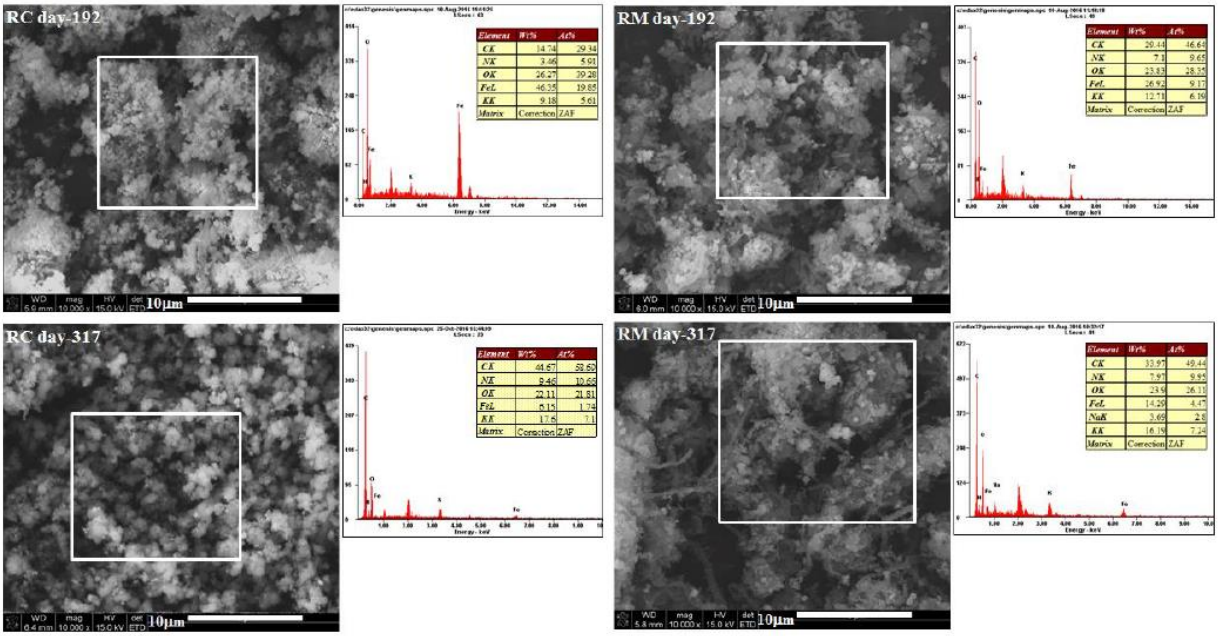

Fig. 5-5. Scanning electron microscopy images and energy-dispersive X-ray spectroscopy spectra of the digestate samples collected on days 192 and 317.

It is worth noting that the Fe content of the digestate decreased markedly over time in RM as well as RC, which agrees well with the temporal changes in fixed suspended solids (FSS) concentrations (Fig. 5-7). These indicate there was a loss of magnetite by washout during the reactor operation. FSS is considered a rough but reasonable indicator of magnetite content because the substrate contains only a limited amount of FSS (<150 mg/L). Not surprisingly, the FSS concentration in RC decreased steeply to 133 mg/L, particularly after cessation of magnetite supplementation. This accords well with the morphological change of the digestate in

RC, where fine magnetite particles apparently disappeared between days 192 and 317 (Fig. 5-5). Although RM showed a lesser and delayed decrease in the FSS concentration because of the recycling of magnetite, there was still a considerable decrease from 2375 to 733 mg/L. This indicates that magnetite recycling from the effluent was not complete, which could be related to the increase in biomass concentration (measured as volatile suspended solids (VSS)) as a result of magnetite recycling (Fig. 5-7). Cells aggregated with magnetite should be captured by magnetic separation and recovered with magnetite from the effluent (Fig. 5-2). In this case, an increase in biomass concentration beyond a certain level may limit the effectiveness of magnetite separation using a fixed magnetic setting. Also, the conditioning film could be formed on the surface of magnetite by the adsorption of organic matters and it is known to encourage primary biofilm formation by providing suitable environment for biological attachment [117]. This may cause a continuous, gradual loss of magnetite from the system owing to the decreased electrical conductivity. Another possibility is handling loss during sampling, separation, resuspension, and reinjection, which may result in significant magnetite loss over time. Given that RC was suddenly upset with a continuous loss of magnetite by washout (Fig. 5-3 and Table 5-2), maintaining a magnetite concentration above a certain threshold in the mixed liquor appears to be important for process stability. These observations suggest the need for further studies to determine the threshold concentration of magnetite and avoid its loss during long-term continuous operation.

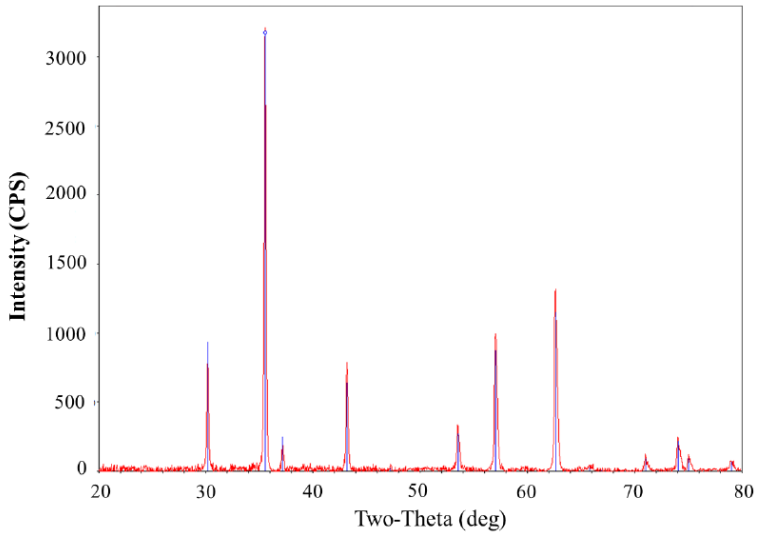

Fig. 5-6. XRD spectra of the reactor digestate sample from RM on day 317. The spectrum of pure magnetite (red line) is shown for reference.

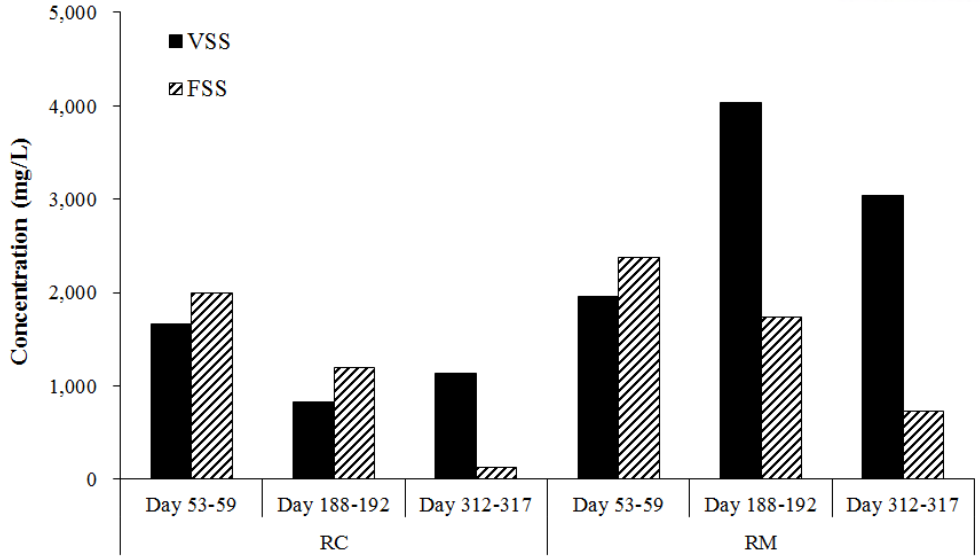

Fig. 5-7. Changes in volatile suspended solid and fixed suspended solid concentrations in the reactors (VSS, volatile suspended solids; FSS, fixed suspended solids).

5-3-3. Effect of biomass retention

The results presented above suggest that magnetite particles formed aggregate structures with cells and promoted DIET by bridging cell connections owing to their conductive nature [47, 48]. The formation of complex biomass-magnetite aggregates made an interesting contribution to biomass retention in the reactors. By recycling magnetite, active biomass involved in the aggregate structures should also be recovered and recycled to the reactor. This can help retain a high biomass density so as to increase solids retention time (SRT), which can be achieved by a sequencing batch operation. The effect of biomass recycling is well reflected in the differences in VSS concentrations between the experimental reactors (Fig. 5-7). The VSS concentration in RM increased significantly (up to 2.1-fold) after the start of magnetite recycling and remained at a much higher level (2.7–4.8-fold) than that in RC. It is notable that, corresponding to the enhanced biomass retention, MPR and Y_M increased by 18.4% and 15.5%, respectively, in RM (Table 5-2). The decreased levels of VSS, MPR, and Y_M in RM toward the end of the experiment can be attributed to the loss of magnetite and, in turn, biomass and DIET activity over the course of the experiment.

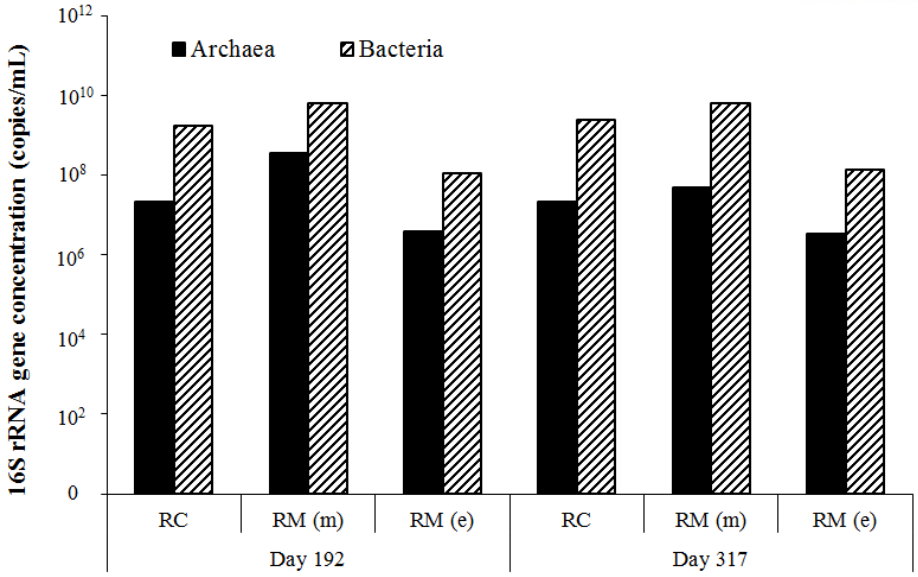

Fig. 5-8. Archaeal and bacterial 16S rRNA gene concentrations in reactor biomass samples (m, mixed liquor; e, effluent).

Enhanced biomass retention by magnetite recycling is further supported by the real-time PCR results. On both days 192 and 317, RM retained markedly higher bacterial (2.8–3.4-fold) and archaeal (2.2–15.5-fold) abundance, measured as 16S rRNA gene concentration in the mixed liquor, compared to RC (Fig. 5-8). Additionally, the determination of the microbial population in the RM effluent after magnetite separation indicated significantly lower levels of bacteria (48.7–54.6-fold) and archaea (14.4–91.9-fold) than in the RM mixed liquor. This indicates that a significant portion of biomass washed out from the reactor was recycled together with magnetite by magnetic separation. Slow-growing microbes can take more direct advantage of an increase in SRT, and microbial diversity is generally higher for longer SRTs. The remarkable emergence of filamentous forms after a long period of magnetite recycling in RM (Fig. 5-5) is also attributable to the enhanced biomass retention, given that filamentous microbes often have lower specific growth rates than non-filamentous ones. Filamentous *Methanosaeta* species, primarily responsible for converting acetic acid to methane, have very long doubling times of several days [118]. Extended retention of biomass may have helped such slow-growing microbes flourish in abundance over time in the reactor. A previous study had attempted to use magnetic foam glass particles as biofilm carrier coupled with their magnetic separation for enhanced biomethanation [119]. However, the authors used an artificially structured support material for biofilm development and did not look into the potential effect on DIET activity, in contrast to the present study, which introduces a novel and convenient approach based on the self-aggregation of microbial cells and magnetite particles.

5-3-4. Microbial community structure and activity

For deeper insight into the underlying ecology, 16S rRNA gene-targeted NGS analysis was performed at the RNA (i.e., cDNA) as well as the DNA levels on four reactor samples: RC day-192 mixed liquor, RC day-317 mixed liquor, RM day-317 mixed liquor, and RM day-317 effluent. Samples were taken before the termination of magnetite supplementation to RC (day 192) and at the end of the experiment (day 317) to assess the influence of magnetite on the microbial communities in the reactors. It is generally accepted that DNA- and RNA-based community analyses reflect the abundance and the metabolic activity of individual microbial populations in a community, respectively [120, 121]. A total of 169,374 reads (93,260 for DNA- and 76,114 for RNA-based analyses) were produced and classified into 227 OTUs (13 archaeal and 207 bacterial OTUs). Taxonomic affiliations of major OTUs (>2% of the total bacterial or archaeal reads in at least one sample) are presented in Table 5-3.

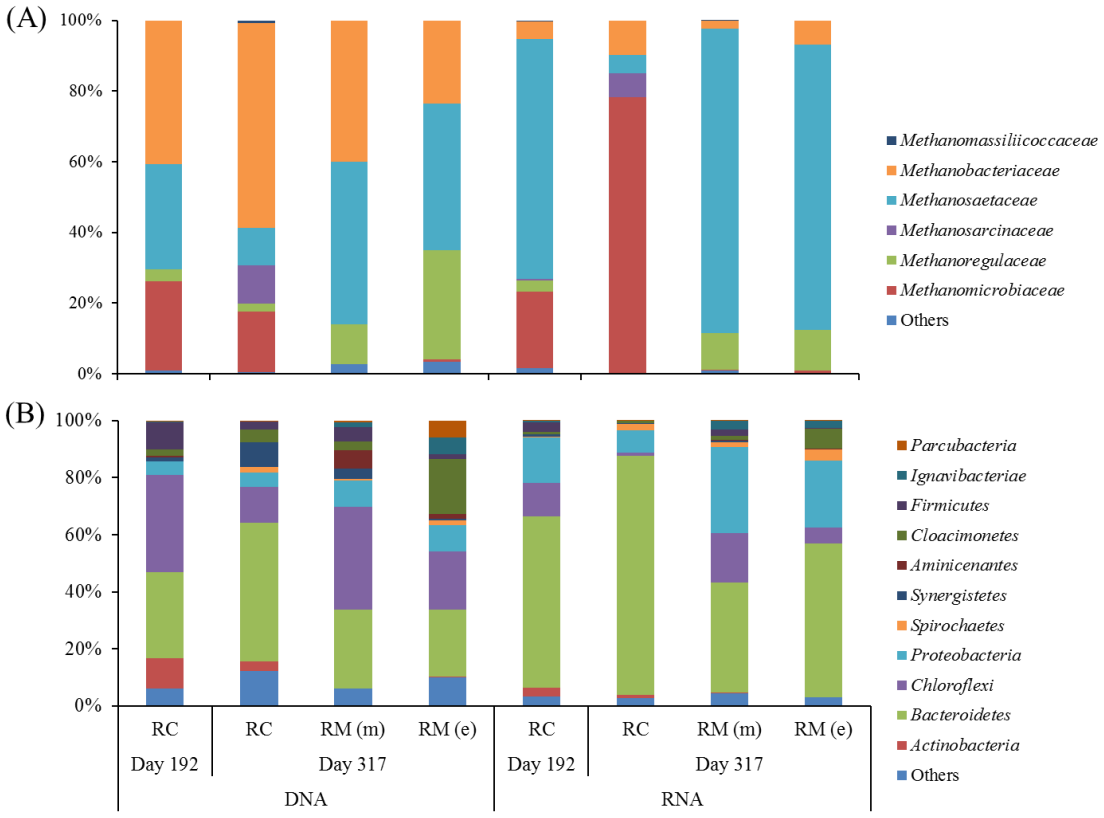

Fig. 5-9. Relative distribution of archaeal (A) and bacterial (B) sequences in the 16s rRNA libraries for each reactor biomass sample (m, mixed liquor; e, effluent)

Table 5-3 Relative abundance and taxonomic affiliation of major OTUs (>2% of the total bacterial or archaeal readings in at least one sample)[a].

	OTU no.	Nearest taxon	Similarity (%)	16S rRNA gene libraries[b]				16S rRNA libraries[b]				Accession no.	Classification[c]
				RC-192	RC-317	RM-317m	RM-317e	RC-192	RC-317	RM-317m	RM-317e		
Archaea	a1	*Methanosaeta concilii*	98.3	13.9	3.6	38.0	34.5	49.3	4.9	71.4	72.8	KM408635	*Methanosaeta*
	a2	*Methanolinea tarda*	96.9	2.3	0.8	6.8	27.2	3.0	0.0	9.4	11.1	KP109880	*Methanolinea*
	a3	*Methanosaeta harundinacea*	98.3	15.8	7.1	8.1	7.1	18.7	0.2	14.7	7.9	CP003117	*Methanosaeta*
	a4	*Methanobacterium beijingense*	97.6	39.3	46.9	36.4	22.4	5.0	7.9	2.2	6.6	KP109878	*Methanobacterium*
	a5	*Methanoculleus receptaculi*	98.3	25.2	17.2	0.0	0.7	21.7	78.3	0.2	0.7	NR043961	*Methanoculleus*
	a6	Clone OAS_33-8	98.3	1.1	1.4	4.3	3.5	0.3	0.0	1.2	0.4	LC108820	*Methanoregulaceae*
	a7	*Methanobacterium formicicum*	98.3	1.0	10.7	1.0	0.3	0.0	1.7	0.0	0.0	KX344121	*Methanobacterium*
	a8	*Methanobacterium subterraneum*	99.0	0.4	0.4	2.7	0.8	0.0	0.2	0.1	0.4	KY684741	*Methanobacterium*
	a9	*Methanosarcina mazei*	98.2	0.0	10.8	0.0	0.0	0.3	6.7	0.0	0.0	KX826992	*Methanosarcina*
Bacteria	b1	*Parabacteroides chartae*	99.0	14.3	37.3	0.8	4.2	33.3	59.9	3.0	11.7	NR109439	*Parabacteroides*
	b2	Clone D12	99.0	9.6	0.0	19.0	3.1	4.9	0.0	12.1	4.6	KR003431	*Bacteroidetes*
	b3	Clone SSOTU85	99.0	27.3	7.8	19.9	8.8	8.2	0.6	7.3	1.8	HM346756	*Chloroflexi*
	b4	Clone GZKB119	99.0	4.7	0.1	4.0	4.9	19.7	0.0	14.2	15.8	AJ853611	*Flavobacteriales*
	b5	*Ca.* Cloacamonas acidaminovorans[d]	99.0	2.3	1.2	3.2	19.2	0.7	0.3	1.5	7.1	CU466930	*Ca.* Cloacamonas
	b6	Clone 4D-F	99.0	0.0	4.2	0.0	0.0	0.0	12.9	0.3	0.3	JX843997	*Bacteroidetes*

b7	*Petrimonas mucosa*	97.6	0.2	0.1	1.3	10.2	0.6	0.1	3.1	18.9	LT608328	*Porphyromonadaceae*
b8	*Geobacter hephaestius*	97.9	0.4	0.4	0.3	0.1	5.2	1.9	4.6	0.5	AY737507	*Geobacter*
b9	*Atopobium parvulum*	94.5	10.5	3.2	0.0	0.0	2.9	1.2	0.0	0.0	KU851139	*Atopobium*
b10	Clone WWB10	99.6	4.7	7.2	0.1	0.0	1.7	0.6	0.2	0.0	KX255714	*Bacteria*
b11	*Saccharofermentans acetigenes*	95.9	6.4	0.0	0.2	0.1	2.8	0.0	0.2	0.0	NR115340	*Saccharofermentans*
b12	*Smithella propionica*	98.3	0.1	0.0	2.3	0.3	0.8	0.0	10.8	0.8	NR024989	*Smithella*
b13	Clone EMTBioanoB-6	98.6	1.0	8.6	3.5	0.4	0.4	0.1	0.5	0.0	KM819496	*Synergistaceae*
b14	Clone ORSFAM_g01	98.3	0.1	0.0	6.6	0.8	0.0	0.0	4.5	0.7	EF393281	*Chloroflexi*
b15	Clone 7N186hH15	97.9	0.6	1.8	3.4	3.3	0.2	0.0	1.5	0.7	KJ854102	*Chloroflexi*
b16	Clone EGSB_20_2-25	98.6	0.0	0.0	1.1	4.5	0.0	0.0	2.6	2.3	KJ881299	*Ignavibacterium*
b17	*Serratia* sp. HPPRK4	99.0	1.8	0.2	0.2	1.5	0.6	0.1	1.4	5.4	KU605754	*Serratia*
b18	Clone Pav-121	98.3	0.5	0.0	6.2	1.8	0.1	0.0	0.3	0.2	DQ785307	*Aminicenantes* gis[e]
b19	Clone QEEB3AA02	96.6	0.0	0.0	1.6	3.9	0.0	0.0	0.3	1.2	CU917606	*Bacteria*
b20	Clone B30_129	98.3	0.1	0.5	0.5	1.8	0.3	0.5	1.6	3.9	KP258901	*Spirochaetaceae*
b21	*Pseudomonas fluorescens*	98.6	0.2	0.7	0.1	1.7	0.1	1.6	0.8	5.9	KY458552	*Pseudomonadaceae*
b22	Clone OTU-BMAR60-8	98.6	0.3	0.3	0.5	5.8	0.0	0.0	0.0	0.1	KF493719	*Parcubacteria* gis
b23	Clone B6_178	98.6	2.1	0.1	1.7	3.9	0.5	0.0	0.5	0.7	HQ689282	*Anaerolineaceae*
b24	Clone 1716	99.6	0.0	0.0	0.4	0.6	0.0	0.0	2.8	3.8	KX36762	*Syntrophobacteraceae*
b25	Clone P-24	99.0	0.0	0.1	0.7	0.2	0.1	0.3	3.3	0.2	KC011442	*Bacteroidetes*

b26	*Syntrophobacter sulfatireducens*	99.0	0.1	0.0	1.2	0.1	0.1	0.0	3.0	0.2	NR043073	*Syntrophobacter*
b27	Clone OTU_330	99.3	0.0	3.3	0.0	0.0	0.0	0.5	0.0	0.0	LT624316	*Ca.* Cloacamonas
b28	*Geobacter pickeringii*	96.2	0.5	0.1	0.0	0.0	3.1	0.0	0.0	0.0	CP009788	*Geobacter*
b29	Clone 02d06	98.3	0.8	0.0	2.5	0.2	0.1	0.0	0.3	0.0	GQ138219	*Acidaminococcaceae*
b30	Clone NBBOT0308_39	98.6	0.0	2.2	0.0	0.0	0.0	1.5	0.0	0.0	JQ072419	Subdivision3 gis
b31	Clone NBLE311E	98.6	0.1	2.1	0.0	0.0	0.0	0.1	0.0	0.0	GU389857	*Veillonellaceae*

[a] OTUs, operational taxonomic units. Cells with relative abundance values are colored in a heatmap-like fashion: red for archaeal and blue for bacterial sequences.

[b] Labeled with the corresponding reactor name followed by the time of biomass sampling in days (m, mixed liquor; e, effluent).

[c] The lowest rank assigned by RDP Classifier at an 80% confidence threshold.

[d] *Ca.*, *Candidatus*.

[e] gis, genera *incertae sedis.*

The DNA-based analysis results show that the methanogen community structure in RC changed significantly between days 192 and 317. *Methanosarcinaceae*, not detected on day 192, emerged to account for 10.8% of the total archaea, while the relative abundance of *Methanosaetaceae* declined 2.8-fold (Fig. 5-9A). *Methanosarcinaceae* did not occur in the day-317 mixed liquor and effluent samples of RM, and *Methanosaetaceae* dominated the RM methanogen community. These aspects indicate that magnetite likely had a significant effect on the development of the methanogen community structure in the experimental reactors. Under stable conditions with magnetite supplementation or recycling (i.e., RC day-192 and RM day-317 samples), *Methanosaetaceae* occurred in high relative abundance, particularly in the RM samples. The significance of *Methanosaetaceae* as the major methanogen group responsible for methanogenesis was also confirmed at the RNA level. *Methanosaetaceae* dominated the 16S rRNA libraries (68.0–86.1%) in the RC day-192 and RM day-317 samples, suggesting that *Methanosaetaceae* was more actively involved in methanogenesis than other methanogens in the reactors. The fact that *Methanosaetaceae* with high substrate affinity often dominate methanogen communities under stable AD conditions with low residual VFA levels [108] supports this observation (Fig. 5-4). Although *Methanosaetaceae* is generally known as a strictly aceticlastic family, it has recently been reported that *Methanosaeta* species can reduce carbon dioxide to methane using electrons delivered from exoelectrogenic bacteria via DIET [122]. Therefore, *Methanosaetaceae* (OTU-a1 and -a3) appear to be involved in both DIET-based and aceticlastic methanogenesis in the experimental reactors. On the other hand, *Methanobacteriales* dominated the reactor methanogen community (58.0%) under imbalance conditions without magnetite available (i.e., RC day-317 sample). This could be related to the accumulation of VFAs, particularly propionic acid, at the end of the experiment in RC (Fig. 5-4), given that hydrogen from the syntrophic oxidation of propionic acid can support the growth of hydrogenotrophic methanogens. It is notable that *Methanomicrobiales* accounted for 78.3% of the 16S rRNA library from the RC day-317 sample, suggesting that *Methanomicrobiales* was more metabolically active than other methanogens around day 317 in RC. It therefore appears that *Methanomicrobiales* (particularly OTU-a5) likely contributed most to the methanogenic activity, although *Methanobacteriales* was numerically more abundant, possibly owing to its faster growth rate compared to *Methanomicrobiales* [122], when RC was imbalanced toward the end of the experiment.

The bacterial community structure was much more diverse than the archaeal community structure in the analyzed biomass samples (Fig. 5-9B). The retrieved bacterial 16S rRNA gene sequences belonged to 24 known phyla, with part of the total sequences (3.1–7.5%) being classified as unknown. The phyla with relative abundances lower than 1% in all samples were classified as “Others” in Fig. 5-9B. *Bacteroidetes*, *Chloroflexi*, and *Proteobacteria*, frequently observed in abundance in mesophilic AD environments, commonly occurred as major bacterial phyla in the 16S rRNA gene libraries. They also accounted for the majority in the 16S rRNA libraries from the reactor samples (>82.0%). Notably, these major phyla responded differently to the presence of magnetite. The relative 16S rRNA abundance of *Bacteroidetes* was apparently higher (1.4–2.2-fold) in the

RC day-317 sample collected under magnetite-depleted conditions, while contrarily, those abundances of *Proteobacteria* and *Chloroflexi* were much higher (2.2–3.9-fold and 11.7–17.3-fold, respectively) in the RC day-192 and RM day-317 samples collected under magnetite-stimulated conditions. This suggests that *Proteobacteria* (particularly OTU-b8, -b12, -b17, -b24, -b26, and -b28) and *Chloroflexi* (particularly OTU-b3, -b14, -b15, and -b23) populations were likely involved in DIET via magnetite particles for CO_2-reducing methanogenesis in the experimental reactors. A putative role of *Chloroflexi* as electroactive bacterial partner in DIET has also been reported in previous studies [111, 123]. *Geobacter* species and their relatives, which are well-known exoelectrogenic bacteria, belong to the class *δ-Proteobacteria*, which occupied most of the total *Proteobacteria* sequences (>82.3%) in the 16S rRNA libraries from the RC day-192 and RM day-317 samples (data not shown). These observations further support the notion that magnetite likely stimulated the activity of electroactive microbes, thus changing the microbial community structure and activity. Another point to note is that these phyla, whose members appear to be involved in DIET, showed higher relative metabolic activity (i.e., higher relative 16S rRNA abundance) in the mixed liquor biomass (cell-magnetite aggregates; Fig. 5-5) than in the effluent biomass (magnetite-free cell flocs) sampled on day 317. This implies that putatively electroactive *Proteobacteria* and *Chloroflexi* populations were more metabolically active in terms of physical attachment to magnetite particles [91].

Archaeal and bacterial cluster dendrograms constructed based on the OTU distribution in the 16S rRNA gene and 16S rRNA libraries are shown in Fig. 5-10. As apparent in the phylum distribution (Fig. 5-9), the DNA- and RNA-based analyses produced different clustering patterns for both archaeal and bacterial communities. The RNA-based analysis results for archaeal and bacterial communities showed similar clustering patterns, where the RC day-317 library was very remotely related (Sorensen similarity <0.4) to the other relatively closely related libraries, with the RM day-317 mixed liquor and effluent libraries being most closely clustered. These clustering patterns are well associated with the process performance data and operating conditions (Tables 5-1 and 5-2). On the other hand, compared to in the RNA-based clustering patterns, variations in process performance were not well reflected in the DNA-based clustering patterns, although the RC day-317 library was also distantly related to the RM day-317 mixed liquor library. The RNA-based cluster analysis appears to provide a more relevant picture of the correlation between microbial communities and reactor performance. This is attributable to the fact that microbial communities first respond to environmental stimuli at the activity level followed by the population level, whose influence could be particularly pronounced for slow-growing microbes such as methanogens [121].

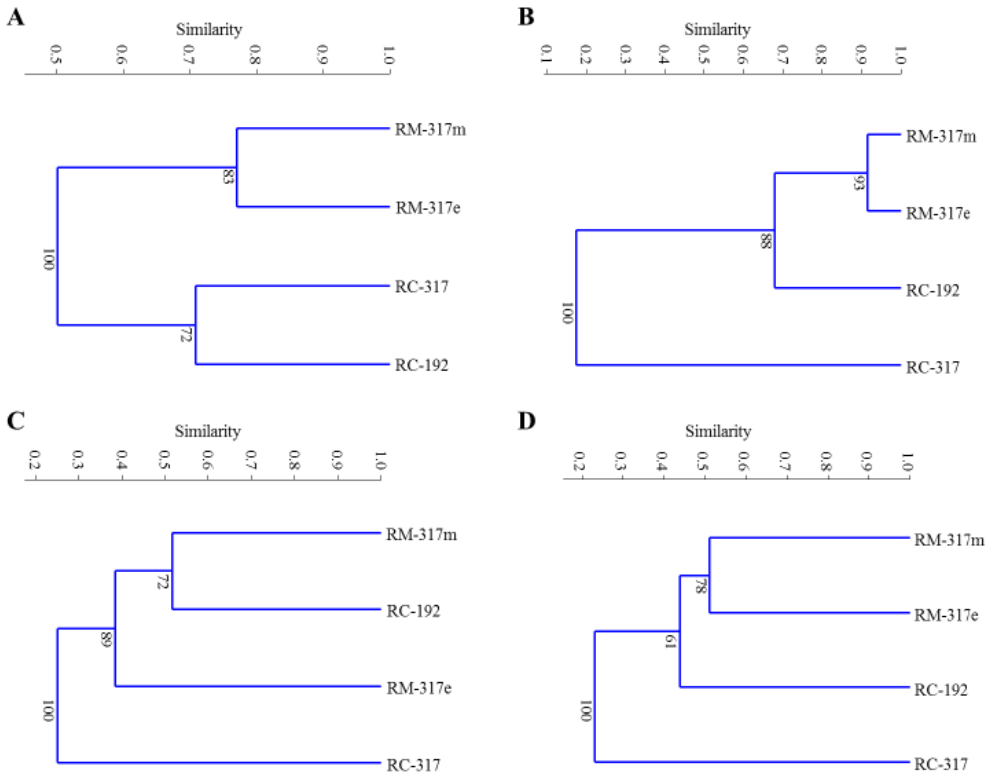

Fig. 5-10. Cluster dendrograms generated based on the OTU distribution in the archaeal 16S rRNA gene (A) and 16S rRNA (B) libraries and the bacterial 16S rRNA gene (C) and 16S rRNA (D) libraries

5-3-5. Bacterial populations involved in interspecies electron transfer

Fig. 5-11 shows the relative abundances of *Geobacter*, *Smithella*, and *Syntrophobacter*, which are well-known *δ-proteobacterial* genera involved in IET under anaerobic conditions, in the 16S rRNA gene and 16S rRNA libraries. *Geobacter* is a representative exoelectrogenic genus and has been reported to perform DIET using different conductive materials, including magnetite, as electrical conduits to provide electrons for CO_2-reducing methanogenesis [22, 41, 124]. Notably, the relative metabolic activity of *Geobacter* was significantly higher (2.4–4.2-fold higher relative 16S rRNA abundance) in the RC day-192 and RM day-317 mixed liquor samples than in the RC day-317 sample. This supports the notion that magnetite likely promoted the activity of DIET-associated microbes and, in turn, enhanced the methanogenic performance in the experimental reactors. A recent study reported the formation of a DIET relationship between *Geobacter* and *Methanosaeta* for the reduction of CO_2 to methane [27]. Given that *Methanosaetaceae* was the most metabolically active methanogen group when magnetite was available (Fig. 5-9), the reactor microbial communities could develop an electric syntrophy in the presence of magnetite.

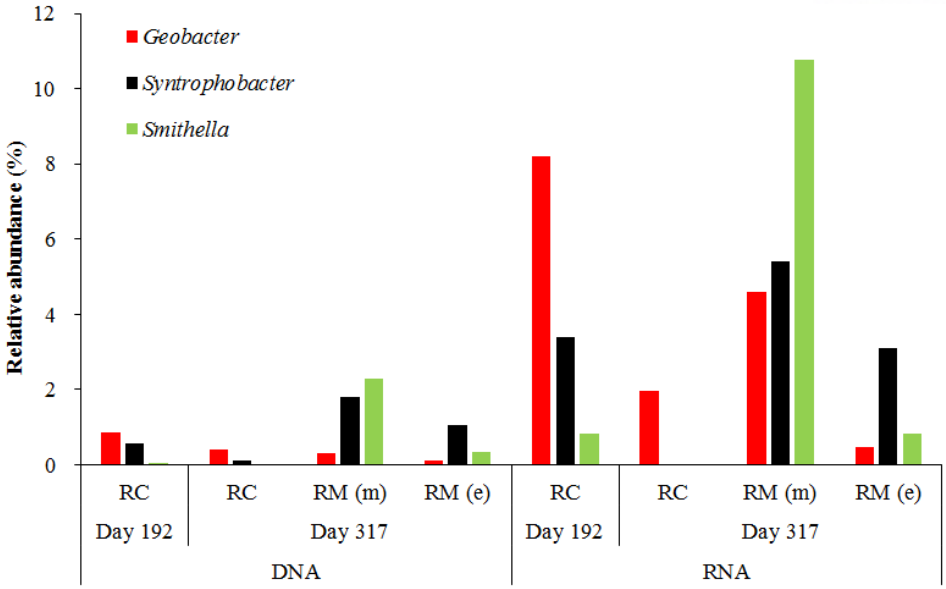

Fig. 5-11. Relative abundance of representative interspecies electron transfer-associated bacteria in the 16S rRNA gene and 16S rRNA libraries for each reactor

Both *Smithella* and *Syntrophobacter* can grow on propionate in syntrophic association with methanogens for growth [125]. These syntrophic propionate oxidizers require hydrogen-consuming partners to keep the hydrogen partial pressure low enough for propionate oxidation to be thermodynamically favorable. This may explain their extremely low population and activity levels in the RC day-317 sample, when the system was severely imbalanced owing to a buildup of propionate. Although *Smithella* and *Syntrophobacter* play significant roles in hydrogen-mediated IET to hydrogenotrophic methanogens, their participation in DIET has not been reported so far and has been suggested to be unlikely in previous studies [124, 126]. Therefore, their high metabolic activity in the RC day-192 and RM day-317 samples may indicate that magnetite promotes the activity of microbes involved in indirect as well as direct IET in the long term. However, it should be noted that *Methanosaetaceae*, which cannot utilize hydrogen, was the most metabolically active methanogen group in those samples, with hydrogenotrophic methanogens being of relatively minor importance. This implies that the syntrophic propionate-oxidizing populations might be somehow associated with DIET via magnetite in the experimental reactors.

5-4. Summary

Magnetic separation and recycling of effluent magnetite was investigated in an attempt to support magnetite-promoted DIET in a continuous AD process without adding extra magnetite. The proposed magnetite recycling method proved effective in maintaining enhanced DIET and methanogenic activities during a long-term operation (>250 days). Magnetite recycling helped retain a high biomass density (i.e., increased SRT) by

returning active biomass aggregated with magnetite to the reactor. *Methanosaeta* was likely the major methanogen group responsible for the DIET-based methanogenesis. DIET via magnetite particles as electrical conduits was likely the main mechanism for the enhancement of biomethanation performance and stability.

6. (STUDY 4) INDIVIDUAL AND COMBINED EFFECTS OF MAGNETITE ADDITION AND EXTERNAL VOLTAGE APPLIDAION ON ANAEROBIC DIGESITON

6-1. Introduction

Adding a conductive material is a simple and effective method to promote DIET in AD; its positive effect on the process performance has been demonstrated in Study 1–3 and other previous studies using conductive materials such as magnetite [41, 47, 111, 127], activated carbon [40, 128-130], biochar [39, 124], and carbon fibers [131, 132]. Conductive material likely serves as a conduit for electron flow between electroactive syntrophic partners. Early studies on this phenomenon were mostly performed using defined culture media with simple substrates to confirm the effect of DIET via conductive materials (mDIET). Increasingly, studies have attempted to accelerate methanogenesis by promoting mDIET in mixed cultures treating real wastewater [132-134]. Another, more direct way to promote DIET in a digester is applying an external voltage through electrodes submerged in the mixed liquor, which results in a reactor configuration similar to a single-chamber microbial electrolysis cell (MEC). Although MEC is basically a system for hydrogen evolution, methane is also produced by electromethanogenesis in MECs with biocathodes [86, 135]. Electromethanogenesis involves DIET via anodic oxidation of organic matter by exoelectrogenic bacteria coupled with cathodic reduction of CO_2 to CH_4 by electrotrophic methanogens. A beneficial effect of the stimulation of electromethanogenesis by applying external voltage on the AD performance has been reported [136-138].

Increasing efforts are being made to more effectively promote DIET in AD processes by adding highly conductive materials with large specific surface area, such as nano-sized graphene [139, 140] and carbon nanotube [141], or by improving the electrochemical properties of electrodes by coating with conductive catalysts [142, 143]. However, although previous studies have promoted DIET by adding conductive material or by applying external voltage, few have considered their combined effect. To fill this gap, this study investigated the individual and combined effects of magnetite addition and external voltage application using graphite felt electrodes in lab-scale continuous digesters treating dairy wastewater. The particle size of the magnetite used (100–700 nm) was small enough to aggregate with microbial cells and enter the porous structure of the electrodes; as such, the structure and electrochemical properties of the electrode biofilms could be influenced by the magnetite particles. For more comprehensive insight into the behavior of digester microorganisms, changes in microbial community structure and in AD performance under different DIET-promoting conditions were analyzed. The findings of this study provide better understanding of the effects of different DIET-promoting strategies on AD performance.

6-2. Materials and methods

6-2-1. Bioreactor operation

Four identical continuously stirred anaerobic digesters with a 2-L working volume, namely RC (without magnetite addition and external voltage application), RM (with magnetite addition only), RE (with external voltage application only), and RME (with magnetite addition and external voltage application), were operated on cheese whey, a dairy wastewater. The digesters were inoculated with anaerobic sludge from a biogas plant treating sewage sludge and fed with diluted cheese whey (5 g/L as soluble chemical oxygen demand [sCOD]) supplemented with 400 mg/L NH_4Cl to avoid process deterioration due to nitrogen depletion [111]. The basic physicochemical characteristics of the inoculum and substrate are shown in Table 6-1. A low inoculation ratio of 0.5% (v/v) was employed to avoid excessive growth of predominant populations and to more clearly observe the influence of different operating conditions on the development of microbial communities. The digesters were first run in repeated batch mode for four cycles for microbial acclimation and enrichment before continuous daily feeding of the substrate.

RM and RME were continuously supplemented with magnetite (particle size, 100–700 nm) by amending the substrate to achieve a final Fe concentration of 20 mM. RE and RME were equipped with two graphite felt electrodes of the same dimension (2 × 7 × 1 cm, specific area = 0.868 m^2) connected with a titanium wire. A constant voltage of 0.6 V was applied between the electrodes using a potentiostat (WMPG1000S, WonATech, Korea) while continuously monitoring the current at 10-min intervals. In RM, RE, and RME, magnetite addition and/or external voltage application were started immediately after inoculation. The digesters were operated at decreasing hydraulic retention times (HRTs) from 20 to 7.5 days. The time period and operating conditions for each experimental phase are presented in Fig. 6-1. All digesters were maintained at pH 7.0 and 35°C throughout the experiment with an automatic pH and temperature control systems. Each digester was continuously mixed with an overhead stirrer at 150 rpm.

Table 6-1. Physicochemical characteristics of inoculum and substrate

Parameter	Unit	Anaerobic sludge	Cheese whey
Total COD	mg/L	24,230 (629)[a]	5,519 (12)
Soluble COD	mg/L	1,254 (314)	4,859 (24)
Total solids	mg/L	30,400 (283)	5,100 (141)
Total volatile solids	mg/L	17,300 (424)	4,800 (283)
Total suspended solids	mg/L	25,500 (236)	700 (141)
Volatile suspended solids	mg/L	15,667 (0)	800 (0)

[a] Standard deviations are in parentheses.

	Operating conditions (HRT/Magnetite addition/External voltage application)					
Period	Day 0–93	Day 94–303	Day 304–433	Day 434–503	Day 504–581	Day 582–631
RC	20/No/No	20/Yes/No			12.5/Yes/No	7.5/Yes/No
RM	20/Yes/No	15/Yes/No		12.5/Yes/No	10/Yes/No	7.5/Yes/No
RE	20/No/Yes	15/No/Yes	12.5/No/Yes		12.5/Yes/Yes	7.5/Yes/Yes
RME	20/Yes/Yes	15/Yes/Yes	12.5/Yes/Yes	10/Yes/Yes	7.5/Yes/Yes	

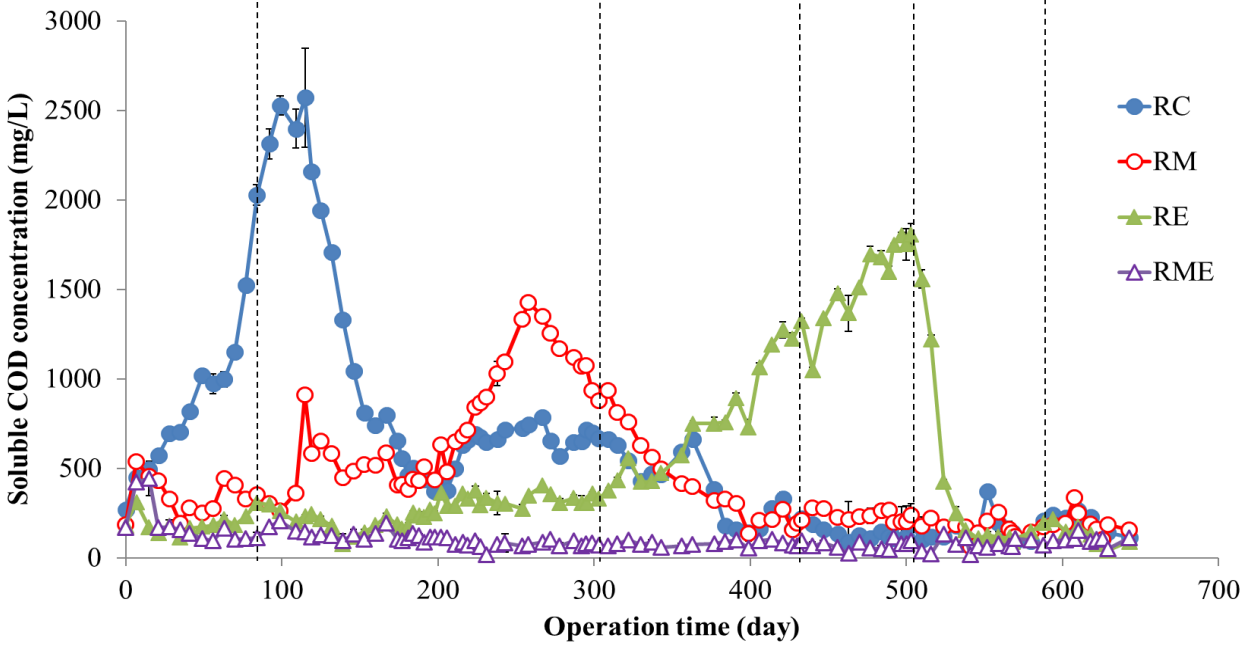

Fig. 6-1. Digester operating conditions and changes in residual soluble chemical oxygen demand (COD) concentration over the experimental phases.

6-2-2. Fluorescence in situ hybridization

One milliliter of the digester mixed liquor sample (RME at an HRT of 7.5 days) for fluorescence in situ hybridization (FISH) analysis was washed three times with PBS followed by overnight fixation in 1 mL of 4% paraformaldehyde at 4°C in a tube. The fixed samples were washed twice with PBS and loaded onto a slide, followed by dehydration in an ethanol series of increasing concentrations (50%, 80%, and 100%) for 3 min each. The dried samples were incubated in 10 μL of hybridization buffer (0.9 M NaCl, 0.01% sodium dodecyl sulfate, 20 mM Tris-HCl, pH 7.2, and 35% formamide) with oligonucleotide probes (50 ng/μL each) at 46°C for 1.5 h. The hybridization buffer was then replaced with washing solution (200 mM NaCl, 0.01% sodium dodecyl sulfate, 20 mM Tris-HCl, pH 7.2, and 5 mM EDTA), and then incubated at 48°C for 20 min. The samples were further washed with distilled water and suspended in 50% (v/v) glycerol solution before microscopic observation [144]. The FISH images were acquired using a Nikon Eclipse Ci-L microscope (Japan) equipped with a Nikon Intensilight C-HGFI fluorescent lamp (Japan) and a Nikon DS-Fi3 camera. Two fluorescently labeled oligonucleotide probes, *Geobacter*-specific GEO825 (5'-TACCCGCRACACCTAGT-3') and *Methanothrix*-specific MX825 (5'-TCGCACCGTGGCCGACACCTAGC-3') probes, with TAMRA and FAM, respectively [138], were used to hybridize samples.

6-2-3. Energy efficiency calculation

The energy efficiency relative to electrical input and the energy in the substrate recovered as methane (EE) were calculated using the modified equation of a previous study [145]:

$$\mathrm{EE} = \frac{\mathrm{n_m}\Delta G_m}{\int_0^{\mathrm{t}} \mathrm{I}E_{ap}\mathrm{dt} + \mathrm{COD_{fed}}Y_m\Delta G_m} \qquad (6-1)$$

where n_m is the number of moles of CH_4 in the collected biogas, ΔG_m is a molar Gibbs free energy of CH_4 oxidation by oxygen to carbon dioxide (−817.97 kJ/mol), I is the current intensity, E_{ap} is the applied voltage between electrodes, COD_{fed} is the concentration of COD in the influent substrate and Y_m is a theoretical CH_4 yield (mol CH_4/g COD).

6-3. Results

6-3-1. Anaerobic digestion performance

To compare AD performance and stability among four digesters, hydraulic loading was gradually

increased with periodic monitoring of organic removal and methane production efficiencies. Changes in operating conditions such as HRT, magnetite addition, and external voltage application throughout the experimental period are presented in Fig. 6-1 RC failed to reach a steady state at 20-day HRT, while the other digesters achieved stable performance. With the rapid accumulation of sCOD in RC, acetate and propionate were detected as the major VFA composition (Fig. 6-2), suggesting an imbalanced syntrophic relationship between acidogenic bacteria and methanogens [146]. RM deteriorated at an HRT of 15 days, showing serious performance deterioration (sCOD removal < 71.5%, methane yield < 0.218 L/g $sCOD_{fed}$; Table 6-2). With a further decrease in HRT to 12.5 day, RE also experienced imbalanced AD performance (sCOD removal < 64.5%, methane yield < 0.177 L/g $sCOD_{fed}$; Table 6-2). RME maintained nearly complete sCOD removal (> 97.3%) and high methane yield (> 0.262 L/g $sCOD_{fed}$) during all experimental phases, while the HRT was reduced to 7.5 days. These results suggest that RME was superior to the other digesters in maintaining stable and high AD performance under high hydraulic loading conditions.

The sCOD concentration in RM at HRT of 15 days was highly accumulated (up to 1429.6 mg/L) after 11 turnovers of the working volume. It is worth noting that RM recovered from the upset and showed stabilized performance (<274.8 mg/L) after another 10 volume turnovers at 15-day HRT without changing its operating conditions. Once restored, RM maintained stable AD performance comparable to that of RME at reduced HRTs of 12.5–7.5 days. Meanwhile, RC and RE did not recover from the performance deterioration, continuously showing serious sCOD and VFA accumulations at HRTs of 20 and 12.5 days, respectively. The difference in the behaviors of both digesters from RM can be attributed to the presence or absence of magnetite, which can promote mDIET between syntrophic partners involved in the anaerobic oxidation of fatty acids [41, 47, 111]. To verify the effect of mDIET stimulation on syntrophic VFA degradation and process stabilization, magnetite (20 mM as Fe) was added to the substrate for RC and RM from days 99 and 504, respectively. Despite the continuous mode operation without changing the operational conditions (i.e., without changing HRT), RC and RE showed rapid recovery of their methane-producing and VFA-degrading performances and reached a steady state. Their restored efficiencies were maintained at lower HRTs. After each digester was sufficiently stabilized at HRTs of 7.5–12.5 days (> 6 volume turnovers), a very short HRT of 7.5 days was applied to all digesters from day 582. From day 582 to the end of the experiment (day 634), all digesters maintained comparable stable AD performance in terms of sCOD removal (97.0%–98.5%) and methane yield (0.262–0.289 L/g $sCOD_{fed}$) for more than 8 volume turnovers. These results suggest that magnetite addition more significantly contributes to the recovery of AD performance and stability, although external voltage also had a beneficial effect on performance stability. Methane content in biogas measured in each steady-state period was always higher in digesters with voltage application (i.e., RE and RME) than without (i.e., RC and RM), regardless of magnetite application (Table 6-2). This may be attributable to electromethanogenesis by electrotrophic methanogens in the biocathode. Unlike RC and RM, electrons that are used for methane generation can be donated not only from the substrate but also from external voltage in RE and RME; therefore, extra methane production possibly

occurred via electromethanogenesis by CO_2 reduction in the biocathode [86].

Fig. 6-3 presents the volatile suspended solid (VSS) concentrations in the effluent. At the same HRT conditions, VSS concentrations in the presence of magnetite were always higher than those in the absence of magnetite. In addition, VSS concentration remained relatively constant or slightly increased despite the reduction in HRT in all digesters. These observations suggest that magnetite addition could improve microbial growth or biomass retention inside digesters.

EE values of four digesters obtained in each phase are shown in Fig. 6-4. Relatively lower EE values in RC at 20-day HRT and RE at 12.5-day HRT reflect the failure to achieve steady state. Except for these two phases, EE values among the digesters under the same HRTs were comparable. The EE values seem to be mainly determined by the differences among output energy by methane production, rather than input energy by external voltage application. Electrical energy input is much smaller than energy contained in the substrate (< 1.0% in all phases) or energy recovered as methane (< 1.2% in all phases). This suggests that external voltage application to the AD process does not bring a significant positive effect on methane and energy yield, although it can improve the stability and resilience of anaerobic digesters against decreasing HRTs (Fig. 6-1).

Table 6-2. Digester performance data

Reactor	Fe_3O_4 addition	Period	HRT	MPR [a]	Methane content	Y_M [b]	sCOD removal [c]
		Days	Day	mL/d	%	L/g COD_{fed}	%
RC	No [d]	0–93	20	47.3	71.9	0.095	60.9
	Yes	94–503	20	151.1	68.8	0.302	96.6
	Yes	504–581	12.5	241.3	68.2	0.302	97.8
	Yes	582–631	7.5	378.3	67.6	0.284	97.2
RM	Yes	0–93	20	136.8	70.0	0.276	93.4
	Yes	94–433	15	202.1	67.5	0.303	96.3
	Yes	434–503	12.5	254.4	68.2	0.318	95.7
	Yes	504–581	10	306.8	67.9	0.307	97.3
	Yes	582–631	7.5	385.4	67.7	0.289	97.0
RE	No	0–93	20	137.5	72.7	0.273	94.4
	No	94–303	15	212.1	68.1	0.318	93.4
	No [d]	304–503	12.5	140.5	74.4	0.176	64.4
	Yes	504–581	12.5	233.5	69.8	0.292	97.7
	Yes	582–631	7.5	352.2	70.8	0.264	98.5
RME	Yes	0–93	20	138.6	71.3	0.277	97.3
	Yes	94–303	15	199.0	71.0	0.298	98.4
	Yes	304–433	12.5	229.6	70.4	0.287	98.4
	Yes	434–503	10	288.6	71.0	0.289	98.3
	Yes	504–631	7.5	349.6	74.1	0.262	98.2

[a] MPR, methane production rate.

[b] Y_M, methane yield per COD fed (COD_{fed}).

[c] sCOD, soluble chemical oxygen demand.

[d] failed to reach steady state.

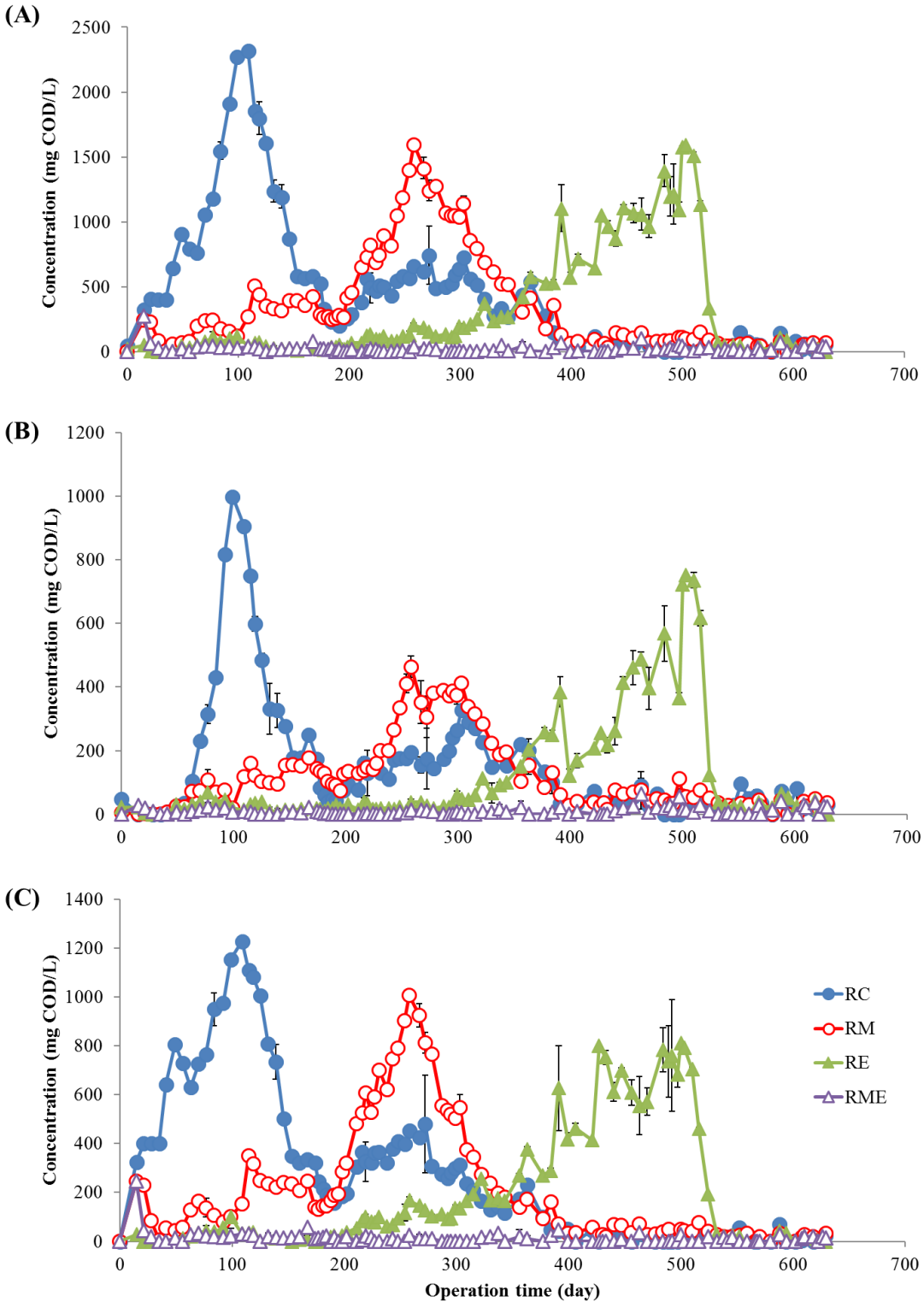

Fig. 6-2. Profiles in the residual concentrations of total volatile fatty acids (A), acetic acid (B), and propionic acid (C).

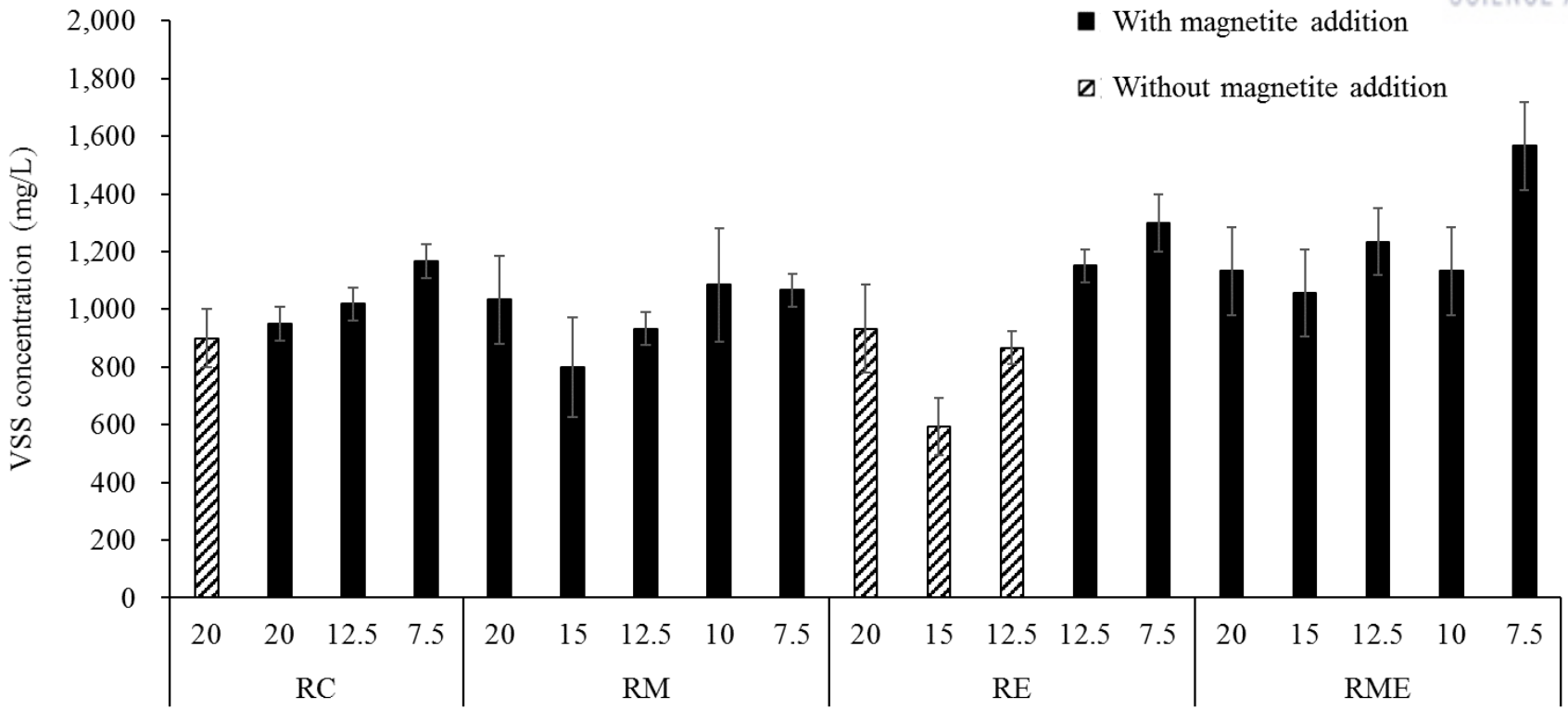

Fig. 6-3. Variations in volatile suspended solid (VSS) concentration in each digester over the experimental phases. The numbers on the x-axis represent the corresponding HRT.

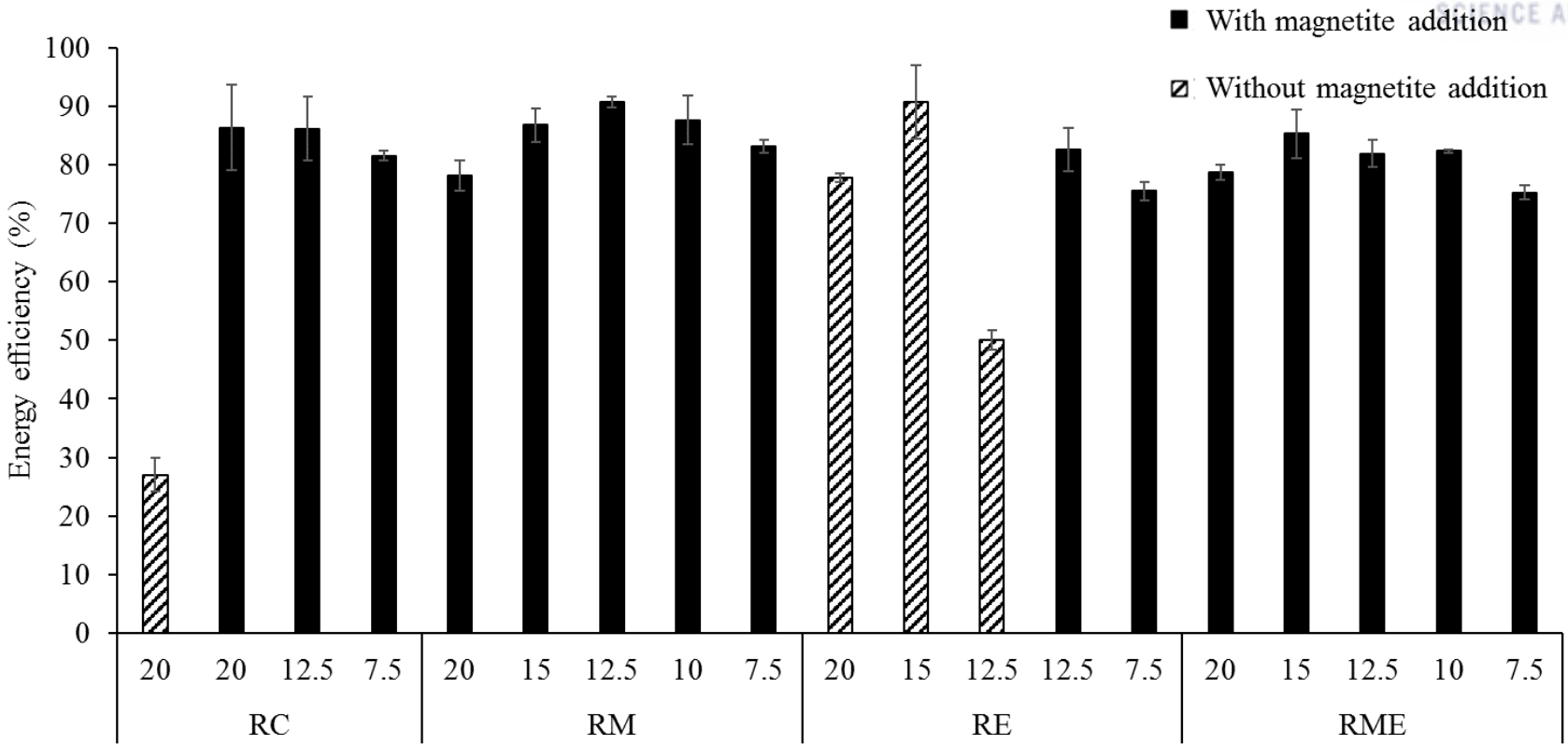

Fig. 6-4. Energy efficiency calculated in each experimental phase.

6-3-2. Morphology and composition of electrode biofilms

Pieces of the electrodes in RE and RME with biofilm were taken from the digesters for further analyses. Fig. 6-5 shows SEM observations of each sample collected on day 504. Various forms and sizes of microbial cells were colonized at the surface of the anode and cathode for both digesters. Much thicker biofilms formed at the electrodes in RME (Fig. 6-5C and 6-5D) compared with those in RE (Fig. 6-5A and 6-5B). This structure might be attributed to the agglomeration of magnetite particles with microbial cells in RME. Similar observations have been reported in previous studies, which presented aggregate structures between magnetite particles and cells in DIET-stimulated environments [47, 48, 133]. It is notable that the anode and cathode biofilms in RE are all of similar morphology and structure, while those in RME are totally different from each other. In RME, small granule-like structures (d = 5–10 μm) occur in the cathode biofilm, while the anode surface is totally covered by a thick layer of biofilm. Although the detailed mechanism remains unknown, magnetite significantly affected biofilm development and electrochemical reactions on the anode and cathode.

The anode and cathode biofilms in RME were further characterized using EDS mapping on day 504 (Fig. 6-6). Despite totally different biofilm structures, it was similarly observed that iron and oxygen showed remarkably higher density and intensity in the biofilm matrices than in the other regions of both electrodes. This result indicates that magnetite (Fe_3O_4) is embedded in the biofilm structure as a main component, along with microorganisms, and plays an important role in developing both anode and cathode biofilm structures. The XRD analysis results obtained from pieces of both electrodes in RE and RME at the end of the experiments (on day 631) also support this possibility. From, Fig. 6-7, all samples showed peak matching with reference peaks of pure magnetite, supporting the observation that magnetite was incorporated into biofilm matrices and existed in an original form without chemical transformation. Given that magnetite is a conductive iron oxide and that it is well distributed inside the biofilm, it promotes electron transfer between the electrode and electroactive microorganisms relatively distant from the electrode surface, as well as the DIET between electro-syntrophic partners [147].

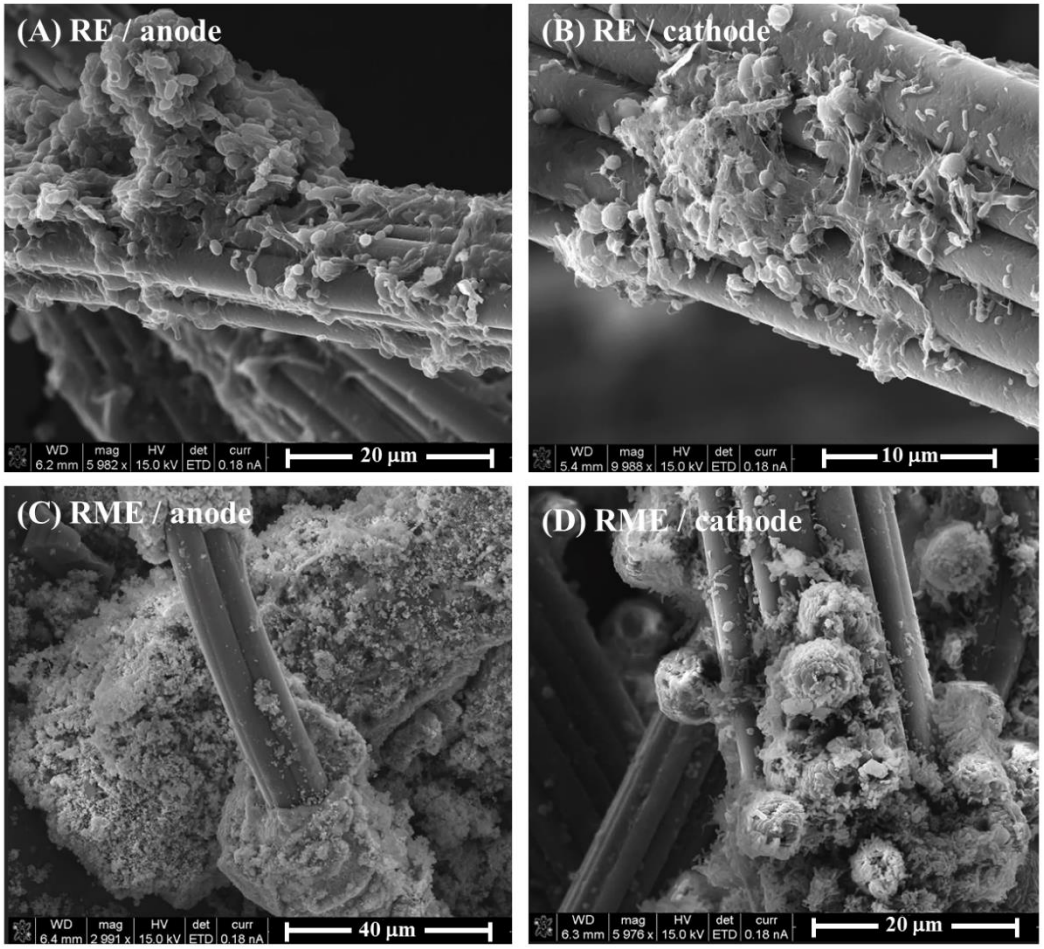

Fig. 6-5. Scanning electron microscopy images of anode (A, C) and cathode (B, D) in RE (anaerobic digester with external voltage application only) and RME (anaerobic digester with magnetite addition and external voltage application) on day 504.

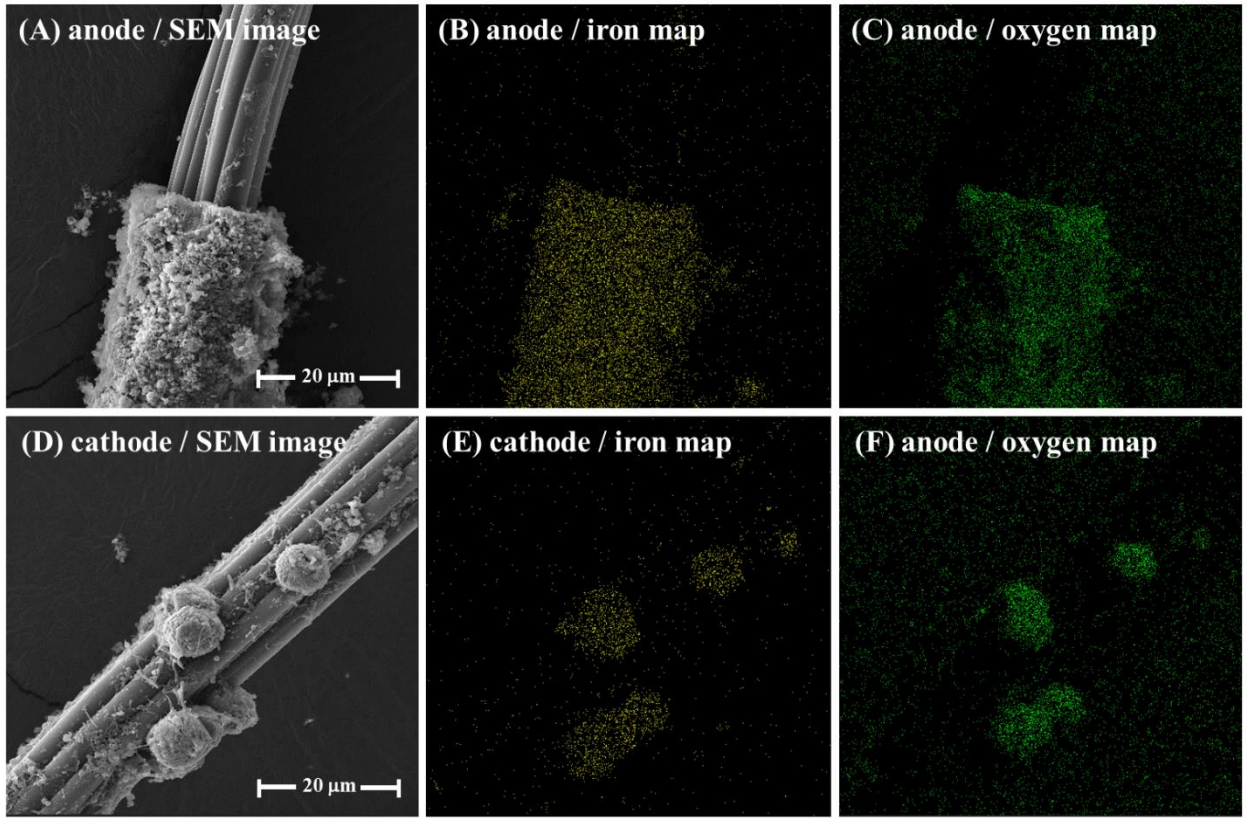

Fig. 6-6. Images of the RME (magnetite addition and external voltage applied) electrode on day 504. (A and D) Scanning electron microscopy images and (B, C, E, and F) energy dispersive X-ray spectroscopy mapping images (B and E for iron, C and F for oxygen).

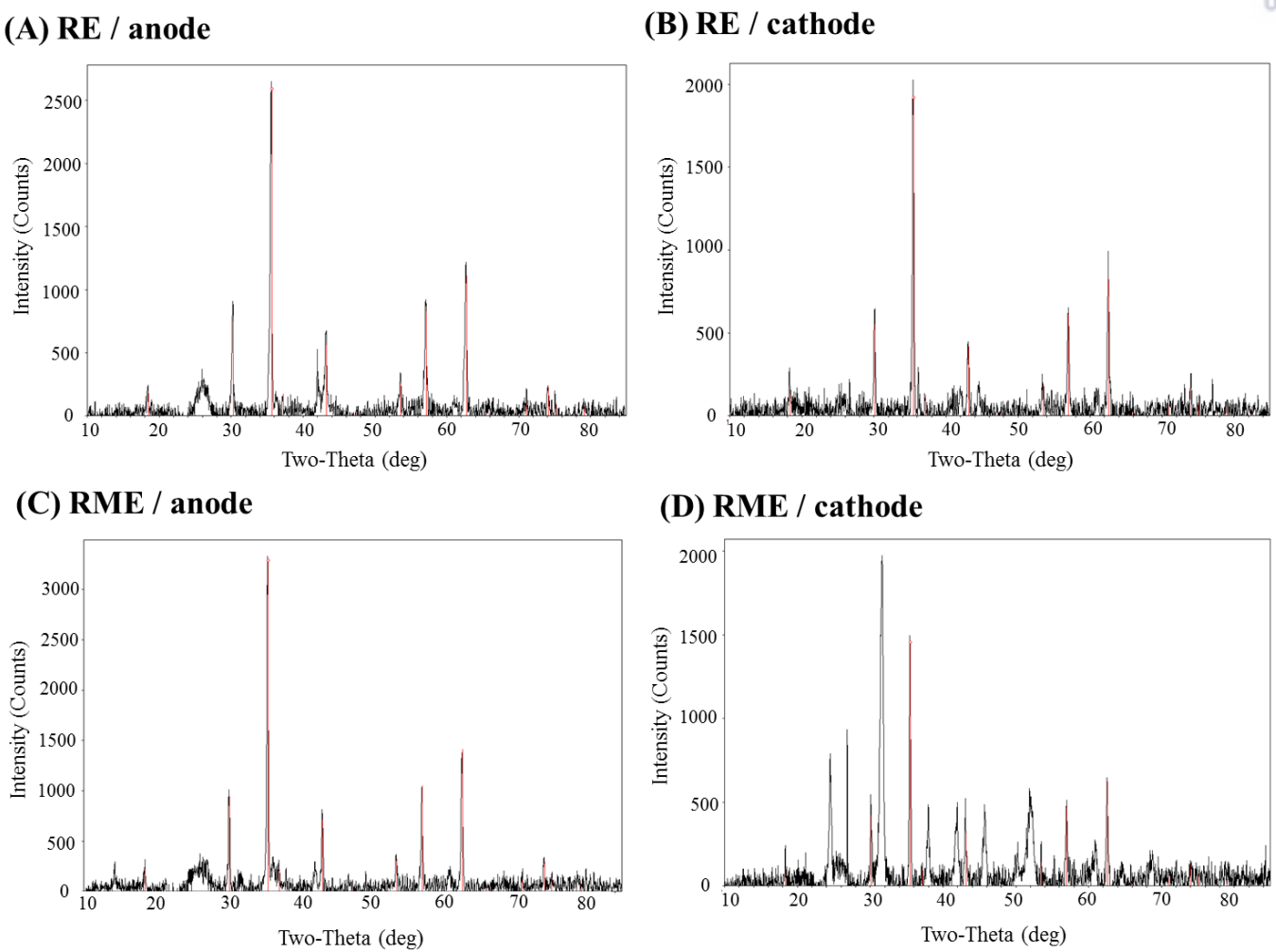

Fig. 6-7. X-ray diffraction analysis results of electrodes at day 631. The spectrum of pure magnetite is shown for reference as a red line.

6-3-3. Planktonic and biofilm microbial community structures

Mixed liquor samples for the analysis of planktonic microbial community structure were taken from each digester under steady-state conditions at HRTs of 20, 15, and 7.5 days (Fig. 6-1). As RC did not reach steady state at 20-day HRT, samples were collected on day 84 before magnetite was supplied. To observe the difference between suspended and attached microbial community structures, the biofilm communities formed on the electrodes of RE and RME were analyzed. Pieces of biofilm samples were collected on the last day of experiments (day 631) when both digesters were operated under steady-state conditions at HRT of 7.5 days. A total of 266,970 reads were produced (an average of 17,798±3,181 reads per sample) and classified into 305 OTUs (30 archaeal and 273 bacterial OTUs). Taxonomic affiliations and relative abundances of major OTUs (≥ 3% of the total archaeal or bacterial reads in at least one sample) are listed in Table 6-3.

Archaeal taxonomic abundances in each sample were ordered by Family level and are presented in Fig. 6-8A. Under 20-day HRT conditions, *Methanosaetaceae* was the most abundant methanogen family in all digesters (≥ 53.7% of the total archaeal reads) except for RC, which deteriorated with rapid VFA build-up and a drop in methane production rate (Table 6-2 and Fig. 6-2). *Methanosarcinaceae* was rarely detected in RM, RE, and RME, accounting for 0.1%–2.0% of the total archaeal reads, while its relative abundance was much higher in RC (10.9%). A different distribution of methanogens in RC from other digesters at the HRT of 20 days might be attributable to VFA build-up due to process imbalance. All of the sequences belonging to *Methanoseataceae* and *Methanosarcinaceae* are members of the genera *Methanothrix* and *Methanosarcina*, respectively. The general consensus is that *Methanothrix* outcompetes *Methanosarcina* in anaerobic digesters with low steady-state acetate concentration because *Methanothrix* have lower maximum growth rates on acetate but higher substrate affinity (i.e., lower minimum threshold) for acetate utilization compared with *Methanosarcina* [148]. The changes in relative abundance of *Methanosaetaceae* observed in this study could be affected by the presence of magnetite particles, given that it has been recently discovered that *Methanothrix* can reduce carbon dioxide to methane by directly accepting electrons from their electroactive DIET partners [27]. Indeed, except for the RM sample at 15-day HRT right after recovery from system imbalance, higher relative abundance of *M. concilli* was observed in all samples under magnetite-supplemented conditions (19.5%–85.2% in archaeal OTUs), suggesting that *M. concilli* can be involved in the electrosyntrophic mechanism by using magnetite as an electron conduit (Table 6-3). Meanwhile, the relative abundance of *Methanobacteraceae* was significantly higher in external voltage-applied environments (i.e., RE and RME), regardless of magnetite addition. OTUs A2, A4, and A5, which are affiliated with *Methanobacterium* species, mainly accounted for the *Methanobacteriales* population (Table 6-3). This suggests that it is possible that hydrogen produced from biocathode via biotic and/or abiotic pathways and *Methanobacterium* used it for their metabolism (i.e., hydrogenotrophic methanogenesis). Furthermore, some observations suggest that the direct uptake of electrons from the cathode to reduce carbon dioxide to methane (i.e., electromethanogenesis) and

hydrogen-mediated methanogenesis could occur simultaneously in the biocathode of electromethanogenesis cells [149-151]. Most previous studies have reported the enrichment of *Methanobacterium* at the methane-producing biocathode, which is in accordance with the present study [86, 149, 152]. *Methanomicrobiaceae* represented a 60.3% proportion of archaeal sequences in the RC sample at 20-day HRT when performance deterioration occurred. *Methanospirillaceae* dominated the archaeal community (92.1% of archaeal sequences) in the RM sample at 15-day HRT when the digester was recovering from upset. Both families are hydrogenotrophic and their populations served as syntrophic partners of VFA-degrading bacteria, particularly under perturbed conditions [153].

A more diverse structure was observed in the bacterial community (Fig. 6-8B). The retrieved bacterial sequences belonged to 21 known phyla, but 5.9% of the total sequences were unclassified as known phyla. The abundantly present phylum in AD environments, such as *Bacteroidetes*, *Chloroflexi*, *Proteobacteria*, *Firmicutes*, and *Thermotogae* were dominant; 62.2%–90.2% of bacterial sequences belonged to these phyla in each sample. A point to note is that the relative abundances of *Proteobacteria* and *Chloroflexi* were remarkably higher in voltage-applied digesters, particularly at shorter HRTs. At 7.5-day HRT in RE and RME, both phyla showed high relative abundances (> 26.6% together) in both planktonic and biofilm bacterial communities. Given that the two phyla together accounted for less than 16.9% in other bacterial libraries, the external voltage application and increased OLR are suggested to be major reasons for the enrichment of *Proteobacteria* and *Chloroflexi*. Most *Proteobacterial* sequences (82.0%–99.7%) were assigned to the class *δ-Proteobacteria*, to which *Geobacter* and many other exoelectrogenic bacteria belong [154, 155]. The enrichment of *δ-Proteobacteria* in electrode biofilms has been widely observed in different bioelectrochemical system [149, 156-158]. Similarly, *Chloroflexi* showed high relative abundances in RE and RME for the 7.5-day HRT, both in the planktonic (23.7%–27.3%) and biofilm (14.4%–28.3%) bacterial communities. It has been recently reported that *Chloroflexi* is abundant in DIET-stimulated conditions and their putative role as DIET partners has been suggested [133, 159]. Here, *Thermotogae* took 6.2%–14.1% of the relative abundances in total bacterial reads in the mixed liquor samples of all digesters at the longest HRT condition (i.e., 20-day HRT), but their relative abundance decreased significantly as HRT was reduced. This observation may be in part related to the relatively slow growth rate of *Mesotoga* (optimal doubling time on xylose at 37°C, 16.5 h; [160]) given that *Thermotogae* was mostly represented by OTU B6, which was assigned to the genus *Mesotoga* (Table 6-3). In this context, the occurrence of *Thermotogae* with considerable relative abundances (8.3%–17.7% of the total bacterial reads) in the electrode biofilms of RE and RME at a very short HRT (7.5 days) may be attributable to the attached-growth mode, which prevents hydraulic washout of biomass. Of note is that a considerable fraction of the bacterial sequence (5.6%–18.7%) retrieved from the electrode biofilms is unclassified at the phylum level. Therefore, microbial communities in electro-syntrophic AD environments are still largely unknown and further study is needed to identify the microorganisms in electrode biofilms that are involved in electron-donating or -accepting mechanisms.

Table 6-3 Relative abundance and taxonomic affiliation of major operational taxonomic units (OTUs; ≥ 3% of the total bacterial or archaeal readings in at least one sample)[a]

OTU no.	Classification[b]	Planktonic samples											Biofilm samples				Closest cultivated species[c]	Accession no.	Similarity (%)
		HRT (20 d)				HRT (15 d)			HRT (7.5 d)				HRT (7.5 d)						
		RC	RM	RE	RME	RM	RE	RME	RC	RM	RE	RME	RE-a[d]	RE-c[e]	RME-a[f]	RME-c			
Archaea																			
A1	*Methanothrix*	0.5	85.2	63.3	53.7	6.8	12.2	19.5	77.1	47.4	67.4	57.4	20.4	29.0	58.7	51.6	*Methanosaeta concilii*	KM408635	98.6
A2	*Methanobacterium*	0.7	0.3	0.0	0.1	0.0	81.8	0.1	0.0	0.0	12.2	0.7	68.3	51.8	1.3	14.6	*Methanobacterium beijingense*	NR028202	98.6
A3	*Methanofolis*	58.4	0.2	11.8	4.1	3.1	2.2	0.1	3.5	1.0	2.0	0.0	6.3	10.9	19.0	22.2	*Methanofollis liminatans*	NR028254	98.6
A4	*Methanobacterium*	0.0	0.0	0.0	0.0	0.0	0.0	61.6	0.0	0.0	0.5	5.4	0.1	0.1	4.0	1.5	*Methanobacterium formicicum*	JN205058	97.6
A5	*Methanobacterium*	0.7	4.5	0.4	0.8	0.0	0.0	0.1	0.0	0.0	0.7	9.8	0.2	0.7	4.5	1.9	*Methanobacterium subterraneum*	MF992205	97.3
A6	*Methanobacterium*	21.1	2.5	9.2	33.9	0.0	2.3	0.8	0.0	0.0	2.9	13.7	1.1	1.8	3.1	2.2	*Methanobacterium formicicum*	LN734822	98.6
A7	*Methanospirillum*	0.0	0.0	0.0	0.0	88.7	0.0	0.0	11.7	42.1	2.2	0.0	0.1	0.0	0.0	0.0	*Methanospirillum stamsii*	NR117705	97.6
A8	*Methanomicrobia*	0.0	0.0	0.0	0.0	0.0	0.0	0.0	0.0	0.0	0.0	0.0	0.0	0.0	5.0	0.0	*Methanosaeta pelagica*	NR113571	88.9
A9	*Methanobacterium*	0.0	0.0	0.0	0.0	0.0	0.0	0.0	0.0	0.0	0.0	8.5	0.0	0.0	1.2	0.5	*Methanobacterium palustre*	DQ649333	98.6
A10	*Methanocculleus*	1.0	2.0	8.4	0.6	0.3	1.0	14.2	2.6	0.0	6.1	1.4	1.5	2.9	0.8	0.9	*Methanoculleus chikugoensis*	KP702949	99.0
A11	*Methanobacterium*	0.0	4.9	0.8	0.4	0.0	0.2	0.4	0.0	0.0	0.1	0.1	0.0	1.0	0.2	1.4	*Methanobacterium beijingense*	MF407520	96.2
A12	*Euryarchaeota*	0.0	0.0	0.6	3.3	0.0	0.2	0.0	0.0	1.3	3.5	1.4	1.4	0.9	0.6	0.6	*Methanobrevibacter millerae*	KP123404	86.6
A13	*Methanosarsina*	10.9	0.3	2.0	0.1	0.0	0.0	0.0	0.4	0.0	0.0	0.0	0.0	0.1	0.6	0.1	*Methanosarcina barkeri*	CP009526	99.3
A14	*Archaea*	0.0	0.0	0.0	0.0	0.0	0.0	2.3	3.3	1.0	1.4	0.3	0.3	0.2	0.1	0.3	*Methanothermobacter tenebrarum*	NR113002	80.7
A15	*Methanothrix*	0.0	0.0	2.2	0.2	1.0	0.0	0.0	0.9	6.3	0.4	0.0	0.2	0.3	0.0	1.4	*Mehtanosaeta harundinacea*	NR043203	98.6
A16	*Methanobrevibacter*	5.3	0.0	0.2	0.0	0.0	0.0	0.0	0.0	0.0	0.0	0.0	0.0	0.0	0.0	0.0	*Methanobrevibacter arboriphilus*	FJ533154	99.3

Bacteria																			
B1	*Macellibacteroide*	0.1	0.3	3.1	3.8	55.8	0.2	48.3	40.2	54.0	15.3	15.8	0.6	0.3	1.4	3.2	*Parabacteroides chartae*	NR109439	98.6
B2	*Bacteroides*	0.5	0.0	6.4	0.0	18.4	11.1	0.0	26.4	8.5	9.5	6.8	0.2	0.0	1.7	2.3	*Bacteroides pyogenes*	HF558365	98.6
B3	Bacteria	2.4	4.1	5.2	5.9	1.5	8.5	2.9	5.6	5.6	1.2	0.3	3.4	2.5	0.3	0.7	*Rectinema cohabitans*	NR156915	94.2
B4	*Bacteroidetes*	0.0	0.0	24.5	23.1	0.0	0.0	0.6	0.0	0.0	3.0	2.4	0.4	0.0	0.1	0.4	*Labilibacter aurantiacus*	NR156071	87.7
B5	*Smithella*	0.0	0.0	0.0	0.0	1.0	0.0	1.2	1.2	0.5	0.3	9.4	6.4	1.3	13.7	21.1	*Smithella propionica*	NR024989	98.6
B6	*Mesotoga*	8.4	14.1	6.2	7.5	0.0	0.4	3.6	0.3	0.0	0.7	2.2	8.3	17.7	13.5	14.7	*Mesotoga infera*	LS974202	98.6
B7	*Petrimonas*	25.0	8.5	1.8	20.6	0.5	3.2	3.9	0.2	0.2	1.8	2.5	0.8	0.5	1.4	1.8	*Petrimonas sulfuriphila*	LT558828	98.6
B8	*Anaerolineaceae*	0.0	0.5	0.0	0.0	0.0	0.0	12.1	0.0	0.0	0.4	26.5	0.9	0.2	24.3	17.1	*Levilinea saccharolytica*	KT183424	89
B9	*Bacteria*	0.0	0.0	0.0	0.0	0.1	0.0	1.6	0.1	0.1	0.2	0.4	16.5	9.5	1.0	3.5	*Deferrisoma camini*	NR118216	81.9
B10	*Bacteroidetes*	3.8	21.1	0.1	0.7	0.0	0.0	0.7	0.0	0.0	0.8	2.4	0.0	0.0	0.1	0.3	*Carboxylicivirga mesophila*	NR133714	89.7
B11	*Acidaminococcaceae*	1.8	3.2	4.8	3.2	1.3	0.0	3.1	1.3	1.3	1.5	1.5	0.1	0.0	0.1	0.2	*Succinispira mobilis*	NR028868	94.8
B12	*Bacteria*	0.0	0.0	0.0	0.0	2.5	0.0	0.0	1.0	14.2	0.0	0.0	0.0	0.0	0.0	0.0	*Paenibacillus limicola*	NR159295	86.6
B13	*Bacteroidetes*	2.0	0.0	0.5	1.2	0.0	0.2	0.0	0.4	0.0	0.3	0.6	3.5	1.6	0.8	0.6	*Solitalea canadensis*	KF528160	98.3
B14	*Geobacter*	0.0	0.0	0.0	0.0	0.0	0.0	0.0	0.0	0.0	0.0	0.0	10.9	0.1	10.0	0.0	*Geobacter anodireducens*	CP014963	98.6
B15	*Bacteroides*	0.0	0.0	0.0	0.0	0.0	25.4	0.0	0.0	0.0	0.0	0.0	0.0	0.0	0.0	0.0	*Bacteroides cellulosilyticus*	LT223636	98.3
B16	*Bacteria*	0.0	0.0	1.4	0.0	0.0	0.0	0.0	0.0	0.0	20.4	0.0	5.6	11.0	0.0	0.0	*Rubrobacter spartanus*	NR158052	86.6
B17	*Coriobacteriaceae*	0.0	0.0	0.0	0.0	0.0	15.6	0.0	0.0	0.0	0.0	0.0	0.2	2.0	0.0	0.0	*Atopobium parvulum*	KU851139	94.2
B18	*Acholeplasma*	0.0	0.0	0.0	0.0	0.0	0.0	0.0	8.1	5.4	0.0	0.2	0.0	0.0	0.1	0.1	*Acholeplasma manati*	FJ590759	98.3
B19	Candidatus *Cloacamonas*	6.4	0.7	1.8	6.6	0.1	0.0	0.3	0.0	0.0	0.1	0.2	0.3	1.5	1.0	2.0	Candidatus *Cloacamonas acidaminovorans*	CU466930	97.9
B20	*Synergistaceae*	2.1	1.7	4.9	1.4	1.1	0.1	0.8	3.7	0.5	0.8	0.1	2.2	0.5	0.1	0.1	*Cloacibacillus porcorum*	CP016757	90.7
B21	*Aminivibrio*	8.5	1.5	2.0	2.2	0.9	0.6	2.0	0.7	0.4	1.2	1.8	2.0	0.8	0.8	0.8	*Aminovibrio pyruvatiphilus*	NR113331	96.9

B22	*Saccharofermentans*	0.0	6.9	0.0	0.0	0.0	0.0	0.0	0.0	0.0	6.7	0.0	0.9	0.2	0.0	0.0	*Saccharofermentans acetigenes*	NR115340	95.9
B23	*Syntrophobacter*	2.0	3.9	0.7	4.9	0.0	0.1	0.0	0.0	0.0	0.0	0.0	0.2	4.8	0.4	0.7	*Syntrophobacter sulfatireducens*	NR043073	98.6
B24	*Actinomycetales*	0.0	0.8	15.2	7.0	0.0	0.0	1.4	0.0	0.0	0.4	1.8	0.9	0.3	0.3	0.4	*Miniimonas arenae*	NR112996	95.9
B25	*Proteiniphilum*	0.0	0.0	0.0	0.0	0.0	15.9	0.0	0.0	0.0	0.0	0.0	0.0	0.0	0.0	0.0	*Ruminobacillus xylanolyticum*	KY434316	96.9
B26	Candidatus *Cloacamonas*	0.0	0.5	0.0	0.3	3.2	0.0	0.0	0.0	0.0	0.0	0.0	0.0	0.5	0.1	0.3	Candidatus *Cloacamonas acidaminovorans*	CU466930	89.3
B27	Bacteroidetes	0.0	0.0	4.1	0.0	0.0	0.0	2.1	0.0	0.0	0.0	0.1	0.0	1.2	0.1	0.4	*Lentimicrobium saccharophilum*	NR149795	90.4
B28	Bacteroidetes	4.1	11.1	0.1	0.0	0.0	0.8	0.0	0.0	0.0	0.0	0.0	0.0	0.0	0.0	0.0	*Paludibacter propionicigenes*	AB910740	91.1
B29	*Bacteria*	0.0	0.0	0.0	0.0	0.0	0.0	2.0	0.0	0.0	0.0	3.2	0.0	0.0	2.1	2.2	*Acetivibrio cellulolyticus*	JQ820024	87.3
B30	*Bacteroidetes*	0.0	0.0	0.0	0.0	0.0	0.0	0.3	0.0	0.0	0.1	0.9	0.7	0.9	3.1	4.8	*Labilibacter aurantiacus*	NR156071	89.7
B31	*Bacteroidales*	0.0	0.0	0.0	0.0	0.0	0.0	0.0	0.0	0.0	5.1	0.0	4.7	1.5	0.0	0.0	*Mariniphaga sediminis*	NR137221	91.4
B32	*Bacteroidetes*	0.0	0.0	0.0	0.0	0.0	0.3	0.0	0.4	0.3	9.3	0.4	0.1	0.1	0.0	0.0	*Ralstonia solanacearum*	CP011998	86.9
B33	*Bacteria*	0.0	0.0	0.0	0.0	0.2	0.0	0.0	0.0	0.0	0.0	6.6	0.0	0.0	4.9	4.4	*Aminomonas paucivorans*	NR114458	90
B34	*Corynebacterium*	5.1	3.0	0.0	0.0	0.0	0.0	0.0	0.0	0.0	0.0	0.0	0.0	0.1	0.1	0.0	*Corynebacterium diphtheriae*	LR134538	98.6
B35	*Ignavibacteriaceae*	0.0	0.0	0.0	0.0	0.0	0.0	3.1	0.0	0.0	0.2	0.5	0.2	0.4	0.5	0.6	*Meliobacter roseus*	MG264298	91.8
B36	*Clostiridium*	5.7	0.0	0.1	0.0	2.4	0.0	0.0	0.0	0.1	0.0	0.2	0.0	0.0	0.1	0.1	*Clostridium aldenense*	NR043680	98.3
B37	*Anaerolineaceae*	0.1	0.3	2.6	4.9	0.0	0.4	0.6	0.0	0.0	0.3	0.1	1.6	0.9	0.8	0.6	*Pelolinea submarina*	NR133813	93.5
B38	*Anaerolineaceae*	0.2	0.6	0.0	0.1	0.0	1.1	0.9	0.0	0.0	0.8	0.2	4.2	1.1	1.3	0.9	*Longilinea arvoryzae*	NR041355	92.8
B39	*Thermovirga*	0.0	0.1	2.7	0.0	0.0	0.2	0.0	0.0	0.0	0.0	0.0	0.6	13.3	0.4	1.3	*Thermovirga lienii*	NR074606	92.4
B40	*Syntrophaceae*	0.0	0.0	0.0	0.0	0.0	0.0	0.0	0.0	0.0	7.2	0.1	1.5	0.4	0.0	0.0	*Smithella propionica*	NR024989	94.8
B41	*Anaerolineaceae*	0.0	0.0	0.0	0.0	3.9	0.0	0.0	0.0	0.0	0.0	0.0	0.1	0.2	0.1	0.1	*Pelolinea submarina*	NR133813	94.5
B42	*Desulfovibrio*	3.4	0.0	0.2	0.0	0.0	3.4	0.0	0.0	0.0	0.0	0.0	0.0	0.0	0.0	0.0	*Desulfovibrio vulgaris*	CP001197	97.3
B43	*Bacteroidetes*	0.0	0.0	0.0	0.0	0.0	0.0	0.0	0.0	0.0	2.0	0.4	3.2	2.5	0.2	0.4	*Lentimicrobium saccharophilum*	NR149795	91.7

B44	*Bacteroidetes*	6.3	1.2	0.0	0.0	0.0	0.2	0.0	0.0	0.0	0.0	0.0	0.0	0.0	0.0	0.0	*Lutaonella thermophila*	NR044451	87.6
B45	*Blautia*	0.0	0.0	4.7	0.1	0.0	0.0	0.0	0.0	0.0	0.0	0.0	0.0	0.0	0.0	0.0	*Blautia producta*	CP035945	99
B46	*Bacteria*	0.0	0.0	0.3	0.1	0.0	6.2	0.0	0.0	0.0	0.0	0.0	0.0	0.1	0.0	0.0	*Polymorphobacter multimanifer*	NR125454	80.7
B47	*Geobacter*	3.3	0.3	0.4	0.2	0.1	0.2	0.0	0.0	0.0	0.1	0.1	0.2	0.1	0.1	0.1	*Geobacter argillaceus*	NR043575	97.6
B48	*Bacteroidetes*	0.0	0.0	0.0	0.0	0.0	0.0	0.0	0.0	0.6	0.0	0.0	1.5	3.6	0.0	0.0	*Ralstonia solanacearum*	CP011998	86.9
B49	*Peptococcaceae*	0.0	0.1	0.0	0.0	0.0	0.0	0.0	0.0	0.0	0.0	0.0	3.3	2.0	0.0	0.0	*Cryptanaerobacter phenolicus*	NR025757	97.6

[a] OTUs, operational taxonomic units. Cells with relative abundance values are colored in a heatmap-like fashion: red for archaeal and blue for bacterial sequences.

[b] The lowest rank assigned by RDP Classifier at an 80% confidence threshold.

[c] Closest cultivated sequences were determined by BLAST search against the NCBI 16S rRNA sequence database.

[d] a, anode biofilm

[e] c, cathode biofilm

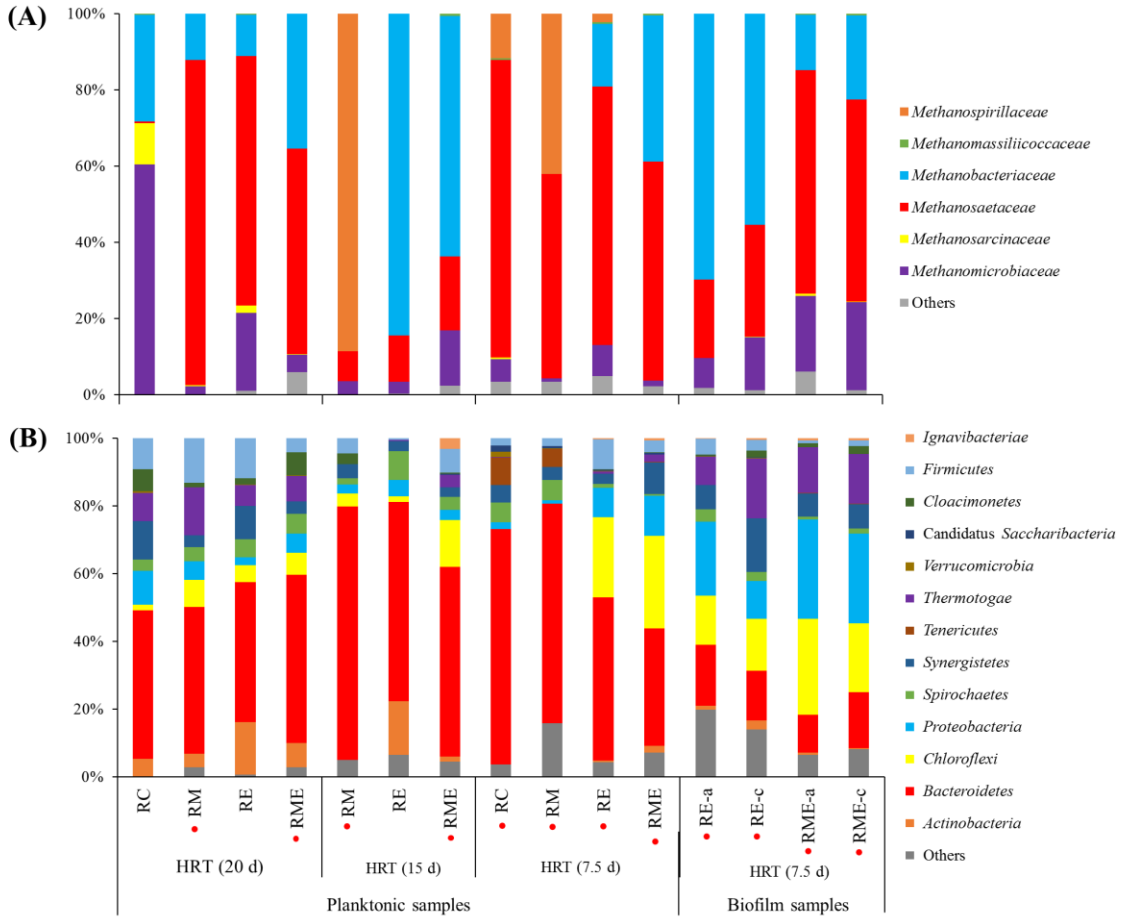

Fig. 6-8. Taxonomic distributions. Taxonomic distribution of archaeal (A) and bacterial (B) sequences in the 16S rRNA gene libraries of the digester biomass samples. The suffixes '-a' and '-c' indicate anode and cathode, respectively. The samples collected under magnetite-supplemented conditions are marked with red dots.

6-3-4. Bacteria involved in interspecies electron transfer

Fig. 6-9 shows changes in the relative abundances of bacterial genera, putatively involved in interspecies electron transfer in the digesters, in relation to DIET stimulation by adding magnetite and/or applying external voltage. *Geobacter* is a well-known exoelectrogenic genus that is frequently found in diverse DIET-stimulated environments and bioelectrochemical systems [37, 41, 133, 137]. The relative abundance of *Geobacter* was remarkably higher in anode biofilms in both RE and RME (10.1%–11.0%), whereas other samples except the mixed liquor from RC at 20-day HRT showed lower relative abundances of *Geobacter* (< 0.4%; Fig. 6-9A). This observation corresponds to the fact that *Geobacter* species can degrade organic matter and transport electrons produced from organic matter oxidation to the anode. Most *Geobacter*-related sequences retrieved from the anode biofilms were assigned to OTU B14, which is closely related (≥ 97% sequence similarity) to *Geobacter anodireducens* and *Geobacter sulfurreducens*, both of which are frequently found in anodic biofilms in various bioelectrochemical systems [161, 162]. Interestingly, a considerable population of *Geobacter* (3.3% of total bacterial reads) was observed in the mixed liquor sample of RC at 20-day HRT, and all of the sequences were assigned to OTU B47 closely related to *Geobacter argillaceus*. This OTU may have contributed to IET reactions in the digester; however, the lower relative abundance of methanogenic DIET partners (i.e., *Methanosaetaceae* and *Methanosarcinaceae*) indicates that it is unlikely that OTU B47 formed DIET syntrophy with methanogens.

Syntrophobacter and *Smithella* were abundantly found in the biofilm communities rather than the planktonic communities (Figs. 6-9B and 6-9C). Both are known to degrade propionate in AD environments based on the syntrophic relationship with hydrogen-consuming partners [163]. High relative abundances of both genera might be because biofilm can provide the attached growth-environment, which secures a long residence time sufficient for growth of these slow-growing syntrophic propionate degraders (e.g., several tens of hours of doubling time for *Sytrophobacter* and *Smithella*; [164]). It is also possible that the promotion of DIET could form a microenvironment that prevents intermediates (i.e., hydrogen and acetate) from being accumulated and thus reduces the possibility of inhibiting propionate oxidation by intermediate accumulations. [165, 166]. It is notable that *Synthophobacter* showed a relative abundance of < 5%, while *Smithella* was not detected for all planktonic bacterial libraries at 20-day HRT. This observation could be explained by the out-competition of *Smithella* by *Syntrophobacter* on propionate, likely owing to the faster growth rate of the latter [164]. Of note is that the *Syntrophobacter*-related sequences were overwhelmingly dominated (> 94.5%) by one OTU (B23) in the planktonic bacterial libraries at this HRT, whereas more diverse and evenly distributed *Syntrophobacter*-related OTUs were observed in the bacterial libraries at lower HRTs, particularly in the biofilm communities. The significantly different compositions of *Syntrophobacter*-related populations indicate that they may have served various functions in the microbial communities depending on the application of external voltage and/or OLR.

One interesting thing to note is that changes in the relative abundance of *Parabacteroides* were correlated with the presence of magnetite particles, regardless of voltage application (Fig. 6-9D). They were extremely abundant in planktonic communities under magnetite-supplemented conditions, while very little was observed in the attached samples or in the absence of magnetite. *Parabacteroides* species can ferment carbohydrates into diverse VFAs in anaerobic environments and have been found in various conductive material-added environments such as magnetite, granular activated carbon, and multi-wall carbon nanotubes [95, 167, 168]. Although it is unclear whether *Parabacteroides* species are electroactive, their abundant growth under DIET-simulated conditions have been reported [169]. In the present study, their population drastically increased in RM when HRT was reduced from 20 to 15 day, correlating with the recovery from upset in this period (Fig. 6-1 and Table 6-2). This suggests that *Parabacteroides* might play an important role in maintaining stable AD performance under magnetite-supplemented conditions.

6-3-5. Changes in archaeal and bacterial community structures

Fig. 6-10 presents archaeal and bacterial cluster dendrograms and NMS analysis results based on OTU distributions in each sample. The cumulative r^2 for ordination axes in NMS plots were 0.873 and 0.70 for archaeal and bacterial community data, respectively, suggesting that these plots accounted for 87.3% and 70.0% of the total variance in the analyzed data, respectively. The values of instability and final stress for both plots are low enough to be acceptable [96]. The bacterial community structures in all digesters showed remarkably different compositions (Sorensen distance [D_S] > 0.39) at 20-day HRT conditions; that is, the different operating conditions (magnetite addition or/and external voltage application) affected the development of microbial communities. Meanwhile, the archaeal community structure of the RC sample at 20-day HRT was distantly related (D_S > 0.72) to other samples at the same HRT condition, but which showed higher similarities to each other (D_S < 0.42). This likely reflects the fact that RC failed to reach a steady state at 20-day HRT, unlike the other digesters. Both archaeal and bacterial community structures shifted drastically in RM when HRT was reduced from 20 to 15 days, reflecting the serious imbalance in AD performance and the following recovery after 11 turnovers of the working volume. The overall statistical results indicate that bacterial community structure showed much larger variability by operating conditions as compared with the archaeal community structure. Lower diversity and a narrower substrate spectrum of archaea compared with bacteria in AD environments is one possible reason [170, 171]. In particular, bacterial community structures are clearly clustered by HRT condition and growth type (i.e., planktonic vs. biofilm samples). For the biofilm bacterial communities of RE and RME, structures were clustered according to the operating conditions of the digesters, rather than to the electrode type (i.e., anode and cathode). This could be due to the single-chamber configuration in which bioelectrochemical reactions occur in one chamber without physical separation between the anode and cathode. Similarly, De Vrieze et al. [172] observed that there was no significant difference in

bacterial composition between anode and cathode biofilms in single-chamber anaerobic digesters in the presence of electrodes and even more abundant methanogenic populations were observed in anode biofilms than in cathode biofilms. The different microbial community structures between the anode and cathode biofilms in both digesters seem to be related to the difference in the abundance of key microorganisms involved in electrochemical reactions (e.g., *Geobacter*; Fig. 6-9A). Once all digesters reached steady state at 7.5-day HRT, the microbial community structures under the same operating conditions (i.e., RC and RM with magnetite addition only, and RE and RME with magnetite addition and voltage application) were more closely aligned compared with the previous period. This suggests that the strategies used in this experiment for DIET stimulation affected the formation and development of microbial community structures.

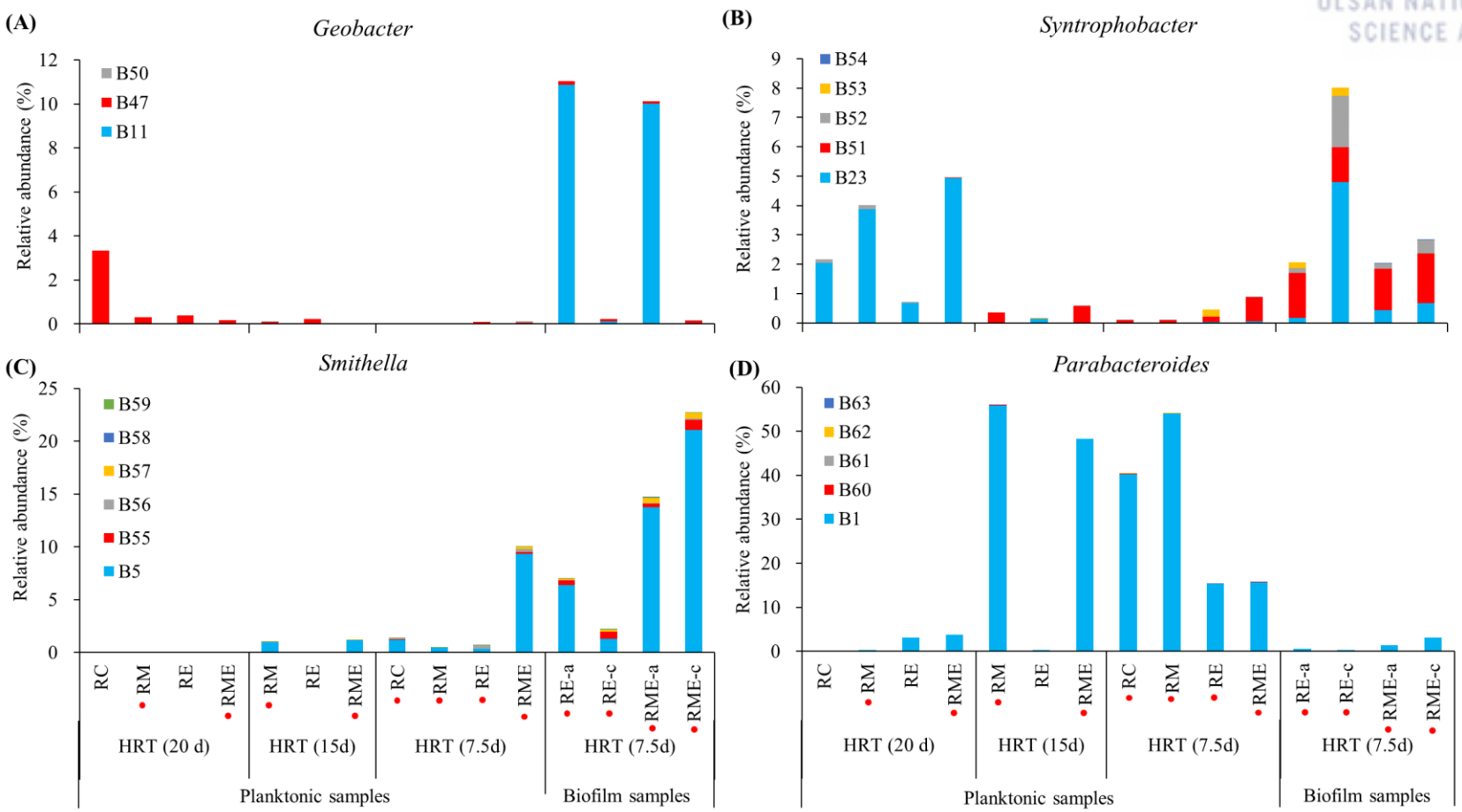

Fig. 6-9. Relative bacterial abundances. Relative abundances of *Geobacter* (A), *Syntrophobacter* (B), *Smithella* (C) and *Parabacteroides* (D) in the bacterial 16S rRNA gene libraries. The suffixes '-a' and '-c' indicate anode and cathode, respectively. The samples collected under magnetite-supplemented conditions are marked with red dots.

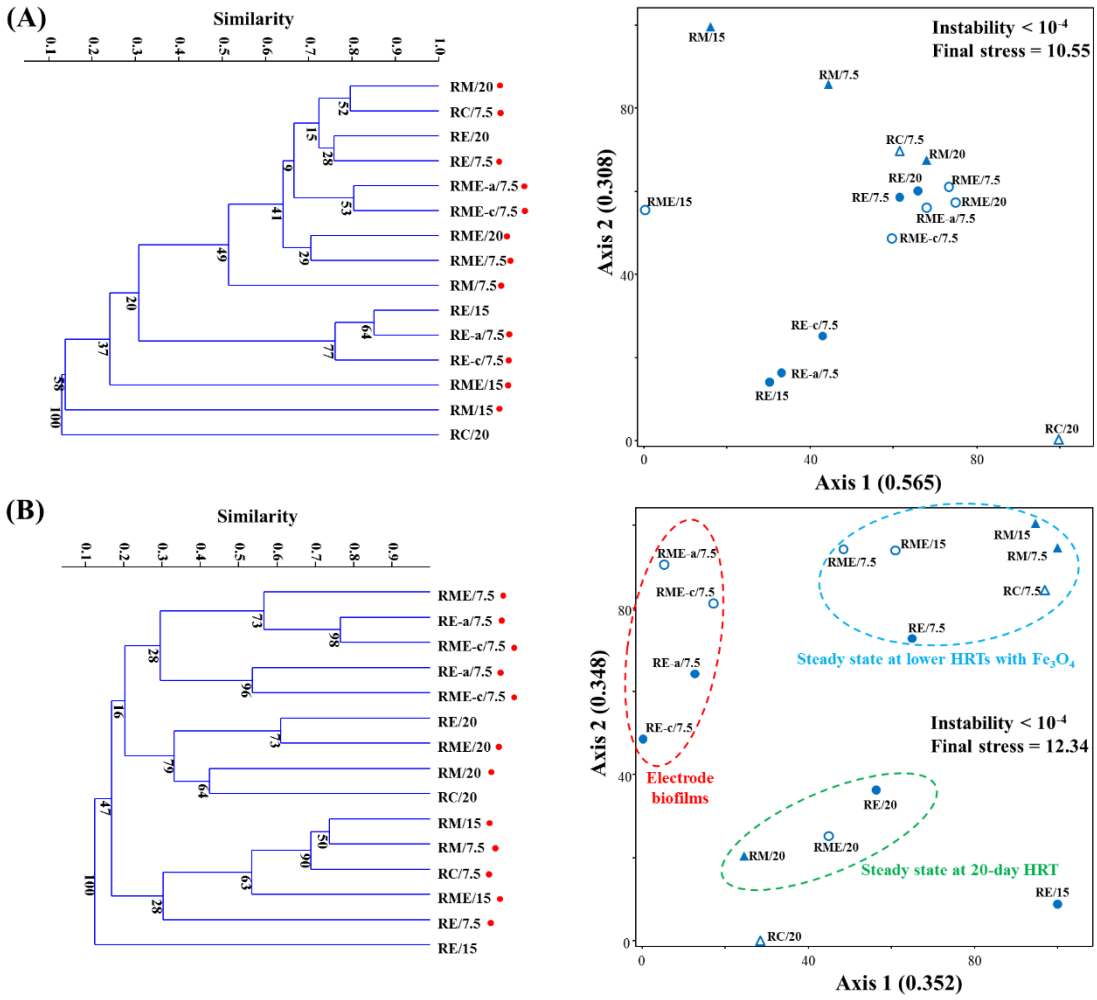

Fig. 6-10. Cluster dendrograms and nonmetric multidimensional scaling (NMS) plots constructed based on the operational taxonomic unit (OTU) distribution. (A) Archaeal and (B) bacterial 16S rRNA gene libraries. Microbial community profiles are labeled with the corresponding digester names and hydraulic retention times (HRTs) in days. The suffixes '-a' and '-b' indicate anode and cathode, respectively. The samples collected under magnetite-supplemented conditions are marked with red dots in cluster dendrograms

6-4. Discussion

The results of this study demonstrate that both the individual and combined effects of two strategies for DIET stimulation, magnetite supplementation (20 mM as Fe) and voltage application (0.6 V between electrodes) were beneficial for improving AD performance and stability under the conditions employed. Under a voltage-applied environment, RME showed better performance in the AD process and better maintained stability compared with RE. RME maintained its AD performance stably without process deterioration from 20- to 7.5-day HRT, while RE experienced severe deterioration at 12.5-day HRT before the recovery from upset by magnetite addition. This indicates that magnetite addition can bring additional improvements to methanogenic performance and stability when applied to an AD system with external voltage application for DIET stimulation. This is consistent with previous research results, which reported improved electrocatalytic activity of H_2-producing biocathode in magnetite-supplemented MEC [173]. The authors suggest that the improvement was attributed to the increased conductivity of the biofilm-electrode interface by magnetite addition. Zhen et al. [174] also reported that semi-conductive crystals such as magnetite could be precipitated and deposited on the surface of electrodes in MEC, and could thus enhance electron exchange between microorganisms. In the present study, enhanced electrical connections between microorganisms via deposited magnetite on the electrode surface is supported by thick biofilms or granule-like structures formed on the electrode of RME (Fig. 6-5). In the case of RM, it showed a temporary deterioration at 15-days HRT, but recovered without a change in its operating conditions and maintained stable performance until HRT was reduced to 7.5 days. Eleven turnovers of the working volume were needed for system recovery and significant transition in microbial community structure was accompanied by performance changes (Figs. 6-8 and 6-10). In this period, the population of *Methanospirillaceae* significantly increased (88.7%). Lerm et al. [175] reported that bacterial and archaeal community structures could be drastically changed after organic shock and perturbation of process performance. Under this imbalanced condition, *Methanospirillum hungatei*, which is known to utilize hydrogen produced from VFA degradation, became more dominant, which is in agreement with the results of the present study. In terms of the process stability, RME showed higher resistance against changes in HRT and high organic loading rate, while RE also had better resilience than RC. Given that RC failed to reach steady state at 20-day HRT but recovered and maintained its high AD performance after magnetite was supplied, magnetite seems to have a beneficial effect on process stability. The effect of magnetite on the resilience of process imbalance has been reported in previous work [111].

An important point to highlight is that higher methane yield was observed in RC and RM with magnetite addition alone compared with that in RE and RME with both magnetite addition and external voltage application, even though sCOD removal efficiencies were slightly lower, but still high (>97.0%), in RC and RM at 7.5-day HRT (Table 6-2). The results suggest that DIET stimulation by magnetite addition alone can sufficiently improve AD performance under high hydraulic loading pressure. Digesters without electrical

energy input, although small, are economically more feasible than those with it (Fig. 6-4). The lower methane yield in RE and RME compared with RC and RM indicates that there was a loss of electrons to alternative electron sinks other than methanogenesis. One possibility is the precipitation of electrochemical byproducts. EDS analysis confirmed a considerable amount of calcium in a granule-like structure on the cathode biofilm of RME (Fig. 6-11). [176] and [177] reported the precipitation of CaP or Ca_3PO_4 on biocathode of MEC and the authors mentioned that the production of these compounds could be due to a high local pH at the cathode and a continuous supply of Ca^{2+} and phosphate buffer solution. Furthermore, some divalent metal ions (e.g., Ca^{2+} and Fe^{2+}) can enhance granulation by being used as linking materials to bind extracellular polymers [178]. Considering that the cheese whey substrate of this study contained considerable Ca^{2+} (35.0±8.0 mg/L; data not shown), electrons at the cathode could be used to produce complexes of calcium-based byproducts and microorganisms. Another possibility is the production of specific biomass or electroactive protein, which is enriched by electrocatalytic conditions at the cathode. As presented in Fig. 6-3, VSS concentrations in the effluent at 7.5-day HRT was higher in RE and RME compared with that in RC and RM, suggesting a high biofilm growth and detachment rate and/or high suspended cell growth rate. Carbon and electrons sinks other than methanogenesis might be stimulated in this phase, including an increase in non-methanogenic biomass or electrochemical byproduct at the surface of electrodes. Similarly, Lee et al. [179] observed lower methane and higher biomass concentrations in voltage-applied experiments than in a control without voltage; they suggest the electrons used for biomass synthesis as a major reason. In addition, hydrogen consumption by hydrogenotrophic bacteria such as sulfate-reducing, nitrate-reducing, and homoacetogenic bacteria, at the cathode could cause the decrease in methane production. In this study, 0.6 V between electrodes was applied in RE and RME, and so it is electrochemically possible to generate hydrogen and enrich hydrogen-consuming bacteria at the cathode [180].

Magnetite not only impacts on AD performance and stability, but can also affect biofilm development on electrodes. In general, long-term operation of bioelectrochemical systems is difficult owing to the thickening of biofilm and precipitation of electrochemical byproducts on electrode surfaces. A biofilm thickness over a certain threshold can minimize the interface between electrode and electroactive microorganisms and render electron transfer inefficient across the biofilm thickness [181]. However, as seen in Fig. 6-5, much thicker and more compact biofilm structures were formed under the presence of magnetite particles in RME compare with RE. The reason why RME could maintain a higher AD performance than RE, despite the thick biofilm, is in part attributed to the high conductivity of magnetite (160 μS/cm;[168]. Biofilms incorporating magnetite particles (d = 100–700 nm) could be formed under the continuous supply of magnetite particles in feed (Figs. 6-6 and 6-7). Biofilm could thicken without losing its conductivity at both inner and surface areas, and so would maintain sufficient conductivity to promote DIET. Furthermore, rough and uneven surfaces of magnetite-embedded biofilm could provide favorable conditions for the attached growth of microorganisms and help to enrich the electroactive biomass on electrodes. Liu et al. [147] attempted to dope an electroactive

biofilm with magnetite particles to improve the performance of microbial fuel cells; they compared current production efficiencies between interior-doped biofilm (i.e., electrodes doped by magnetite located inside biofilm using a magnetic field) and surface-doped biofilm (i.e., electrodes doped by magnetite on the surface only). The interior-doped biofilm improved the microbial fuel cell efficiency more by forming conductive networks among electroactive bacteria within biofilm. In the present study, RME was continuously supplemented with magnetite particles with feed from time 0; magnetite can localize both on the surfaces of electrodes and inside biofilm with even distribution and can help to facilitate DIET and electron transfer between the electrode and attached microorganisms. This could a major reason that RME maintained high AD performance for such a long time (631 days), given that RE failed to reach steady state after 504 days, even with a less thick biofilm.

The results suggest that magnetite addition alone is a better approach than combined magnetite addition and external voltage application in terms of energy efficiency and economic feasibility to achieve stable high-rate AD under long-term operation. The improved performance and recovery from upset in all digesters was mainly attributed to DIET-mediated syntrophy. Magnetite particles did not undergo chemical transformation in either mixed liquor or the electrodes during the long-term experiment (Figs. 6-7 and 6-12). Furthermore, the Fe(II) concentration remained under 3.5 mg/L during whole operational period for all digesters (data not shown), suggesting that it is unlikely that magnetite was released and used as a redox shuttle for extracellular electron transfer [41, 47]. In this study, *Geobacter* and *Methanothrix* seem to be potential DIET partners, considering changes in their abundance under DIET-stimulated environment. This is further supported by the FISH analysis results, which showed that *Geobacter* and *Methanothrix* were closely located with magnetite particles under magnetite-supplemented conditions (Fig. 6-13). Magnetite seems to play a role as an electron conduit between two microorganisms to facilitate DIET [41]. The electric syntrophy between *Geobacter* and *Methanothrix* has been reported by many studies under defined and mixed-culture conditions [27, 138, 182].

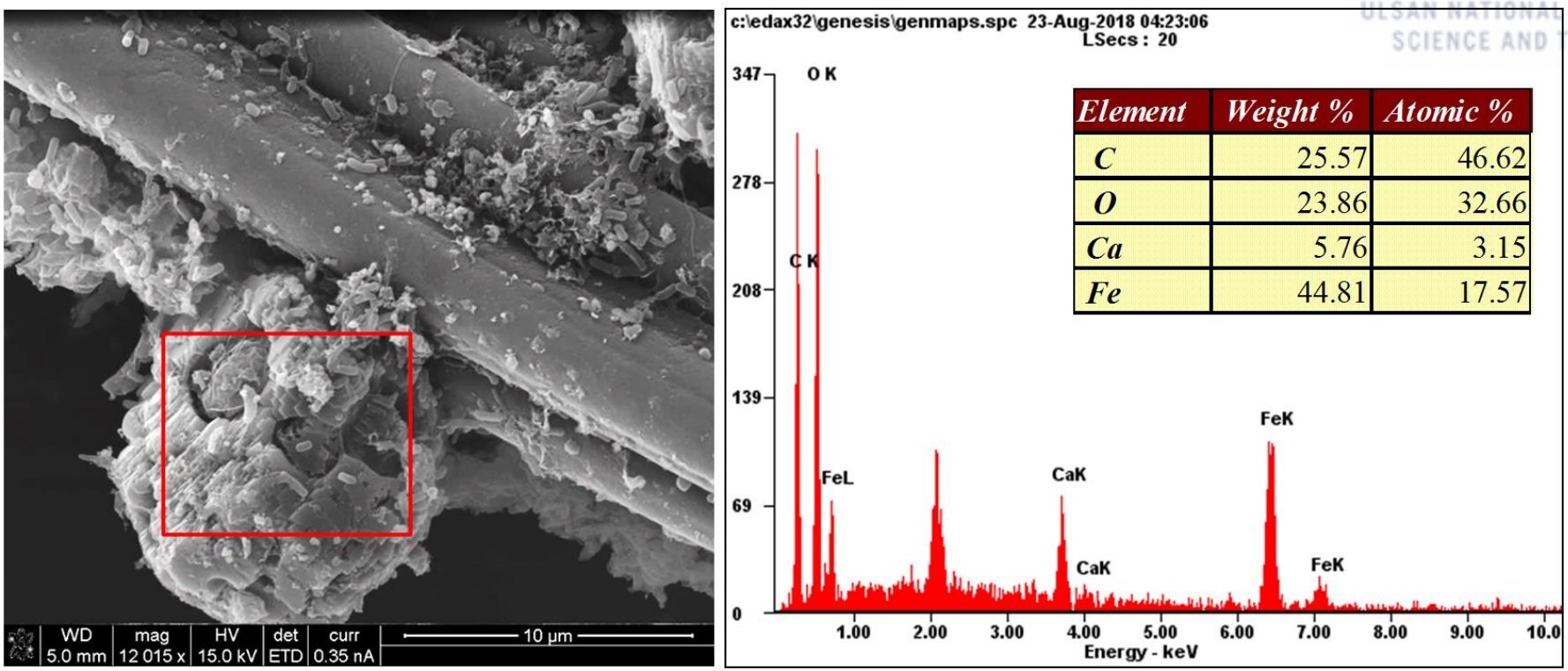

Fig. 6-11. Scanning electron microscopy images and energy dispersive X-ray spectroscopy results of biofilm on an RME (anaerobic digester with magnetite addition and external voltage application) cathode.

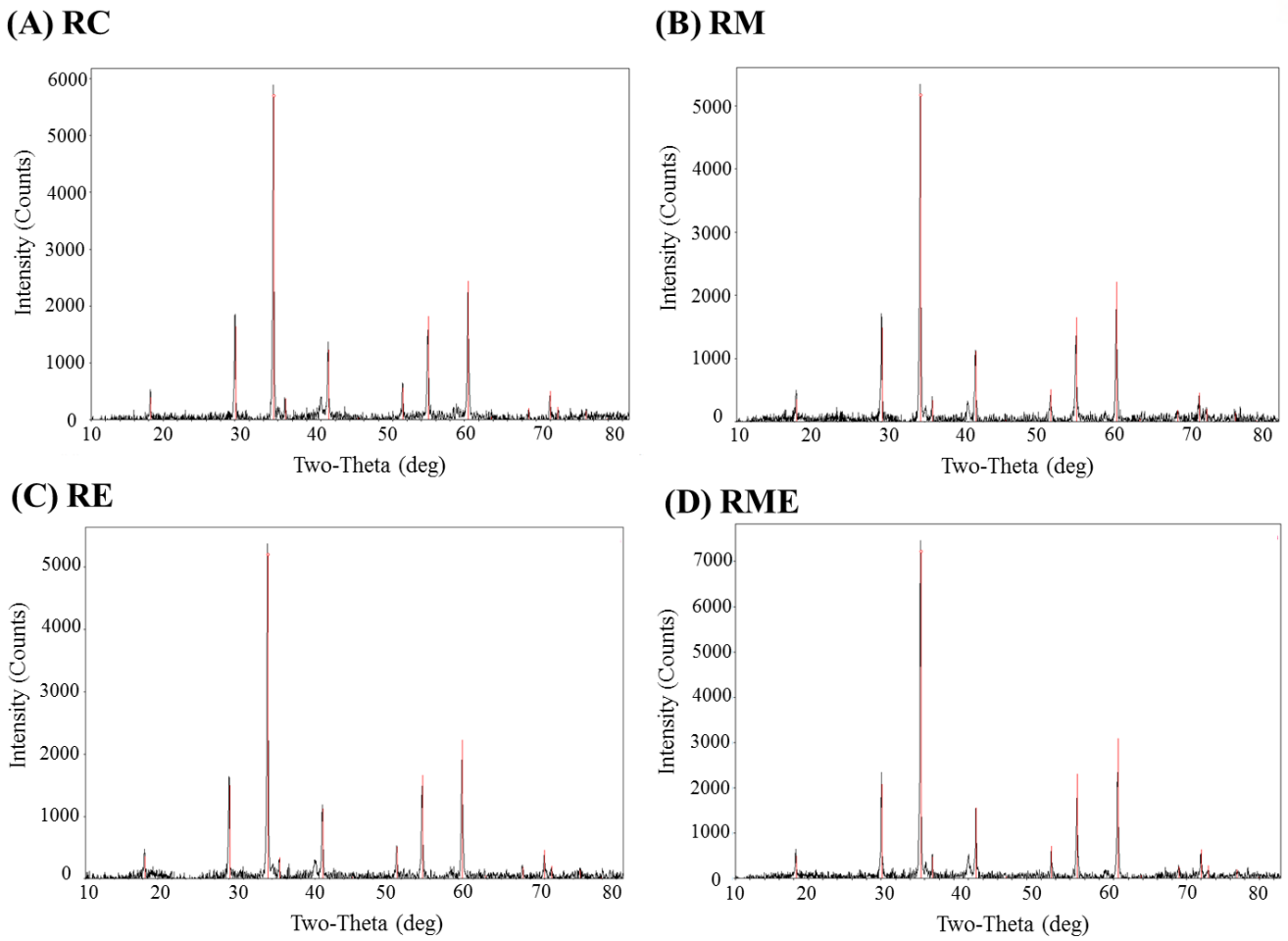

Fig. 6-12. X-ray diffraction analysis results of mixed liquors samples of digesters at a hydraulic retention time (HRT) of 7.5 day. The spectrum of pure magnetite is shown for reference as a red line.

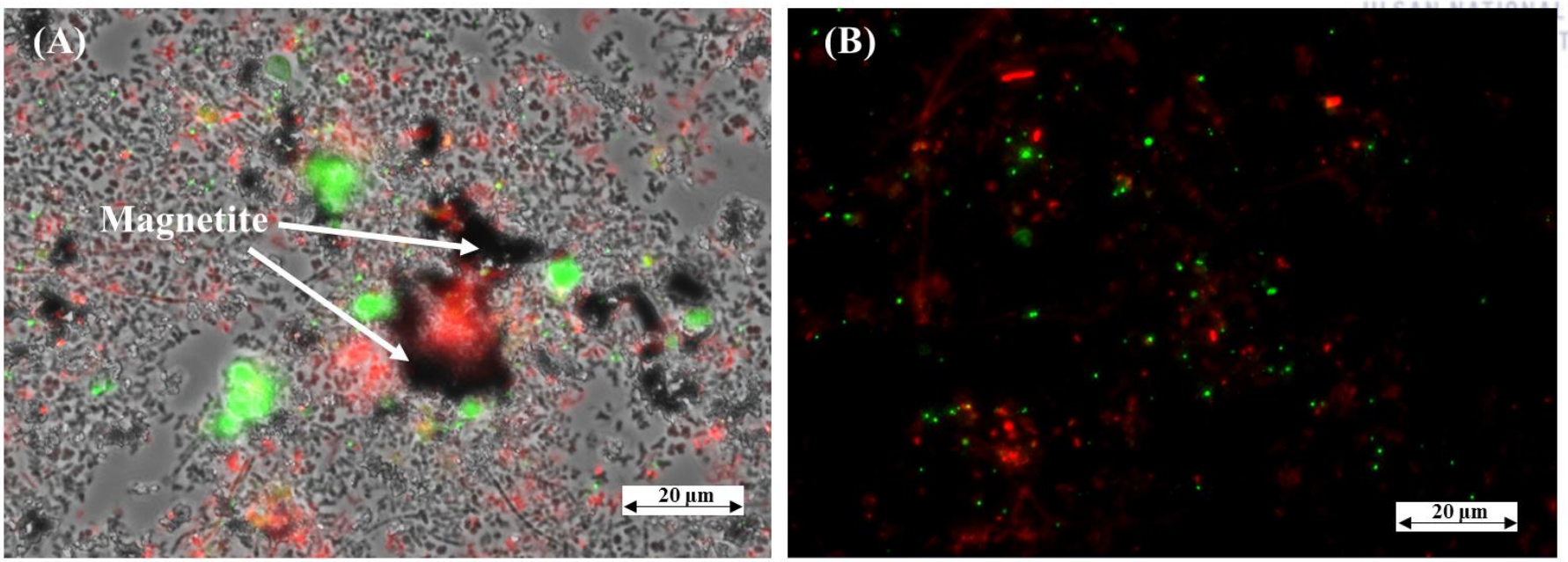

Fig. 6-13. Fluorescent in situ hybridization (FISH) analysis of mixed liquor samples of RME (anaerobic digester with magnetite addition and external voltage application) at a hydraulic retention time (HRT) of 7.5 day (red, *Geobacter*; green, *Methanothrix*).

6-5. Summary

The individual and combined effects of magnetite addition and external voltage application were investigated in a continuous AD process over 631 days. The overall results suggest that both individual applications are beneficial to stimulate DIET. However, magnetite has a more significant effect on enhancing AD performancethan does external voltage; in particular, the digester with magnetite addition alone showed comparable organic removal efficiency and even higher methane yield at lower HRTs compared with the digester with both applications combined. Under magnetite-supplemented and/or external voltage-applied conditions, several (putative) electroactive microorganisms were enriched and likely involved in DIET. Magnetite, as an electron transport conduit, appears to have played an important role in developing electro-syntrophic associations between exoelectrogenic bacteria and electrotrophic methanogens in both the mixed liquor and electrode biofilms. In summary, among the experimental conditions employed in this study, magnetite addition alone was the best approach for promoting DIET in AD and thereby enhancing digester performance and stability in terms of energy efficiency and implementation costs, particularly at lower HRTs. This study provides a reference for exploiting two different strategies to promote DIET in the AD processes. However, further investigations on the effect of DIET promotion with, for example, different types and doses of conductive materials and different ranges of voltage potentials, are needed.

7. CONCLUSION

DIET in AD environments can be achieved by the direct transfer of electrons between different microbial species through a biological electrical connection. DIET is energetically more advantageous than IIET because it does not need hydrogen to be produced for use as an electron carrier. Thus, DIET can improve methanogenic efficiency and process stability. Several recent studies show that DIET can also be mediated through non-biological conductive materials, such as magnetite, granular activated carbon, biochar, and carbon cloth. In my Ph.D. study, this positive effect of magnetite, a conductive iron oxide, on AD performance and stability was confirmed in real wastewater (cheese whey) with a mixed-culture inoculum. In Study 1, the positive effect of (semi)conductive iron oxides in anaerobic batch reactors was successfully confirmed in terms of energy recovery and organic removal over the control reactor. This finding implied that biostimulation with the (semi)conductive ferric oxides was beneficial for high-rate AD. In Study 2, the effect of magnetite addition was investigated in continuous anaerobic digesters with and without magnetite for a long period. Magnetite supplementation benefited not only the AD performance but also the retention of process stability. In Study 3, magnetite particles were separated and recycled in a continuous process without adding extra magnetite for economic feasibility. The proposed magnetite recycling method effectively maintained enhanced DIET and AD performance. *Geobacter* and *Methanothrix* were likely the major syntrophic partners responsible for the DIET-based methanogenesis. The results of Study 4 suggested that both magnetite supplementation and external voltage application stimulated DIET. However, magnetite had a more significant effect on enhancing AD performance than did external voltage. The combination of both applications effectively maintained stability under very short HRTs. In conclusion, magnetite-promoted DIET improves AD performance and stability by making favorable conditions for electroactive DIET partners for methane production. This study provides a reference for an enhanced understanding of the positive effects of DIET-promoting strategies on AD performance and stability.

REFERENCES

[1] Oller I, Malato S, Sánchez-Pérez J. Combination of advanced oxidation processes and biological treatments for wastewater decontamination—a review. Science of the total environment. 2011;409:4141-66.

[2] Angelidaki I, Ellegaard L, Ahring BK. Applications of the anaerobic digestion process. Biomethanation II: Springer; 2003. p. 1-33.

[3] Appels L, Lauwers J, Degrève J, Helsen L, Lievens B, Willems K, et al. Anaerobic digestion in global bio-energy production: potential and research challenges. Renewable and sustainable energy reviews. 2011;15:4295-301.

[4] Kim J, Lim J, Lee C. Quantitative real-time PCR approaches for microbial community studies in wastewater treatment systems: applications and considerations. Biotechnology advances. 2013;31:1358-73.

[5] Batstone D, Picioreanu C, Van Loosdrecht M. Multidimensional modelling to investigate interspecies hydrogen transfer in anaerobic biofilms. Water research. 2006;40:3099-108.

[6] Li Y, Park SY, Zhu J. Solid-state anaerobic digestion for methane production from organic waste. Renewable and sustainable energy reviews. 2011;15:821-6.

[7] Stams AJ, Plugge CM. Electron transfer in syntrophic communities of anaerobic bacteria and archaea. Nature reviews microbiology. 2009;7:568-77.

[8] Kaparaju P, Buendia I, Ellegaard L, Angelidakia I. Effects of mixing on methane production during thermophilic anaerobic digestion of manure: lab-scale and pilot-scale studies. Bioresource technology. 2008;99:4919-28.

[9] Kim M, Ahn Y-H, Speece R. Comparative process stability and efficiency of anaerobic digestion; mesophilic vs. thermophilic. Water research. 2002;36:4369-85.

[10] Stams AJ. Metabolic interactions between anaerobic bacteria in methanogenic environments. Antonie van Leeuwenhoek. 1994;66:271-94.

[11] Thiele JH, Zeikus JG. Control of interspecies electron flow during anaerobic digestion: significance of formate transfer versus hydrogen transfer during syntrophic methanogenesis in flocs. Applied and environmental microbiology. 1988;54:20-9.

[12] Bélaich J-P, Bruschi M, Garcia J-L. Microbiology and biochemistry of strict anaerobes involved in interspecies hydrogen transfer: Springer science & business media; 2012.

[13] Lovley DR, Goodwin S. Hydrogen concentrations as an indicator of the predominant terminal electron-accepting reactions in aquatic sediments. Geochimica et cosmochimica acta. 1988;52:2993-3003.

[14] Casalot L, Rousset M. Maturation of the [NiFe] hydrogenases. Trends in microbiology. 2001;9:228-37.

[15] Stams AJ, De Bok FA, Plugge CM, Eekert V, Miriam H, Dolfing J, et al. Exocellular electron transfer in

anaerobic microbial communities. Environmental microbiology. 2006;8:371-82.

[16] Schink B. Energetics of syntrophic cooperation in methanogenic degradation. Microbiology and molecular biology reviews. 1997;61:262-80.

[17] Kim BH, Gadd GM. Bacterial physiology and metabolism: Cambridge university press; 2008.

[18] Liu Y, Whitman WB. Metabolic, phylogenetic, and ecological diversity of the methanogenic archaea. Annals of the New York academy of sciences. 2008;1125:171-89.

[19] Boone DR, Johnson RL, Liu Y. Diffusion of the interspecies electron carriers H_2 and formate in methanogenic ecosystems and its implications in the measurement of Km for H_2 or formate uptake. Applied and environmental microbiology. 1989;55:1735-41.

[20] De Bok F, Plugge C, Stams A. Interspecies electron transfer in methanogenic propionate degrading consortia. Water research. 2004;38:1368-75.

[21] Cheng Q, Call DF. Hardwiring microbes via direct interspecies electron transfer: mechanisms and applications. Environmental science: processes & impacts. 2016;18:968-80.

[22] Kato S, Watanabe K. Ecological and evolutionary interactions in syntrophic methanogenic consortia. Microbes and environments. 2010;25:145-51.

[23] Arbeli Z, Brenner A, Abeliovich A. Treatment of high-strength dairy wastewater in an anaerobic deep reservoir: analysis of the methanogenic fermentation pathway and the rate-limiting step. Water research. 2006;40:3653-9.

[24] Jing Y, Wan J, Angelidaki I, Zhang S, Luo G. iTRAQ quantitative proteomic analysis reveals the pathways for methanation of propionate facilitated by magnetite. Water research. 2017;108:212-21.

[25] Storck T, Virdis B, Batstone DJ. Modelling extracellular limitations for mediated versus direct interspecies electron transfer. The ISME journal. 2016;10:621-31.

[26] Leang C, Qian X, Mester T, Lovley DR. Alignment of the *c*-type cytochrome OmcS along pili of *Geobacter sulfurreducens*. Applied and environmental microbiology. 2010;76:4080-4.

[27] Rotaru A-E, Shrestha PM, Liu F, Shrestha M, Shrestha D, Embree M, et al. A new model for electron flow during anaerobic digestion: direct interspecies electron transfer to *Methanosaeta* for the reduction of carbon dioxide to methane. Energy and environmental science. 2014;7:408-15.

[28] Shi L, Squier TC, Zachara JM, Fredrickson JK. Respiration of metal (hydr)oxides by *Shewanella* and *Geobacter*: a key role for multihaem *c*-type cytochromes. Molecular microbiology. 2007;65:12-20.

[29] Eaktasang N, Kang CS, Lim H, Kwean OS, Cho S, Kim Y, et al. Production of electrically-conductive nanoscale filaments by sulfate-reducing bacteria in the microbial fuel cell. Bioresource technology. 2016;210:61-7.

[30] Gorby YA, Yanina S, McLean JS, Rosso KM, Moyles D, Dohnalkova A, et al. Electrically conductive bacterial nanowires produced by *Shewanella oneidensis* strain MR-1 and other microorganisms. Proceedings of the national academy of sciences. 2006;103:11358-63.

[31] Malvankar NS, Tuominen MT, Lovley DR. Lack of cytochrome involvement in long-range electron transport through conductive biofilms and nanowires of *Geobacter sulfurreducens*. Energy and environmental science. 2012;5:8651-9.

[32] Summers ZM, Fogarty HE, Leang C, Franks AE, Malvankar NS, Lovley DR. Direct exchange of electrons within aggregates of an evolved syntrophic coculture of anaerobic bacteria. Science. 2010;330:1413-5.

[33] Malvankar NS, Lovley DR. Microbial nanowires: a new paradigm for biological electron transfer and bioelectronics. ChemSusChem. 2012;5:1039-46.

[34] Holmes DE, Dang Y, Walker DJ, Lovley DR. The electrically conductive pili of *Geobacter* species are a recently evolved feature for extracellular electron transfer. Microbial genomics. 2016;2.

[35] Malvankar NS, Vargas M, Nevin KP, Franks AE, Leang C, Kim B-C, et al. Tunable metallic-like conductivity in microbial nanowire networks. Nature nanotechnology. 2011;6:573-9.

[36] Pirbadian S, Barchinger SE, Leung KM, Byun HS, Jangir Y, Bouhenni RA, et al. *Shewanella oneidensis* MR-1 nanowires are outer membrane and periplasmic extensions of the extracellular electron transport components. Proceedings of the national academy of sciences. 2014;111:12883-8.

[37] Rotaru A-E, Shrestha PM, Liu F, Markovaite B, Chen S, Nevin K, et al. Direct interspecies electron transfer between *Geobacter metallireducens* and *Methanosarcina barkeri*. Applied and environmental microbiology. 2014:AEM. 00895-14.

[38] Chen S, Rotaru A-E, Liu F, Philips J, Woodard TL, Nevin KP, et al. Carbon cloth stimulates direct interspecies electron transfer in syntrophic co-cultures. Bioresource technology. 2014;173:82-6.

[39] Chen S, Rotaru A-E, Shrestha PM, Malvankar NS, Liu F, Fan W, et al. Promoting interspecies electron transfer with biochar. Scientific reports. 2014;4:5019.

[40] Liu F, Rotaru A-E, Shrestha PM, Malvankar NS, Nevin KP, Lovley DR. Promoting direct interspecies electron transfer with activated carbon. Energy and environmental science. 2012;5:8982-9.

[41] Kato S, Hashimoto K, Watanabe K. Methanogenesis facilitated by electric syntrophy via (semi) conductive iron-oxide minerals. Environmental microbiology. 2012;14:1646-54.

[42] Moon J-W, Roh Y, Lauf RJ, Vali H, Yeary LW, Phelps TJ. Microbial preparation of metal-substituted magnetite nanoparticles. Journal of microbiological methods. 2007;70:150-8.

[43] Nidheesh P. Heterogeneous Fenton catalysts for the abatement of organic pollutants from aqueous solution: a review. RSC advances. 2015;5:40552-77.

[44] Sun S, Zeng H. Size-controlled synthesis of magnetite nanoparticles. Journal of the american chemical society. 2002;124:8204-5.

[45] Guskos N, Papadopoulos G, Likodimos V, Patapis S, Yarmis D, Przepiera A, et al. Photoacoustic, EPR and electrical conductivity investigations of three synthetic mineral pigments: hematite, goethite and magnetite. Materials research bulletin. 2002;37:1051-61.

[46] Kato S, Hashimoto K, Watanabe K. Microbial interspecies electron transfer via electric currents through

conductive minerals. Proceedings of the national academy of sciences. 2012;109:10042-6.

[47] Cruz Viggi C, Rossetti S, Fazi S, Paiano P, Majone M, Aulenta F. Magnetite particles triggering a faster and more robust syntrophic pathway of methanogenic propionate degradation. Environmental science and technology. 2014;48:7536-43.

[48] Li H, Chang J, Liu P, Fu L, Ding D, Lu Y. Direct interspecies electron transfer accelerates syntrophic oxidation of butyrate in paddy soil enrichments. Environmental microbiology. 2015;17:1533-47.

[49] Yamada C, Kato S, Ueno Y, Ishii M, Igarashi Y. Conductive iron oxides accelerate thermophilic methanogenesis from acetate and propionate. Journal of bioscience and bioengineering. 2015;119:678-82.

[50] Yang Z, Guo R, Shi X, Wang C, Wang L, Dai M. Magnetite nanoparticles enable a rapid conversion of volatile fatty acids to methane. RSC advances. 2016;6:25662-8.

[51] Zhuang L, Tang J, Wang Y, Hu M, Zhou S. Conductive iron oxide minerals accelerate syntrophic cooperation in methanogenic benzoate degradation. Journal of hazardous materials. 2015;293:37-45.

[52] Hwang S, Hansen C. Characterization of and bioproduction of short-chain organic acids from mixed dairy-processing wastewater. Transactions of the ASAE. 1998;41:795-802.

[53] Lee C, Kim J, Shin SG, O'Flaherty V, Hwang S. Quantitative and qualitative transitions of methanogen community structure during the batch anaerobic digestion of cheese-processing wastewater. Applied microbiology biotechnololgy. 2010;87:1963-73.

[54] Yu Y, Lee C, Kim J, Hwang S. Group-specific primer and probe sets to detect methanogenic communities using quantitative real-time polymerase chain reaction. Biotechnology and bioengineering. 2005;89:670-9.

[55] Muyzer G, De Waal EC, Uitterlinden AG. Profiling of complex microbial populations by denaturing gradient gel electrophoresis analysis of polymerase chain reaction-amplified genes coding for 16S rRNA. Applied and environmental microbiology. 1993;59:695-700.

[56] Hammer O, Harper DAT, Ryan PD. PAST: Palaeontological statistics software package for education and data analysis. Palaeontologia electronica. 2001;4:1-9.

[57] McCune B, Grace JB. Analysis of Ecological Communities. Glenden Beach, OR, USA: MjM Software Design; 2002.

[58] VandeWalle JL, Goetz GW, Huse SM, Morrison HG, Sogin ML, Hoffmann RG, et al. *Acinetobacter, Aeromonas* and *Trichococcus* populations dominate the microbial community within urban sewer infrastructure. Environmental microbiology. 2012;14:2538-52.

[59] Kim J, Lee S, Lee C. Comparative study of changes in reaction profile and microbial community structure in two anaerobic repeated-batch reactors started up with different seed sludges. Bioresource technology. 2013;129:495-505.

[60] APHA-AWWA-WEF. Standard Methods for the Examination of Water and Wastewater. 21st ed.

Washington, D.C.: American Public Health Association; 2005.

[61] Ahring BK. Biomethanation I: Springer; 2003.

[62] Kobayashi T, Yasuda D, Li Y-Y, Kubota K, Harada H, Yu H-Q. Characterization of start-up performance and archaeal community shifts during anaerobic self-degradation of waste-activated sludge. Bioresource technology. 2009;100:4981-8.

[63] Venetsaneas N, Antonopoulou G, Stamatelatou K, Kornaros M, Lyberatos G. Using cheese whey for hydrogen and methane generation in a two-stage continuous process with alternative pH controlling approaches. Bioresource technology. 2009;100:3713-7.

[64] Seifert K, Waligorska M, Wojtowski M, Laniecki M. Hydrogen generation from glycerol in batch fermentation process. International journal of hydrogen energy. 2009;34:3671-8.

[65] Wicher E, Seifert K, Zagrodnik R, Pietrzyk B, Laniecki M. Hydrogen gas production from distillery wastewater by dark fermentation. International journal of hydrogen energy. 2013;38:7767-73.

[66] Khanal SK, Chen W-H, Li L, Sung S. Biological hydrogen production: effects of pH and intermediate products. International journal of hydrogen energy. 2004;29:1123-31.

[67] Caccavo F, Blakemore RP, Lovley DR. A hydrogen-oxidizing, Fe(III)-reducing microorganism from the Great Bay Estuary, New Hampshire. Applied and environmental microbiology. 1992;58:3211-6.

[68] Lovley DR, Phillips EJ, Lonergan DJ. Hydrogen and formate oxidation coupled to dissimilatory reduction of iron or manganese by *Alteromonas putrefaciens*. Applied and environmental microbiology. 1989;55:700-6.

[69] Lay J-J, Li Y-Y, Noike T. Developments of bacterial population and methanogenic activity in a laboratory-scale landfill bioreactor. Water research. 1998;32:3673-9.

[70] Quéméneur M, Hamelin J, Barakat A, Steyer J-P, Carrère H, Trably E. Inhibition of fermentative hydrogen production by lignocellulose-derived compounds in mixed cultures. International journal of hydrogen energy. 2012;37:3150-9.

[71] Tan H-Q, Li T-T, Zhu C, Zhang X-Q, Wu M, Zhu X-F. *Parabacteroides chartae* sp. nov., an obligately anaerobic species from wastewater of a paper mill. International journal of systematic and evolutionary microbiology. 2012;62:2613-7.

[72] Jabari L, Gannoun H, Cayol J-L, Hedi A, Sakamoto M, Falsen E, et al. *Macellibacteroides fermentans* gen. nov., sp. nov., a member of the family *Porphyromonadaceae* isolated from an upflow anaerobic filter treating abattoir wastewaters. International journal of systematic and evolutionary microbiology. 2012;62:2522-7.

[73] Kitahara M, Sakamoto M, Tsuchida S, Kawasumi K, Amao H, Benno Y, et al. *Parabacteroideschinchillae* sp. nov., isolated from *chinchilla* (*Chincilla lanigera*) faeces. International journal of systematic and evolutionary microbiology. 2013;63:3470-4.

[74] Supaphol S, Jenkins SN, Intomo P, Waite IS, O'Donnell AG. Microbial community dynamics in

mesophilic anaerobic co-digestion of mixed waste. Bioresource technology. 2011;102:4021-7.

[75] Baek G, Kim J, Lee C. Influence of ferric oxyhydroxide addition on biomethanation of waste activated sludge in a continuous reactor. Bioresource technology. 2014;166:596-601.

[76] Bertin L, Lampis S, Todaro D, Scoma A, Vallini G, Marchetti L, et al. Anaerobic acidogenic digestion of olive mill wastewaters in biofilm reactors packed with ceramic filters or granular activated carbon. Water research. 2010;44:4537-49.

[77] Ueno Y, Sasaki D, Fukui H, Haruta S, Ishii M, Igarashi Y. Changes in bacterial community during fermentative hydrogen and acid production from organic waste by thermophilic anaerobic microflora. Journal of applied microbiology. 2006;101:331-43.

[78] De Vos P, Garrity GM, Jones D, Krieg NR, Ludwig W, Rainey FA, et al. Bergey's Manual of Systematic Bacteriology: The *Fermicutes*. In: Whitman WB, editor. 2nd ed. New York: Springer; 2009.

[79] Fox JR, Mortimer RJ, Lear G, Lloyd JR, Beadle I, Morris K. The biogeochemical behaviour of U(VI) in the simulated near-field of a low-level radioactive waste repository. Applied geochemistry. 2006;21:1539-50.

[80] Tandukar M, Huber SJ, Onodera T, Pavlostathis SG. Biological chromium(VI) reduction in the cathode of a microbial fuel cell. Environmental science & technology. 2009;43:8159-65.

[81] Zumstein E, Moletta R, Godon J. Examination of two years of community dynamics in an anaerobic bioreactor using fluorescence polymerase chain reaction(PCR) single-strand conformation polymorphism analysis. Environmental microbiology. 2000;2:69-78.

[82] Kim J, Jung H, Lee C. Shifts in bacterial and archaeal community structures during the batch biomethanation of *Ulva* biomass under mesophilic conditions. Bioresource technology. 2014;169:502-9.

[83] Akarsubasi AT, Ince O, Kirdar B, Oz NA, Orhon D, Curtis TP, et al. Effect of wastewater composition on archaeal population diversity. Water research. 2005;39:1576-84.

[84] Dinh HT, Kuever J, Muszmann M, Hassel AW, Stratmann M, Widdel F. Iron corrosion by novel anaerobic microorganisms. Nature. 2004;427:829-32.

[85] Uchiyama T, Ito K, Mori K, Tsurumaru H, Harayama S. Iron-corroding methanogen isolated from a crude-oil storage tank. Applied and environmental microbiology. 2010;76:1783-8.

[86] Cheng S, Xing D, Call DF, Logan BE. Direct biological conversion of electrical current into methane by electromethanogenesis. Environmental science & technology. 2009;43:3953-8.

[87] Smith KS, Ingram-Smith C. *Methanosaeta*, the forgotten methanogen? Trends in microbiology. 2007;15:150-5.

[88] Morita M, Malvankar NS, Franks AE, Summers ZM, Giloteaux L, Rotaru AE, et al. Potential for direct interspecies electron transfer in methanogenic wastewater digester aggregates. mBio. 2011;2:e00159-11.

[89] Kim S-J, Park S-J, Cha I-T, Min D, Kim J-S, Chung W-H, et al. Metabolic versatility of toluene-degrading, iron-reducing bacteria in tidal flat sediment, characterized by stable isotope probing-based metagenomic

analysis. Environmental microbiology. 2014;16:189-204.

[90] Lovely D, Phillips EJP. Rapid assay for microbially reducible ferric iron in aquatic sediments. Applied and environmental microbiology. 1987;53:1536-40.

[91] Liu F, Rotaru A-E, Shrestha PM, Malvankar NS, Nevin KP, Lovley DR. Magnetite compensates for the lack of a pilin-associated *c*-type cytochrome in extracellular electron exchange. Environmental microbiology. 2015;17:648-55.

[92] Lovley, DR. Dissimilatory Fe (III)-and Mn (IV)-reducing prokaryotes. The Prokaryotes: Volume 2: Ecophysiology and biochemistry, 2006; 635-58.

[93] Lovley DR, Phillips EJP. Requirement for a microbial consortium to completely oxidize glucose in Fe(III)-reducing sediments. Applied and environmental microbiology. 1989;55:3234-6.

[94] Scott JP. A method of increasing the virulence of *Clostridium chauvoei* by the use of ferric salts. The journal of infectious diseases. 1926;38:511-3.

[95] Baek G, Kim J, Cho K, Bae H, Lee C. The biostimulation of anaerobic digestion with (semi) conductive ferric oxides: their potential for enhanced biomethanation. Applied microbiology and biotechnology. 2015;99:10355-66.

[96] McCune B, Grace JB, Urban DL. Analysis of ecological communities: MjM software design Gleneden Beach, OR; 2002.

[97] Hill D, Cobb S, Bolte J. Using volatile fatty acid relationships to predict anaerobic digester failure. Transactions of the ASAE. 1987;30:496-0501.

[98] Speece RE. Anaerobic Biotechnology for Industrial Wastewaters. Nashville, TN: Archae Press; 1996.

[99] Kato S, Nakamura R, Kai F, Watanabe K, Hashimoto K. Respiratory interactions of soil bacteria with (semi) conductive iron-oxide minerals. Environmental microbiology. 2010;12:3114-23.

[100] Söllinger A, Schwab C, Weinmaier T, Loy A, Tveit AT, Schleper C, et al. Phylogenetic and genomic analysis of *Methanomassiliicoccales* in wetlands and animal intestinal tracts reveals clade-specific habitat preferences. FEMS microbiology ecology. 2016;92:fiv149.

[101] Wang A, Liu L, Sun D, Ren N, Lee D-J. Isolation of Fe(III)-reducing fermentative bacterium *Bacteroides* sp. W7 in the anode suspension of a microbial electrolysis cell(MEC). International journal of hydrogen energy. 2010;35:3178-82.

[102] Chen S, Niu L, Zhang Y. *Saccharofermentans acetigenes* gen. nov., sp. nov., an anaerobic bacterium isolated from sludge treating brewery wastewater. International journal of systematic and evolutionary microbiology. 2010;60:2735-8.

[103] Grabowski A, Tindall BJ, Bardin V, Blanchet D, Jeanthon C. *Petrimonas sulfuriphila* gen. nov., sp. nov., a mesophilic fermentative bacterium isolated from a biodegraded oil reservoir. International journal of systematic and evolutionary microbiology. 2005;55:1113-21.

[104] Larimer FW, Chain P, Hauser L, Lamerdin J, Malfatti S, Do L, et al. Complete genome sequence of the

metabolically versatile photosynthetic bacterium *Rhodopseudomonas palustris*. Nature Biotechnology. 2004;22:55-61.

[105] Chouari R, Le Paslier D, Daegelen P, Ginestet P, Weissenbach J, Sghir A. Novel predominant archaeal and bacterial groups revealed by molecular analysis of an anaerobic sludge digester. Environmental microbiology. 2005;7:1104-15.

[106] Kawaichi S, Ito N, Kamikawa R, Sugawara T, Yoshida T, Sako Y. *Ardenticatena maritima* gen. nov., sp. nov., a ferric iron- and nitrate-reducing bacterium of the phylum '*Chloroflexi*' isolated from an iron-rich coastal hydrothermal field, and description of *Ardenticatenia classis* nov. International journal of systematic and evolutionary microbiology. 2013;63:2992-3002.

[107] Blanchet E, Pécastaings S, Erable B, Roques C, Bergel A. Protons accumulation during anodic phase turned to advantage for oxygen reduction during cathodic phase in reversible bioelectrodes. Bioresource technology. 2014;173:224-30.

[108] Demirel B, Scherer P. The roles of acetotrophic and hydrogenotrophic methanogens during anaerobic conversion of biomass to methane: a review. Reviews in environmental science and Biotechnology. 2008;7:173-90.

[109] Lee J-Y, Lee S-H, Park H-D. Enrichment of specific electro-active microorganisms and enhancement of methane production by adding granular activated carbon in anaerobic reactors. Bioresource technology. 2016.

[110] Müller B, Sun L, Schnürer A. First insights into the syntrophic acetate-oxidizing bacteria – a genetic study. MicrobiologyOpen. 2013;2:35-53.

[111] Baek G, Kim J, Lee C. A long-term study on the effect of magnetite supplementation in continuous anaerobic digestion of dairy effluent–Enhancement in process performance and stability. Bioresource technology. 2016;222:344-54.

[112] Rognes T, Flouri T, Nichols B, Quince C, Mahé F. VSEARCH: a versatile open source tool for metagenomics. Peer J. 2016;4:e2584.

[113] Kim J, Lee C. Response of a continuous biomethanation process to transient organic shock loads under controlled and uncontrolled pH conditions. Water research. 2015;73:68-77.

[114] Hill DT, Cobb SA, Bolte JP. Using volatile fatty acid relationships to predict anaerobic digester Failure. 1987;30:496.

[115] Stams AJ, Sousa DZ, Kleerebezem R, Plugge CM. Role of syntrophic microbial communities in high-rate methanogenic bioreactors. Water science and technology. 2012;66:352-62.

[116] Rivera I, Bakonyi P, Cuautle-Marín MA, Buitrón G. Evaluation of various cheese whey treatment scenarios in single-chamber microbial electrolysis cells for improved biohydrogen production. Chemosphere. 2017;174:253-9.

[117] Switzenbaum M, Robins J, Hickey R. Immobilization of anaerobic biomass. granular anaerobic sludge;

Microbiology and technology: Puduc Wageningen, The Netherlands; 1988. p. 115-31.

[118] Garcia J-L, Patel BKC, Ollivier B. Taxonomic, phylogenetic, and ecological diversity of methanogenic archaea. Anaerobe. 2000;6:205-26.

[119] Ramm P, Jost C, Neitmann E, Sohling U, Menhorn O, Weinberger K, et al. Magnetic biofilm carriers: The use of novel magnetic foam glass particles in anaerobic digestion of sugar beet silage. Journal of renewable energy. 2014;2014.

[120] Gremion F, Chatzinotas A, Harms H. Comparative 16S rDNA and 16S rRNA sequence analysis indicates that *Actinobacteria* might be a dominant part of the metabolically active bacteria in heavy metal-contaminated bulk and rhizosphere soil. Environmental microbiology. 2003;5:896-907.

[121] Delbès C, Moletta R, Godon J-J. Bacterial and archaeal 16S rDNA and 16S rRNA dynamics during an acetate crisis in an anaerobic digestor ecosystem. FEMS microbiology ecology. 2001;35:19-26.

[122] Liu Y. Methanomicrobiales. In: Timmis KN, editor. Handbook of Hydrocarbon and Lipid Microbiology. Berlin, Heidelberg: Springer Berlin Heidelberg; 2010. p. 583-93.

[123] Byrne JM, Muhamadali H, Coker VS, Cooper J, Lloyd JR. Scale-up of the production of highly reactive biogenic magnetite nanoparticles using *Geobacter sulfurreducens*. Journal of the royal society interface. 2015;12.

[124] Zhao Z, Zhang Y, Holmes DE, Dang Y, Woodard TL, Nevin KP, et al. Potential enhancement of direct interspecies electron transfer for syntrophic metabolism of propionate and butyrate with biochar in up-flow anaerobic sludge blanket reactors. Bioresource technology. 2016;209:148-56.

[125] Bergey DH. Bergey's manual of systematic bacteriology: the proteobacteria: Springer; 2004.

[126] Shrestha PM, Malvankar NS, Werner JJ, Franks AE, Elena-Rotaru A, Shrestha M, et al. Correlation between microbial community and granule conductivity in anaerobic bioreactors for brewery wastewater treatment. Bioresource technology. 2014;174:306-10.

[127] Zhang J, Lu Y. Conductive Fe_3O_4 nanoparticles accelerate syntrophic methane production from butyrate oxidation in two different lake sediments. Frontiers in microbiology. 2016;7:1316.

[128] Lee J-Y, Lee S-H, Park H-D. Enrichment of specific electro-active microorganisms and enhancement of methane production by adding granular activated carbon in anaerobic reactors. Bioresource technology. 2016;205:205-12.

[129] Xu S, He C, Luo L, Lü F, He P, Cui L. Comparing activated carbon of different particle sizes on enhancing methane generation in upflow anaerobic digester. Bioresource technology. 2015;196:606-12.

[130] Yang Y, Zhang Y, Li Z, Zhao Z, Quan X, Zhao Z. Adding granular activated carbon into anaerobic sludge digestion to promote methane production and sludge decomposition. Journal of cleaner production. 2017;149:1101-8.

[131] Zhao Z, Zhang Y, Woodard T, Nevin K, Lovley D. Enhancing syntrophic metabolism in up-flow anaerobic sludge blanket reactors with conductive carbon materials. Bioresource technology.

2015;191:140-5.

[132] Dang Y, Holmes DE, Zhao Z, Woodard TL, Zhang Y, Sun D, et al. Enhancing anaerobic digestion of complex organic waste with carbon-based conductive materials. Bioresource technology. 2016;220:516-22.

[133] Baek G, Jung H, Kim J, Lee C. A long-term study on the effect of magnetite supplementation in continuous anaerobic digestion of dairy effluent–Magnetic separation and recycling of magnetite. Bioresource technology. 2017;241:830-40.

[134] Lei Y, Sun D, Dang Y, Chen H, Zhao Z, Zhang Y, et al. Stimulation of methanogenesis in anaerobic digesters treating leachate from a municipal solid waste incineration plant with carbon cloth. Bioresource technology. 2016;222:270-6.

[135] Yu Z, Leng X, Zhao S, Ji J, Zhou T, Khan A, et al. A review on the applications of microbial electrolysis cells in anaerobic digestion. Bioresource technology. 2018.

[136] Park J, Lee B, Tian D, Jun H. Bioelectrochemical enhancement of methane production from highly concentrated food waste in a combined anaerobic digester and microbial electrolysis cell. Bioresource technology. 2018;247:226-33.

[137] Yin Q, Zhu X, Zhan G, Bo T, Yang Y, Tao Y, et al. Enhanced methane production in an anaerobic digestion and microbial electrolysis cell coupled system with co-cultivation of *Geobacter* and *Methanosarcina*. Journal of environmental sciences. 2016;42:210-4.

[138] Zhao Z, Zhang Y, Wang L, Quan X. Potential for direct interspecies electron transfer in an electric-anaerobic system to increase methane production from sludge digestion. Scientific reports. 2015;5:11094.

[139] Tian T, Qiao S, Li X, Zhang M, Zhou J. Nano-graphene induced positive effects on methanogenesis in anaerobic digestion. Bioresource technology. 2017;224:41-7.

[140] Lin R, Cheng J, Zhang J, Zhou J, Cen K, Murphy JD. Boosting biomethane yield and production rate with graphene: The potential of direct interspecies electron transfer in anaerobic digestion. Bioresource technology. 2017;239:345-52.

[141] Salvador AF, Martins G, Melle-Franco M, Serpa R, Stams AJ, Cavaleiro AJ, et al. Carbon nanotubes accelerate methane production in pure cultures of methanogens and in a syntrophic coculture. Environmental microbiology. 2017;19:2727-39.

[142] Lee B, Park J-G, Shin W-B, Tian D-J, Jun H-B. Microbial communities change in an anaerobic digestion after application of microbial electrolysis cells. Bioresource technology. 2017;234:273-80.

[143] Feng Q, Song Y-C, Bae B-U. Influence of applied voltage on the performance of bioelectrochemical anaerobic digestion of sewage sludge and planktonic microbial communities at ambient temperature. Bioresource technology. 2016;220:500-8.

[144] Hori T, Haruta S, Ueno Y, Ishii M, Igarashi Y. Dynamic transition of a methanogenic population in response to the concentration of volatile fatty acids in a thermophilic anaerobic digester. Applied and

environmental microbiology. 2006;72:1623-30.

[145] Cerrillo M, Viñas M, Bonmatí A. Startup of electromethanogenic microbial electrolysis cells with two different biomass inocula for biogas upgrading. ACS sustainable chemistry & engineering. 2017;5:8852-9.

[146] Wang Y, Zhang Y, Wang J, Meng L. Effects of volatile fatty acid concentrations on methane yield and methanogenic bacteria. Biomass and bioenergy. 2009;33:848-53.

[147] Liu P, Liang P, Jiang Y, Hao W, Miao B, Wang D, et al. Stimulated electron transfer inside electroactive biofilm by magnetite for increased performance microbial fuel cell. Applied energy. 2018;216:382-8.

[148] Bialek K, Kim J, Lee C, Collins G, Mahony T, O'Flaherty V. Quantitative and qualitative analyses of methanogenic community development in high-rate anaerobic bioreactors. Water research. 2011;45:1298-308.

[149] Baek G, Kim J, Lee S, Lee C. Development of biocathode during repeated cycles of bioelectrochemical conversion of carbon dioxide to methane. Bioresource technology. 2017;241:1201-7.

[150] Villano M, Aulenta F, Ciucci C, Ferri T, Giuliano A, Majone M. Bioelectrochemical reduction of CO_2 to CH_4 via direct and indirect extracellular electron transfer by a hydrogenophilic methanogenic culture. Bioresource technology. 2010;101:3085-90.

[151] Siegert M, Yates MD, Call DF, Zhu X, Spormann A, Logan BE. Comparison of nonprecious metal cathode materials for methane production by electromethanogenesis. ACS sustainable chemistry & engineering. 2014;2:910-7.

[152] Batlle-Vilanova P, Puig S, Gonzalez-Olmos R, Vilajeliu-Pons A, Balaguer MD, Colprim J. Deciphering the electron transfer mechanisms for biogas upgrading to biomethane within a mixed culture biocathode. RSC advances. 2015;5:52243-51.

[153] Fotidis IA, Karakashev D, Angelidaki I. Bioaugmentation with an acetate-oxidising consortium as a tool to tackle ammonia inhibition of anaerobic digestion. Bioresource technology. 2013;146:57-62.

[154] Yanuka-Golub K, Reshef L, Rishpon J, Gophna U. Community structure dynamics during startup in microbial fuel cells – The effect of phosphate concentrations. Bioresource technology. 2016;212:151-9.

[155] Ishii Si, Suzuki S, Norden-Krichmar TM, Wu A, Yamanaka Y, Nealson KH, et al. Identifying the microbial communities and operational conditions for optimized wastewater treatment in microbial fuel cells. Water research. 2013;47:7120-30.

[156] Ishii Si, Suzuki S, Yamanaka Y, Wu A, Nealson KH, Bretschger O. Population dynamics of electrogenic microbial communities in microbial fuel cells started with three different inoculum sources. Bioelectrochemistry. 2017;117:74-82.

[157] Siegert M, Yates MD, Spormann AM, Logan BE. Methanobacterium dominates biocathodic archaeal communities in methanogenic microbial electrolysis cells. ACS sustainable chemistry & engineering. 2015;3:1668-76.

[158] Lu L, Xing D, Ren N. Pyrosequencing reveals highly diverse microbial communities in microbial electrolysis cells involved in enhanced H_2 production from waste activated sludge. Water research. 2012;46:2425-34.

[159] Feng Q, Song Y-C, Ahn Y. Electroactive microorganisms in bulk solution contribute significantly to methane production in bioelectrochemical anaerobic reactor. Bioresource technology. 2018;259:119-27.

[160] Nesbø CL, Bradnan DM, Adebusuyi A, Dlutek M, Petrus AK, Foght J, et al. *Mesotoga prima* gen. nov., sp. nov., the first described mesophilic species of the *Thermotogales*. Extremophiles. 2012;16:387-93.

[161] Reguera G, Nevin KP, Nicoll JS, Covalla SF, Woodard TL, Lovley DR. Biofilm and nanowire production leads to increased current in *Geobacter sulfurreducens* fuel cells. Applied environmental microbiology. 2006;72:7345-8.

[162] Sun D, Wang A, Cheng S, Yates M, Logan BE. *Geobacter anodireducens* sp. nov., an exoelectrogenic microbe in bioelectrochemical systems. International journal of systematic and evolutionary microbiology. 2014;64:3485-91.

[163] Brenner D, Krieg N, Staley J. Bergey's manual of systematic bacteriology. Volume 2: The *Proteobacteria* Part A, Introductory Assays. Ed. Springer.(Estados Unidos). 304p; 2005.

[164] Liu Y, Balkwill DL, Aldrich HC, Drake GR, Boone DR. Characterization of the anaerobic propionate-degrading syntrophs *Smithella propionica* gen. nov., sp. nov. and *Syntrophobacter wolinii*. International journal of systematic and evolutionary microbiology. 1999;49:545-56.

[165] Hari AR, Katuri KP, Logan BE, Saikaly PE. Set anode potentials affect the electron fluxes and microbial community structure in propionate-fed microbial electrolysis cells. Scientific reports. 2016;6:38690.

[166] Tholozan J, Samain E, Grivet JP, Albagnac G. Propionate metabolism in a methanogenic enrichment culture. Direct reductive carboxylation and acetogenesis pathways. FEMS microbiology ecology. 1990;6:291-7.

[167] Ambuchi JJ, Zhang Z, Shan L, Liang D, Zhang P, Feng Y. Response of anaerobic granular sludge to iron oxide nanoparticles and multi-wall carbon nanotubes during beet sugar industrial wastewater treatment. Water research. 2017;117:87-94.

[168] Valero D, Rico C, Canto-Canché B, Domínguez-Maldonado J, Tapia-Tussell R, Cortes-Velazquez A, et al. Enhancing biochemical methane potential and enrichment of specific electroactive communities from nixtamalization wastewater using granular activated carbon as a conductive material. Energies. 2018;11:2101.

[169] Toczyłowska-Mamińska R, Szymona K, Król P, Gliniewicz K, Pielech-Przybylska K, Kloch M, et al. Evolving microbial communities in cellulose-fed microbial fuel cell. Energies. 2018;11:124.

[170] Zumstein E, Moletta R, Godon JJ. Examination of two years of community dynamics in an anaerobic bioreactor using fluorescence polymerase chain reaction (PCR) single-strand conformation polymorphism analysis. Environmental microbiology. 2000;2:69-78.

[171] Lever MA. A new era of methanogenesis research. Trends in microbiology. 2016;24:84-6.

[172] De Vrieze J, Gildemyn S, Arends JB, Vanwonterghem I, Verbeken K, Boon N, et al. Biomass retention on electrodes rather than electrical current enhances stability in anaerobic digestion. Water research. 2014;54:211-21.

[173] Gacitua MA, González B, Majone M, Aulenta F. Boosting the electrocatalytic activity of *Desulfovibrio paquesii* biocathodes with magnetite nanoparticles. International journal of hydrogen energy. 2014;39:14540-5.

[174] Zhen G, Kobayashi T, Lu X, Xu K. Understanding methane bioelectrosynthesis from carbon dioxide in a two-chamber microbial electrolysis cells(MECs) containing a carbon biocathode. Bioresource technology. 2015;186:141-8.

[175] Lerm S, Kleyböcker A, Miethling-Graff R, Alawi M, Kasina M, Liebrich M, et al. Archaeal community composition affects the function of anaerobic co-digesters in response to organic overload. Waste management. 2012;32:389-99.

[176] Lei Y, Song B, van der Weijden RD, Saakes M, Buisman CJ. Electrochemical induced calcium phosphate precipitation: importance of local pH. Environmental science & technology. 2017;51:11156-64.

[177] Jeremiasse AW, Hamelers HV, Buisman CJ. Microbial electrolysis cell with a microbial biocathode. Bioelectrochemistry. 2010;78:39-43.

[178] Yu H-Q, Tay J-H, Fang HH. The roles of calcium in sludge granulation during UASB reactor start-up. Water research. 2001;35:1052-60.

[179] Lee J-Y, Park J-H, Park H-D. Effects of an applied voltage on direct interspecies electron transfer via conductive materials for methane production. Waste management. 2017;68:165-72.

[180] Call D, Logan BE. Hydrogen production in a single chamber microbial electrolysis cell lacking a membrane. Environmental science & technology. 2008;42:3401-6.

[181] Borole AP, Reguera G, Ringeisen B, Wang Z-W, Feng Y, Kim BH. Electroactive biofilms: current status and future research needs. Energy & environmental science. 2011;4:4813-34.

[182] Holmes DE, Shrestha PM, Walker DJ, Dang Y, Nevin KP, Woodard TL, et al. Metatranscriptomic evidence for direct interspecies electron transfer between *Geobacter* and *Methanothrix* species in methanogenic rice paddy soils. Applied and environmental microbiology. 2017:AEM. 00223-17.

감사의 글

2010 년도에 학부에 입학했을 때만 해도 2019 년까지 제가 유니스트에서 공부하고 있을 것이라고는 생각하지 못했습니다. 대학원에 진학하고 싶다는 막연한 생각은 가지고 있었지만 대학원 생활이 구체적으로 뭘 하는 것인지, 무엇에 대해서 공부하고 싶은지에 대해서는 한 번도 생각해 본 적이 없었던 것 같습니다. 학부 3 학년 때 우연히(?) 수강했던 이창수 교수님의 수업을 듣고는 교수님의 대단한 영어 및 수업 실력과 '미생물을 이용한 폐기물의 처리'라는 신기한 주제에 매료되어 현재 연구실인 ABLE lab 으로의 진학을 계획하게 되었습니다. 긴 고민의 시간을 가진 것도 아니고 원대한 꿈을 품은 것도 아니지만, 지금 와서 생각해보면 당시 그런 선택을 했던 저 자신을 정말 칭찬하고 싶습니다. 다들 대학원 생활이 힘들고 지친다고 하지만, 저는 이 연구실에서 실험하고 공부하고 동료들과 어울리면서 딱히 슬럼프라는 것을 겪어보지 못했던 것 같습니다. 때때로 작은 스트레스를 받거나 반복되는 일상이 무료했던 적은 있지만, 그럼에도 불구하고 지금에서 돌이켜보면 5 년 반 동안의 삶은 대부분 즐거움과 행복으로 가득했습니다. 새로운 일에 도전하는 것에 겁도 많고 독립심도 부족하고 낯도 많이 가리는 제가 이렇게 만족스러운 대학원 생활을 보낼 수 있었던 것은, 모두 제 주변 사람들의 도움과 애정에서 비롯된 것이라고 생각하기 때문에 이 글을 빌어 그 분들께 감사를 전하고 싶습니다.

가장 먼저, 학부 생활을 비롯하여 거의 7 년에 가까운 시간 동안 부족한 저를 물심양면으로 가르쳐 주시고 성장할 수 있게 도와주신 저희 지도교수님, 이창수 교수님께 감사 인사를 드리고 싶습니다. 이 연구실에 입학했을 때부터 졸업을 앞둔 지금까지도, 제가 알게 된 교수님 중 최고의 교수님이 누구냐고 물어본다면 우리 교수님이라고 자신 있게 말 할 수 있을 만큼 좋은 분을 만나 성공적으로 학위를 마칠 수 있게 되었습니다. 학술적인 측면 뿐 아니라 인생 선배로서 해 주신 조언들 덕분에 제가 많이 성장할 수 있었습니다. 더불어, 학위 심사를 위해 많은 시간을 할애하여 제 연구에 대해 함께 고민해 주신 학위 심사위원 분들께도 감사의 인사를 드립니다. 국내의 혐기소화 기술을 선도하시는 POSTECH 황석환 교수님의 값진 조언들을 들을 수 있어서 영광이었고, 항상 연구 진행에 큰 도움이 되는 질문들을 던져 주신 부산대학교 배효관 교수님, 화학적 측면에서의 전문적인 피드백을 주신 언제 뵈어도 유쾌하신 서울대학교 이창하 교수님, 대학원 기간 동안 가장 큰 도움이 되었던 수업인 수질화학 강의를 진행해 주시고 이와 관련된 조언들을 아끼지 않으신 권영남 교수님께도 깊은 감사를 드립니다. 피펫 사용법도 모르고 솔리드 디쉬를 손으로 집어 무게를 측정하던 아기 대학원생 시절부터 저를 사랑으로 키워 주신 김자애 박사님, 너무너무 감사하고 사랑합니다!

그리고 이 연구실에 들어온 것이 진짜 행운이라고 느껴질 정도로 너무너무 좋은 우리 ABLE 랩 구성원들에게도 감사를 전합니다. 같은 시기에 입학해서 가장 오랫동안 함께 생활한 우리 랩 GC 지킴이 예담이, 아이디어가 너무 샘솟는 나머지 가끔 날 피곤하게 했던 미래의 보육원 원장 규철이, 나랑 취향도 잘 맞고 말도 너무 잘 통해서 수다 떨면서 맥주 마시면 둘 다 절제가 안 되는 현정이, 너무나 도도하고 엄청난 청결&원칙주의자이지만 그래서 가끔 실수할 때 더 귀여운 단비, 이상한 언행 (나 때는 말이야~ 등)을 일삼지만 같이 논문 쓰고 실험할 때는 엄청나게 큰 도움이 되는 진수, 나 때문에 질소 가스에 맞아서 눈썹 털이 다 날아갈 뻔한 은근히 대화가 잘 통하는 한웅이, 조용조용한 목소리로 말해서 잘 안 들리지만 가끔씩 너무 웃기고 귀여운 말을 하는 형민이, 랩에 있을 때 실험도 많이 도와주고 심심할 때는 언제든지 놀아주던 맥주 괴물 학찬 오빠, 그리고 궂은 일도 항상 도와줬던 지훈이를 포함한 인턴둥이들, 다들 너무 고마워. 마지막으로 나랑 성격이 정반대인 것 같으면서도 정말 비슷한 점도 많아서 대학원 생활 내내 내가 정말 많이 좋아하고 의지했던 내 평생 친구 희정이ㅜㅜ 너와의 커피타임, 알코올타임, 수다타임이 없었더라면 대학원 기억의 절반이 없는 거나 다름없을 거야, 앞으로도 평생 내 개그맨 해줘. 진짜 이 감사의 글을 누군가가 본다면 ABLE lab 으로의 진학을 강추하고 싶을 정도로, 매일 생성되는 웃긴 에피소드들과 더불어 최고의 경험과 행복을 선사해 준 고마운 연구실입니다.

학부 1 학년 때부터 지금까지 거의 10 년 째 함께 하는 내 영원한 룸메 효정이, 맛집 탐방 메이트 정하, 내 든든한 버팀목 정식 오빠, 학부 졸업 이후로 자주는 못 보지만 언제 만나도 어색하지 않은 기현이, 민아, 은희, 윤선 언니. 가방 끈만 자꾸 길어지고 아무도 취업 못 하고 있다고 항상 웃겨 했던 나의 복자팸, 태연이, 지혜, 수인이, 예송이, 유림이 (아직도 가방 끈만 늘이고 있는 건 이제 나 밖에 안 남았지만..). 다들 멀리 살면서도 (특히 브라질에 사는 수인이ㅋㅋ) 언양읍에서 공부하는 나 보러 여러 번 울산까지 와 준 내 소중한 친구들. 그리고 멀리 떨어져 있어도 자주 보게 되고 볼 때마다 너무 재밌고 힐링되는 내 청양팸, 스물 아홉이나 되었는데도 만나면 아홉 살처럼 유치하고 허물없이 놀게 되는 세상에서 제일 좋은 내 고향 친구들인 효숙이, 성인이, 은미, 유림이, 솔이. 디펜스 응원한다고 편지랑 선물까지 주면서 날 감동시킨 민정이, 공부하느라 고생 많다고 가끔씩 울산까지 찾아와서 응원해주었던 내 유일한 동네 남사친 권범이, 주기적으로 만나서 수다 떨고 힐링해야 하는 우리 주연 언니, 다들 너무 감사합니다.

마지막으로 내가 제일 사랑하고 존경하는, 언제나 내 편인 우리 가족에게도 감사를 전합니다. 영화 리틀 포레스트처럼 내가 힘들고 스트레스 받고 길을 헤매더라도 언제든 돌아와서 숨을 고를 수 있는 곳을 마련해 주고 싶어서, 나이가 들어도 청양을 떠나지 않을 거라는 우리 엄마. 내가 살아오면서 만난 세상의 어떤 남자와 비교하더라도 최고의 아빠, 최고의 남편, 최고의 교육자인 우리 아빠. 나보다 7 살이나 어리지만, 아주 가끔을 제외하고는 나보다 성숙하고 생각이 깊은 자랑스러운 내 동생 대건이. 어렸을 때부터 매번 받기만 해서 너무 죄송하고 감사한 우리 어머님, 항상 유쾌하셔서 만나면 에너지가 생기는 인간비타민 아버님, 같이 모여서 진영이 험담할 때가 제일 재밌는 아주버님. 내가 어떠한 결정을 하더라도 항상 응원해주고 존중해주는 든든한 가족들 덕분에 성공적으로 박사 학위를 마칠 수 있었다고 생각합니다.

진짜 마지막으로 내 인생 최고의 행운인 내 남편이자 베프이자 인생 멘토인 진영이에게. 나보다 몇 배는 성숙하고 현명한 너를 만났기 때문에 내가 헤매지 않고 무사히 박사 학위를 마칠 수 있었어. 앞으로 너와 함께 할 시간들은 대부분 행복한 일들도 가득하겠지만 힘든 일들도 가끔 찾아올 텐데, 항상 네가 말했던 것처럼 인생은 무수히 많은 점들의 연속이고 우리가 서 있는 곳이 변곡점인지는 지나 보아야 아는 거니까, 어떤 고난이 오더라도 함께 긍정에너지로 극복해보자! 박사 학위 마지막까지 도와주어서 정말 고마워.

2019 년 7 월 ABLE lab 에서

백 가 현